The geothermal utilization of shut-in or abandoned hydrocarbon wells

Technical and economical aspects

Seleyman Ghafuri

MSc Thesis Petroleum Engineering and Geosciences | Delft University of Technology

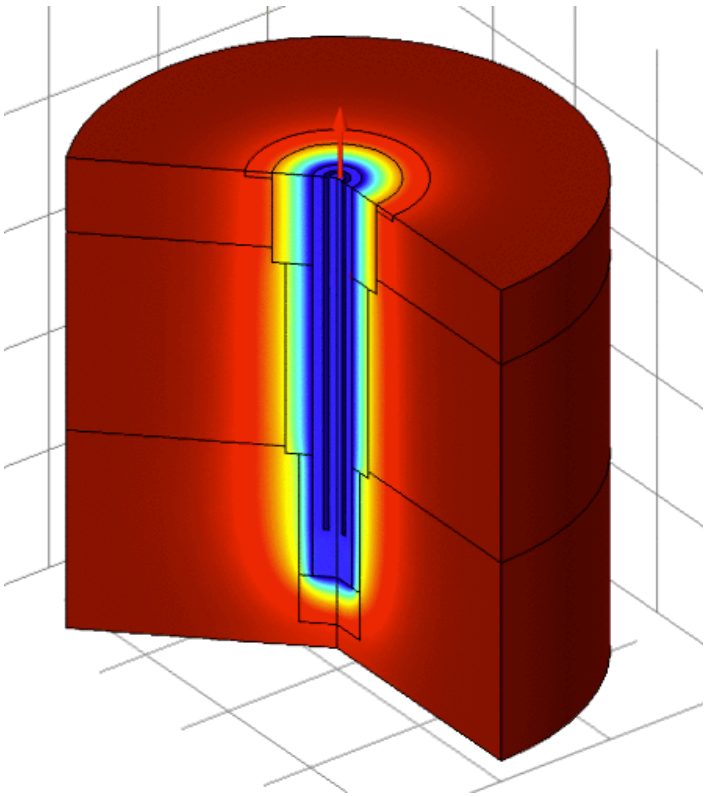

TU Delft

VERMILION ENERGY

The geothermal utilization of shut-in or abandoned hydrocarbon wells:

Technical and economical aspects

By

S. Ghafuri

To obtain the degree of Master of Science in:

Petroleum Engineering and Geosciences

at the Delft University of Technology,
to be defended publicly on Wednesday April 28, 2021 at 3:00 PM.

Thesis committee:	Prof. dr. D. Bruhn	TU Delft, Supervisor and Committee Chair
	Dr. K.H.A.A Wolf	TU Delft
	Dr. P.J. Vardon	TU Delft
	Ir. R. Gibbons,	Vermilion Energy

Abstract

This research is intended to create an insight into the heat exchange occurring in a well and to find ideal well conditions in which the performance of the heat exchange is maximised.
For demonstrating and studying these aspects the well of Grouw-01 is analysed. The well of Grouw-01 is a depleted gas well attained from Vermilion Energy and is in shut-in state.

Re-using these shut-in or abandoned wells can provide fossil fuel-free energy for the local community. Such wells have the potential to be used for geothermal energy generation, either by using them to directly access warm water from a reservoir or as borehole heat exchanger, without direct connection to a potential reservoir. In this study there is no contact with the reservoir. As there is no contact, a method is created in which the injected fluid can reach the surface within the same well. This is done by creating a circulating system of a working fluid in the well in which the heat is extracted from the subsurface and carried to the surface by the working fluid. For the fluid to be able to circulate, a tubing is installed inside the well which is an inner-tubing. Such a well with circulating fluid systems is designed like a Deep Coaxial Borehole Heat Exchanger (DCBHE). The software COMSOL Multiphysics 5.4 is used for the reconstruction of the well design in 3-D. The model is based on the former gas production well Grouw-01, which has been in the shut-in phase for over 5 years. For such systems, the design conditions need to be optimized as these conditions can help increase the heat extraction. The different properties that can influence this are the type of working fluid, the material and thickness (insulation material) of an inner-tubing for fluid circulation, flowrates, outer-well size and injection temperatures.

Finding an ideal design condition is the main goal. The software allowed an intense sensitivity analysis on the properties which can influence the heat extraction. The outcomes of the different sensitivity analyses show that

- The heat capacity of the working fluid is critical for the amount of power that the fluid delivers. Working fluids with high heat capacity deliver a higher power output compared to the working fluids with low heat capacity. However, a working fluid with low heat capacity normally delivers a higher production temperature.
- The flowrate in which the fluid circulates, has an optimum limit in which fluid cooling is minimum during upward flow and heat extraction during downward flow maximum.
- Insulation material of VIT (Vacuum Insulated Tubing) is crucial for the system to function, the properties of the VIT play a prominent role in this. A material with similar thermal properties can function as a replacement for the VIT.
- Increasing the thickness of the inner-tubing (VIT) delivers a higher power output. This power increase is small compared to the increase of inner-tubing thickness.
- The outer-tubing has similar effects on the power output. If the size of the outer-tubing is doubled there is a small increase in power generation.
- The simulated different well depths show a linear relation of the temperature, power output and depth of a well.
- Injection temperature of the working fluid should remain low for higher efficiency.
- Simulating a reversed working fluid cycle, in which the fluid is injected through the inner-well and produced through the outer-well can cool down the working fluid if the flowrate is low.

Based on the amount of energy that the Grouw-01 well can provide to the energy requirements of households, a system of heat supply and demand is created for an economic analysis. In the economic analysis the value of the different materials, project costs and revenues from this geothermal project are analysed in three different cases. The costs involved are divided in capital costs, operational costs and a government take in the form of taxes. The results of the economic analysis showed that the project is financially viable, unless there is an increase in the OPEX or if the project load hours are drastically reduced.

In this thesis, based on sensitivity studies and the literature review, an efficient DCBHE is introduced. In addition, the economics will give an insight into the financial viability of this efficient system. This thesis provides information for geothermal engineers, well engineers, researchers and whoever are interested in alternative energy methods.

Acknowledgement

I was involved in an engineering internship at Vermilion Energy which also provided input to my M.Sc. thesis at the Technical University of Delft. I hope, my thesis supports the company's plan to re-use their shut-in wells and provide heated water as base-load energy to the local community. This thesis is based on extensive literature research and the creation and evaluation of different finite element models to simulate field conditions by using the well data/logs. I hope the resulting document is of use for the geothermal developers of Vermilion Energy.

The project was under supervision of Prof. D. Bruhn and Dr. S. Saeid from the Technical University of Delft and Ir. R. Gibbons from Vermilion Energy. I am grateful for their insight, expertise and coffee moments. At the time of my graduation Dr. S. Saeid, whom I had extensive contact with could not join duo to maternal leave. I hoped she would, as she is the reason for me reaching this point. With all of your help and guidance, I completed my thesis.

In addition, I would like to express my gratitude to Ir. Jeff Davies, who introduced me to the project and set me up at Vermilion. Dr. K.H.A.A. (Karl-Heinz) Wolf and Dr. P.J. (Phil) Vardon, who guided me through my bachelors and currently are in the thesis committee, merci!

The project took a complete one and a half years to finish, during this period there were many things happening in my life and to makes things even more difficult; Corona came into the world. Thanks to my family and friends who supported me and helped me re-charge during the times I needed it, I could finish the extensive but beautiful project.

Thank you all.

S. Ghafuri
Delft, February 2021

Contents

List of figures

List of tables

1. Introduction

1.1. Geothermal energy

In 2015, it was agreed in the Paris Climate Agreement that the release of greenhouse gases should be reduced. The greenhouse gases are the leading cause of global warming and all nations should work together in achieving climate neutrality by 2050 (Nijpels, 2019). The Dutch government has set a target of 49% reduction of greenhouse gases in the Netherlands by 2030 of what was emitted in 1990 (R. Koelemijer, 2017). To reach these goals, the Dutch government subsidizes alternative climate neutral energy forms like geothermal, wind and solar energy. The focus for this research will be on geothermal and how this can be used as an alternative energy source.

Geothermal energy is the heat generated and stored in the subsurface. Extracting this heat and transporting the heat to the surface is usually done with water or steam. Most of the geothermal systems in the Netherlands produce heat from a well doublet system, with a production well from which hot water is produced and once this is cooled down it is re-injected in the injection well (Figure 1-1). In this configuration, the reservoir pressure can be maintained and the reservoir heat extracted. The re-injected water is re-heated in the reservoir as it circulates through pores and fractures of the reservoir and extracts the heat. A potential application of geothermal energy extraction can be found in wells that are shut-in or abandoned, as temperature always increases with depth and thus can be exploited for energy provision. Such shut-in wells can originate from several different environments and industries, for example the petroleum industry. Petroleum companies are actively trying to find ways in which they can re-use their assets, materials, or wells in order to avoid abandonment and associated costs. A considerable opportunity is presented in their re-use for geothermal heat provision. Neighbouring houses and companies could profit from the heat provided by these wells, which is environmentally friendly as well.

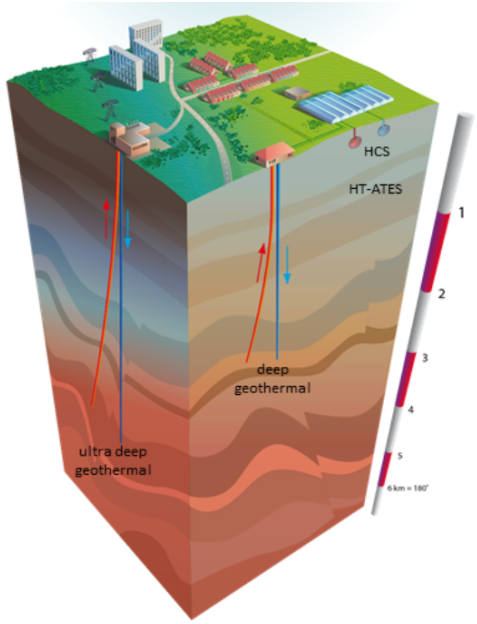

Figure 1-1 Most common geothermal doublet systems(simplified) in 3D with injection(blue) and production (red) wells (M.A.W. Vrijlandt, 2019).

1.2. Geothermal systems and the mono-well

Abandoned hydrocarbon wells have the potential to be used for geothermal energy generation, either by using them to directly access warm water from a reservoir or as borehole heat exchangers, without direct connection to a potential reservoir. There are several different ways fluid can be circulated through a single well in a borehole heat exchanger, as illustrated in Figure 1-2. Options b, c and d are only used for shallow geothermal systems. The only one of these options that remains for deep wells is option a. Therefore, in this study the focus will be placed on the Deep Coaxial Borehole Heat Exchangers or DCBHE (Horne, 1980) as in Figure 1-2a. For this purpose, a tube is inserted in the well to serve as an inner-tube such that the fluid can circulate.

As the fluid is injected (marked as x in Figure 1-2a) and transported to the bottom of the well, the temperature of this fluid will increase since heat is exchanged with the casing and surrounding formation. When the fluid is at the bottom of the well and has reached the bottom hole temperature, it is transported to the surface through the inner-well. Such systems exist already, for example a deep well in Prenzlau, East Germany, with an installed capacity of up to 500 kW_{th} from a depth of 2800m. In combination with a heat pump this system provides approx. 2900 MWh/year to the local district heating network (Schneider et al., 1997). This well was, however, initially drilled as a geothermal well without sufficient hot water at the reservoir and not converted from prior hydrocarbon exploitation. In these systems there has been no sensitivity analysis on the different parameters which improve the heat exchange.

For the project discussed here, we investigate a well which is depleted and shut-in. The focus is on production and injection in a single well, i.e., a mono-well, this means that the well will have an inner-tubing. By having a circulating system, the working fluid can be injected and exchange heat with the surroundings. The function of the inner-tubing is for the working fluid to be transported to the surface once the injected fluid has reached the bottom of the well.

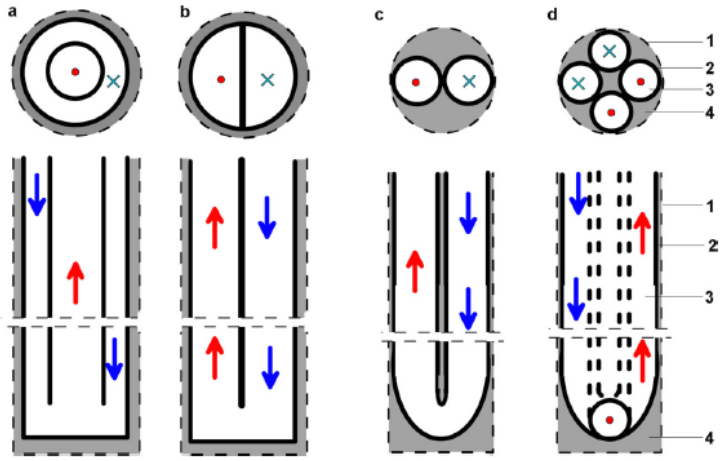

Figure 1-2 Different designs of BHE systems a. Co-axial heat exchanger, b. demi-type heat exchanger, c. single U-pipe, d. double U-pipe heat exchanger, 1.Borehole wall, 2. Heat exchanger pipe, 3. Heat carrier, 4. Sealant. (Tomasz Śliwaa, 2018).

1.3. Previous studies on DCBHE

The circulating system has several components that can regulate the temperature of the working fluid. The components which have an influence on the temperature regulation are the outer-well, inner-well, the working fluids, injection temperature, flowrate changes and geological layering. The influence of these parameters on the overall energy output can be an important factor to optimise the efficiency of the system, as the efficiency is dependent on the temperature difference between the injected and produced working fluid. In this section available literature is examined to understand the influence of these different parts and discuss the results of the different studies.

Well size

An important parameter to investigate in a co-axial well for heat extraction is the size of different well elements; the well diameter and the inner-tubing. The importance and relationship of the inner-tubing and outer-casing size are described by Wang et al. (2009), in this research the relationship between thermal energy extracted and well radius is studied. The experiment results in Figure 1-3-left illustrate that the generated thermal power increases if the size of the outer-casing is increased. This relationship is almost in a linear slope.

A possible cause for the increasing relationship between the thermal power and the outer-casing radius increment can be the larger contact surface of the working fluid with the surrounding subsurface for the heat exchange. This results in a faster depletion of the heat from the surroundings; hence a higher thermal power is achieved. A similar (almost) linear relationship can be seen for a decreasing inner-tubing radius (Figure 1-3-right). Increasing the inner-tubing size leaves less volume in the well for the working fluid to move through. Having less volume with the same amount of working fluid, results in higher flowrate and less time for heat exchange resulting in lower thermal power.

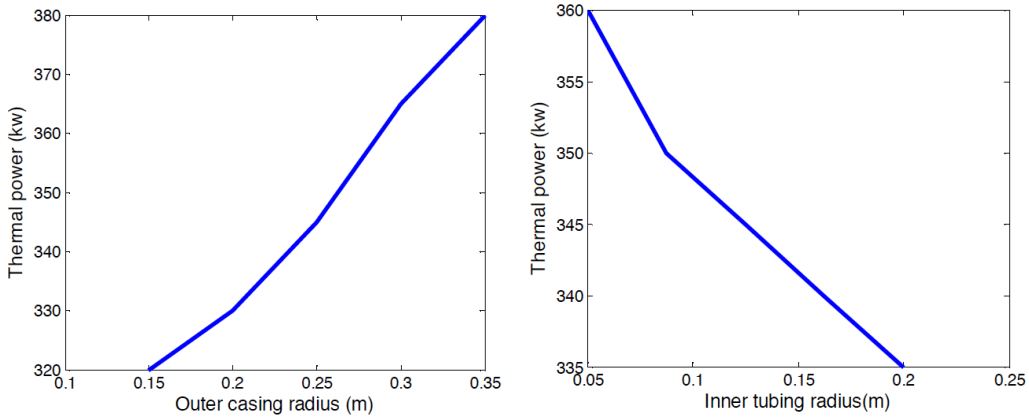

Figure 1-3 The thermal power with an increase in outer casing size (left) or inner-tubing size(right) (Wang M. W., 2009).

Insulation of the inner-tubing

Research of Horne et al. (1980) on the effect of insulation material for the inner-tubing can be seen as a model experiment in this research. Two working fluids were injected in the DCBHE, both working fluids gained in temperature during the downward flow (Figure 1-4). During the upward flow, the case with insulation had a higher working fluid temperature at the surface. The insulation was implemented to have minimum or no cooling of the working fluid during the upward fluid flow. Morita et al. (1995) studied thermal conductivity and showed that for the inner-tubing it is essential to have a low thermal conductivity in order to achieve a large difference in injection and production temperature. This difference can demonstrate the efficiency of transporting the heat from the subsurface to the surface. The effect of thermal conductivity of the inner-tubing is shown in Figure 1-5.

The inner-tubing can vary in thickness, material and design, which all affect the production temperatures. Insulation of the tubing is crucial for transferring the heat in an efficient way to the surface. If the tubing is not insulated the heat would be transferred to the cold injection water, hence it is crucial to have good insulation with low thermal conducting properties. If the tubing has low thermal conductivity the expectation for this is that the heat is transported with minimum heat loss to the surface.

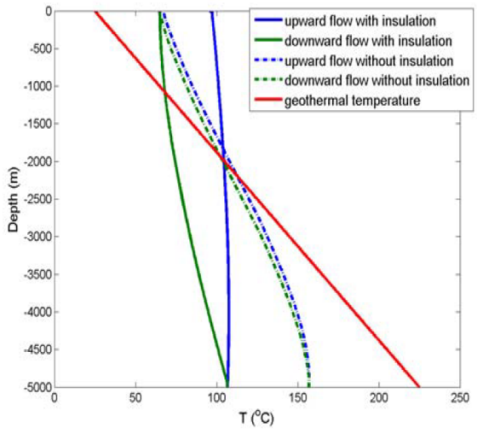

Figure 1-4 Temperature differences for insulated and non-insulated wells based (Horne, 1980).

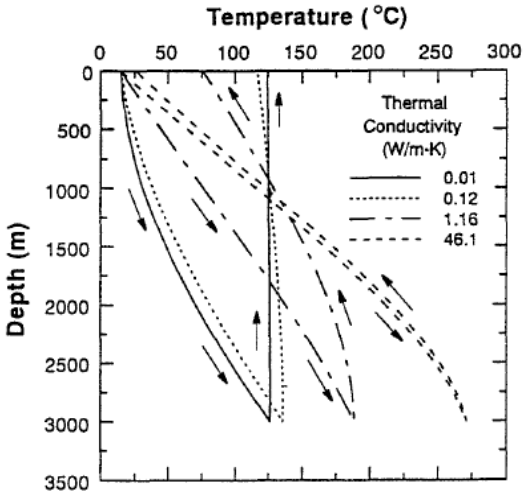

Figure 1-5 The effect of thermal conductivity of the inner-tubing on temperature distribution in the mono-well (Koji Morita, 1995).

Flowrate and injection temperature

A study by Wight et al. (2015) has demonstrated the effects of flowrate and injection temperature change. Figure 1-6 shows the behaviour of the different flowrates. For the higher flowrates there is almost no heat loss during the first 1500-meter well depth. Low flowrates on the contrary show heat loss, if the inlet temperature is higher than the wellbore depth temperature. Figure 1-7 from the same research analyses the difference between high and low inlet temperature. If the inlet temperature is low and flowrate high the working fluid temperature will not decline in the first 1000 meters. If the inlet temperature is high and the flowrate low, then the fluid has more time to exchange heat with the surrounding layers resulting in a decrease in fluid temperature during the first 1000 meters in depth. This effect is seen in Figure 1-7 (left). Based on this study, it is recommended to have a low inlet temperature, in order to have high efficiency in heat extraction.

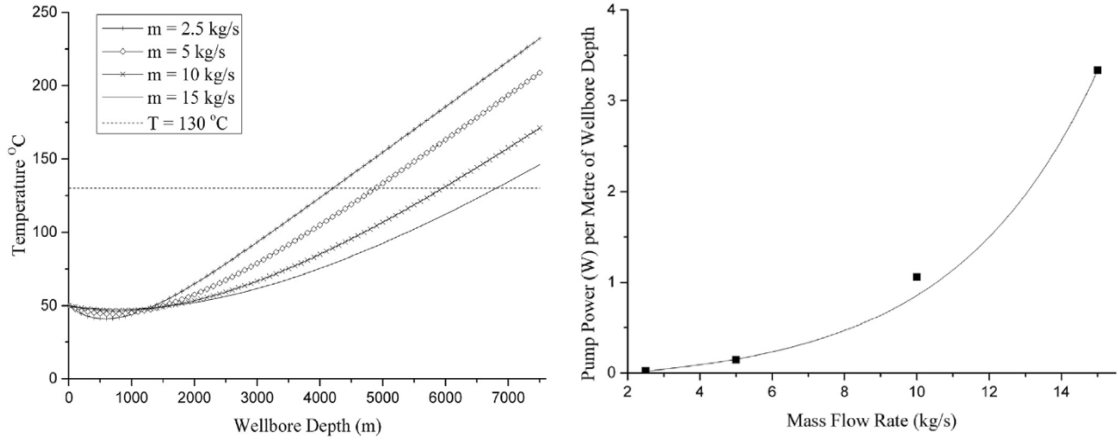

Figure 1-6 The temperature profile for different flowrates (left) and the power requirement for different flowrates (right) (N.M. Wight, 2015).

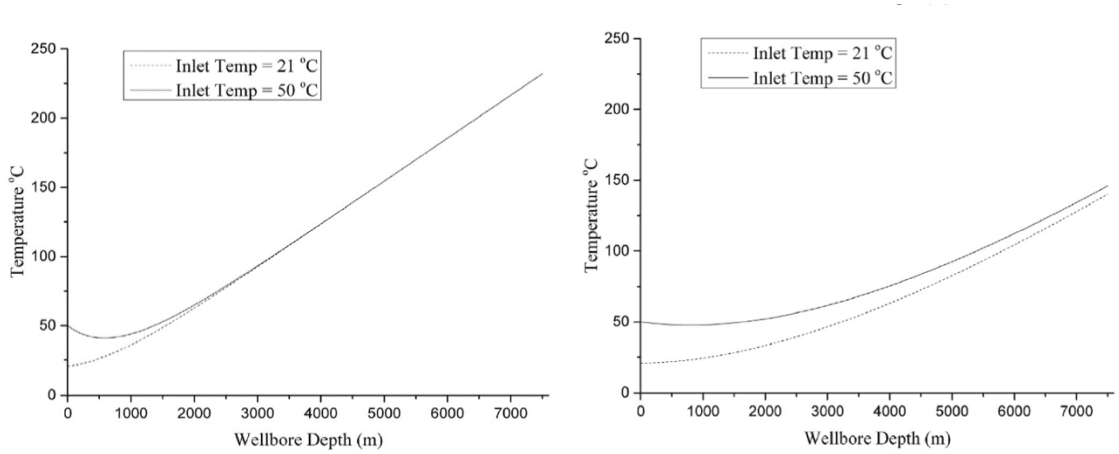

Figure 1-7 The temperature profiles for low flowrates of 2.5 [kg/s](left) and high flowrates of 10 [kg/s](right) with different inlet temperatures (N.M. Wight, 2015).

Pump requirements

A DCBHE requires pumping to inject and produce the working fluid. This is why the power consumption by the pump in such a system also needs to be estimated. The pump requires power to circulate the fluid, the power is used to overcome friction and head differences.

The relative pumping power is also an efficiency criterion. If the pumping power is high compared to the generated power by the DCBHE, then the overall system is not efficient. Using Figure 1-6 (right) from research by Wight et al. (2015) we can have an estimation of the pump power requirement. For a flowrate of 2 kg/s, the pump power would be around 0.05 W per meter of wellbore depth. If the wellbore depth is around 2000 meters, approximately 100 W of power is required to pump the fluid.

Geological influence

A study by Sliwa et al. (2015) conducted on the geology and temperature relationship, demonstrated the influence different geological sections can have on the temperature distribution in the subsurface caused by differences in rock properties. The heat distribution can fluctuate caused by water in the pore space of the geological section (Figure 1-8). The differences of these fluctuations vary per geological section, beyond the thermal transport the geology has no effect on the performance of a closed loop system.

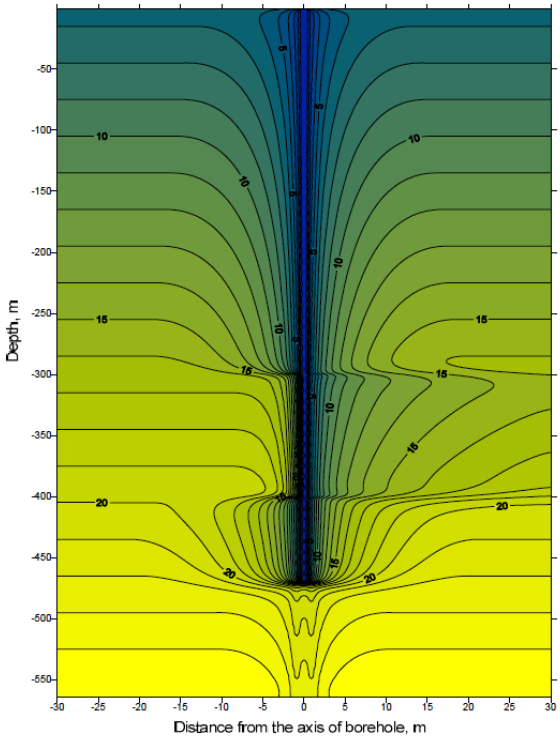

Figure 1-8 Example of an underground water flow at 300-400 m depth impacting the rock mass temperature distribution (Tomasz Sliwa, 2015).

What has not been done in these different research's is an elaborated sensitivity analysis on all the different factors of influence to the heat extraction.

1.4. Objectives of this study

The main objective of this research is to assess the amount of thermal energy that can be extracted from abandoned and shut-in hydrocarbon wells and the duration of the heat extraction. Moreover, to understand which design parameter/s can provide the highest thermal energy while improving on system's efficiency and economics. In order to have an overview of all the different aspects in geothermal mono-well heat extraction, the research question to be clarified and answered in detail is:

How can a mono-well for efficient heat production be developed?

In order to address the main research question, two sub-research questions need to be answered first. The sub-questions are a step-by-step guidance into solving the main research question in an engineering and financial analysis.

How can energy extraction be optimized from the subsurface with a geothermal mono-well and under what condition?
The developed DCBHE generates different amounts of energy from the different well conditions and depths. To find these different conditions and ideal well design, a system is used in which subsurface parameters and operational variable changes determine the efficiency and net energy of the system. The investigated system has a heat pump and a DCBHE pump. The subsurface parameters and operational variables changed are the flowrate, working fluid, injection temperature, inner-tubing material and thickness, outer-tubing thickness and well depth. With the outcome of this efficiency calculation a recommendation can be made for optimal subsurface parameters and operational variable changes.

Is the DCBHE economically viable?
Setting up a closed loop system would require different surface facilities compared to a doublet system. The closed loop system first requires a design and based on this design a thorough cost estimate of the different facilities and equipment required. The costs are deducted from the revenue generated for such systems. The revenue is based on available government policies or the actual market price for heat. Having an estimation of the revenue and costs of the project can determine if the project is economically viable.

In this thesis Grouw-01[1] is taken as the case study. To address the objective of this research a starting point is the characterization of the well by using geological, drilling and available log data. After characterization of Grouw-01 a semi-3D finite element computer model has been designed in order to simulate the well conditions. After the development of the well in COMSOL and simulating the well conditions, a sensitivity study is conducted to show the influence of the different parameters on the energy extraction from the well. The potential of this extracted energy is further analysed with an economic study. Although the analysis is based on the Grouw-01 well, approach and model used in this study can be applied on most wells in the Netherlands.

[1] Grouw-01, is a depleted well earlier used by Vermilion Energy to extract gas. Currently the well is abandoned.

2. Geology and subsurface properties

The Grouw-01 well was drilled to reach the reservoir containing hydrocarbons, primarily methane gas (Table 9.2) at a depth of 1927-1937 m. The physical location of Grouw-01 is in an industrial area, an environment requiring energy for heating. When drilling the Grouw-01 well, different geological data were collected and processed. The collected data provide information on the geological history and structure and the subsurface properties related to heat extraction.

To have a better understanding of the geological layering, one can use the stratigraphy of the area surrounding Grouw-01. Grouw-01 is located between the Vlieland basin and the Friesland platform (Figure 2-1). The stratigraphy of both structural elements is quite similar. For this investigation geological lithostratigraphy of the Friesland platform has been used for the final model. The emphasis has been on the different rock types and their properties, and the thickness of the different geological layers.

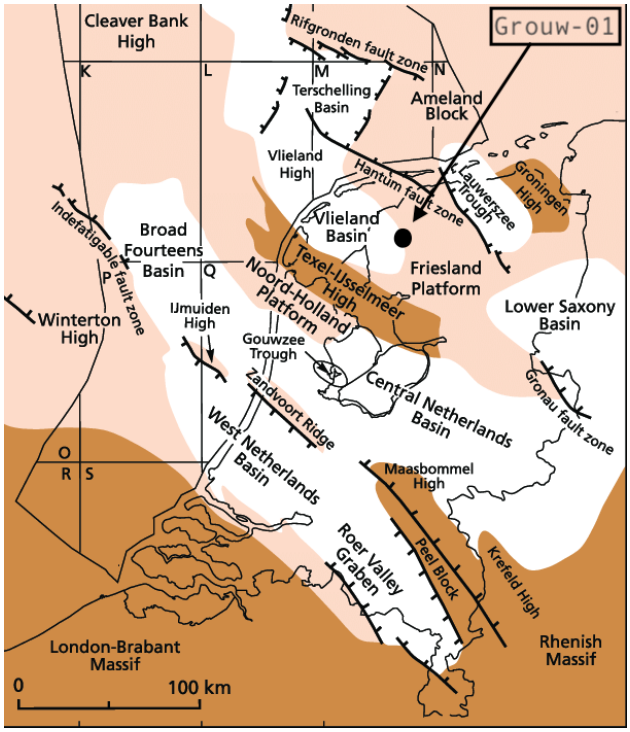

Figure 2-1 The structural elements map for late Jurassic to early Cretaceous with: structural highs (dark brown) platforms (light brown) and basins (white) (Theo Wong, 2007).

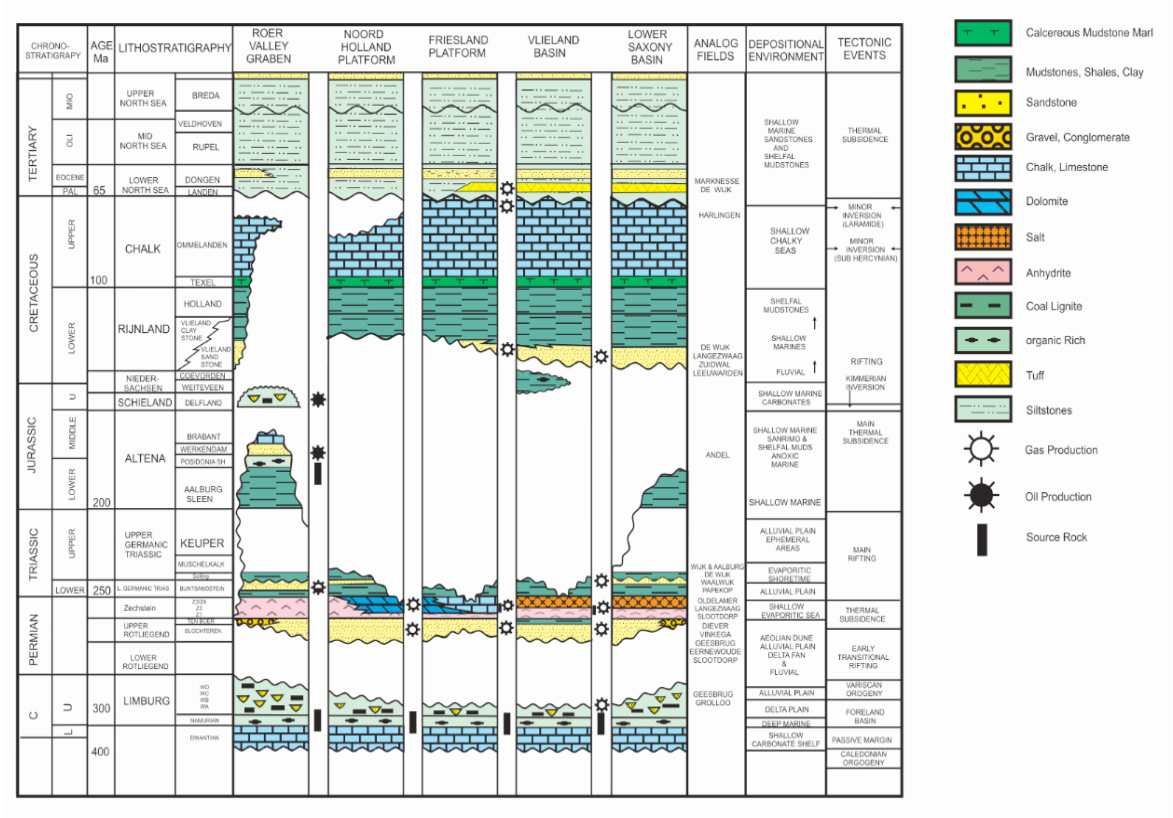

Figure 2-2 The stratigraphic chart of several section in the Netherlands (Vermilion, 2020).

Combining both the chrono-stratigraphy and the stratigraphy of the Friesland platform, the different geological sections can be described with their thicknesses. For this thesis the structural geology has been left out, since the reservoir structure is not needed for further investigation of the mono-well system.

Quaternary	From the surface to the bottom of the Quaternary there has been a deposition of sand in this section. The thickness of the section is approximately 300 meters and consists of sand and sandstone.
Tertiary - Miocene to Oligocene	Most of the formations formed in the Tertiary are siltstones. The thickest siltstone formations are the formations of Breda and Rupel (Nlog, 1979). The layer is between 300 and 708 meters deep.
Tertiary - Eocene to Paleocene	This section has a zone containing sandstone, the sand of Brussels. This is a 90 meter thick sandstone layer, above and below there is siltstone material also containing small parts of claystone (Table 9-4). This layer is between 708 and 798 meters deep. The remaining sections of the Tertiary period consist of siltstones. The siltstone ends at a depth of around 1105 meters.
Cretaceous upper	The Ommelanden formation is composed of limestone, with a thickness of round 630 meters. The upper Cretaceous has large quantities of limestone and chalk. his limestone layer is between 1105 – 1730 meters deep.

The formation of Texel is beneath the Ommelanden formation and consists of mixtures of calcareous mudstone and marl (Figure 2-2). This formation begins at approximately 1790 meters depth.

Cretaceous lower

The lower Cretaceous ends with the Holland formation, a formation from 1790 m to 1835 m depth. The formation contains (from top to bottom): limestone, claystone and limestone.

Between 1835 m and 1922 m depth, the impermeable Vlieland claystone forms a seal for the gas reservoir (Figure 2-2).

The Friesland formation forms the reservoir targeted by Grouw-01 well.

2.1. Geothermal gradient and reservoir temperature

Deep in the earth there is an immense heat available and in large quantities, this heat is transported to the surface so cooling can occur. In this thesis the different aspects of this heat transport are not further discussed. The focus is on the geothermal heat at the well depth, to be more accurate the first 2 kilometers have been temperature logged for the Grouw-01 well, this is useful for creating a computer model to recreate similar conditions (Figure 2-4).

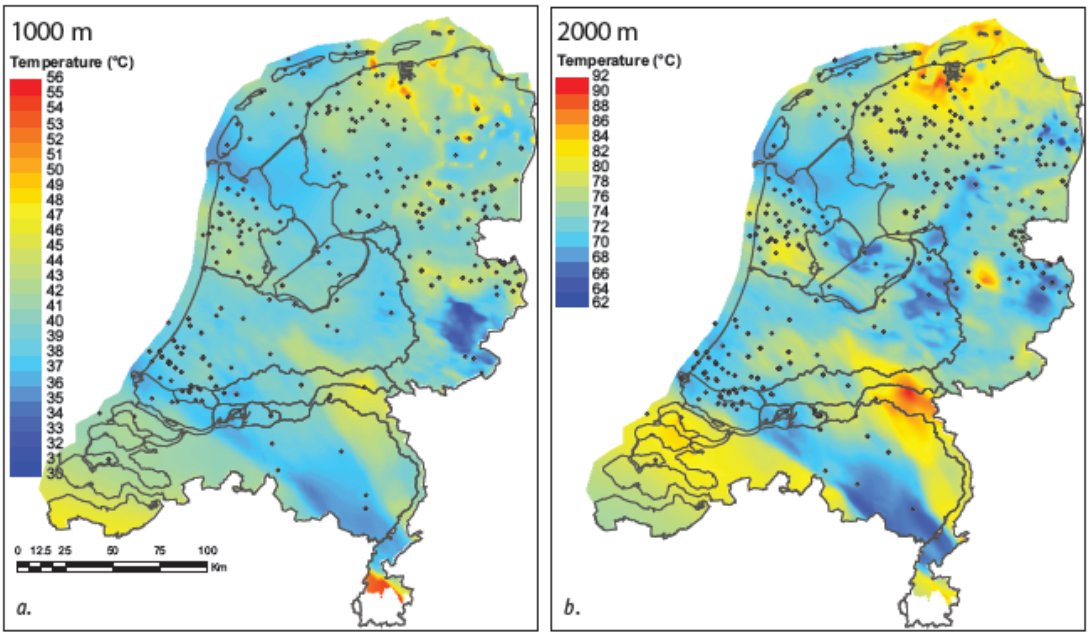

Figure 2-3 Temperatures at 1000 m and 2000 m depth, obtained from measurements in boreholes (D. Bonté, 2012) .

Grouw-01 is located in the northern parts of the Netherlands, where temperatures at 2000 m depth are higher compared to the southern part of the country (Figure 2-3). A possible explanation for the temperature differences could be the difference in geological layering. When, for example, the Roer valley graben in the south and the Friesland platform in the north are compared it can be seen that there are differences in their limestone content (Figure 2-2). The Roer valley graben has lost most of the limestone (during the Cretaceous) contrary to the Friesland platform where the limestone is still intact.

For Grouw-01 to be used as a co-axial heat exchanger, the bottom of the well will be cemented. To have high bottom hole temperatures, this cemented section needs to be at the deepest point possible. For the simulation model, in chapter 3 a depth of 2000 m is taken as the bottomhole depth, although it is possible that the actual created bottomhole will be at 1800 m or 1850 m depending on the safety regulations for cementing wells.

From the temperature log of the Grouw-01 well (Table 2-1) by Elf Petroland (1990), a temperature of roughly $80 - 85^{o}C$ can be expected at a depth of 2000 m. This is in line with the temperature map in Figure 2-3, which is basically a collective borehole temperature display. Alternatively, Schlumberger measured the bottom hole temperature (BHT) in Grouw-01 in 1985, the measured data are displayed in Figure 2-4. The data from Schlumberger of the BHT (Table 9-1) suggests that the temperature is approximately 77.5°C at 1925 meters depth. This is slightly different from the temperature log, which suggests that at the deepest measured point (which is 1909 m) there is a temperature of 80.7°C (Table 2-1).

Table 2-1 Pressure gradients and temperature at different depths for Grouw-01 well (Goepfer, 1990).

Measurement depths		Duration (min)	MRP (Bars.rel)	Pressures (bars.abs)	Temperature (°C)	Gradient (bars/mv)	Equivalent fluid density (g/cc)
m/TH	m/SL						
SAS	+2	30	128,2	128,93	15,5 (NS)		
500	500	30	-	135,11	30,3 (NS)	0,0123	0,125
1000	1000	30	-	140,83	51,4 (NS)	0,0114	0,116
1500	1500	30	-	146,23	67,9	0,0108	0,110
1800	1800	30	-	149,28	75,5	0,0102	0,104
1850	1850	30	-	149,79	78,6	0,0102	0,104
1909	1909	30	-	150,41	80,7	0,0105	0,107

For a realistic scenario both the temperature log and BHT should be compared with their depths. The temperature log shows slightly higher temperatures at 2000 m depth if a linear line is drawn from the last measured points compared to the BHT measured by Schlumberger (Figure 2-4). As seen in Figure 2-3, the average temperature should be in between $78 - 82^{o}C$ for the Friesland area. Having an average of these two different data also generates an average temperature that is close to the data of Figure 2-3.

For this reason, an average temperature between the different measurements is used in the model (chapter 3) as the thermal gradient of the area of Grouw-01. There are also some differences in the average surface temperature in the Netherlands, which is approximately 10°C (A. Lokhorst, 2007), the average surface temperature recorded from the temperature log (Table 2-1) and used in the model, however, is approximately 15°C (Table 2-1). This difference in surface temperatures creates a slightly different thermal gradient, for an identical BHT, resulting in a lower gradient for the higher surface temperature.

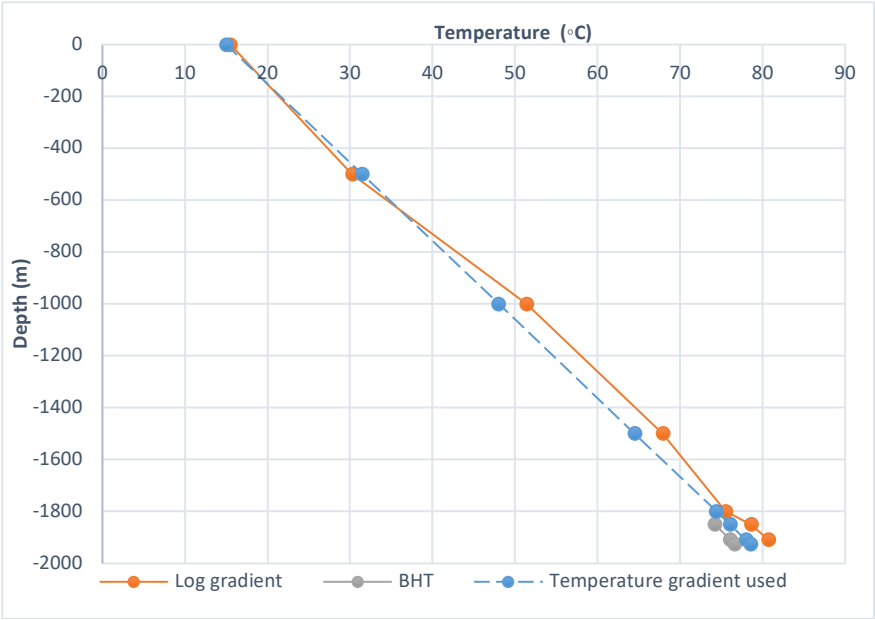

Figure 2-4 Data collected from the temperature logs and the bottom hole temperature measurements (BHT).

Equation 2-1 The geothermal gradient based on temperature log and BHT.

$$T_0 = T_{surface} + 0.033 * z$$

Using the actual data from the log, including the surface temperature, the average temperature gradient for the location can be calculated by Equation 2-1 at the generic depth z in meters, where $T_{surface}$ is the surface temperature (15 $°C$), and 0.033 $deg°C$/m is the thermal gradient.

3. Subsurface model

The software COMSOL Multiphysics has been used to simulate the heat transfer and fluid flow in the DCBHE. The input data and initial conditions are collected from the geological characteristics of the subsurface and the well data gathered from existing reports at Vermillion and further from available literature.

There are several properties that are important for heat transfer, here the focus is mainly on heat capacity and the thermal conductivity of the different materials, working fluids and rocks involved. These properties are used in the heat equation (Equation 3-1). The thermal conductivity often described by λ, is the rate at which heat can be transported through a material. The definitions of a good conductor or an insulator are based on the thermal conductivity of a material. For example, a good conductor has a high thermal conductivity value, as thermal conductivity is defined as 'the heat passing through two materials per time unit, per surface area unit and per unit of temperature' (Vassilis Belessiotis, 2016). The heat capacity is defined as the amount of heat required to raise the temperature of a unit mass of a substance by $1°C$ at specific pressure. The specific heat is explained as the heat capacity for one gram of a substance (Hanrahan, 2012).

3.1. Geometry of the model

To generate a simulation model which is similar to the actual well condition, the well and surrounding geology are defined in a detailed approach. Figure 3-1 is a schematic picture of the well showing the well geometry and completion together with the inner-tubing. The detailed layout of the well is shown in appendix Table 9-4. All parts of the well are implemented with details in the model. However, it must be noted that in Grouw-01 not all the sections were cemented up to the surface, while here for the sake of simplicity uniform cementation is assumed. The properties are described in Table 3-1. As discussed in previous chapters, in order for fluid to circulate in a mono-well an inner-tubing is required.

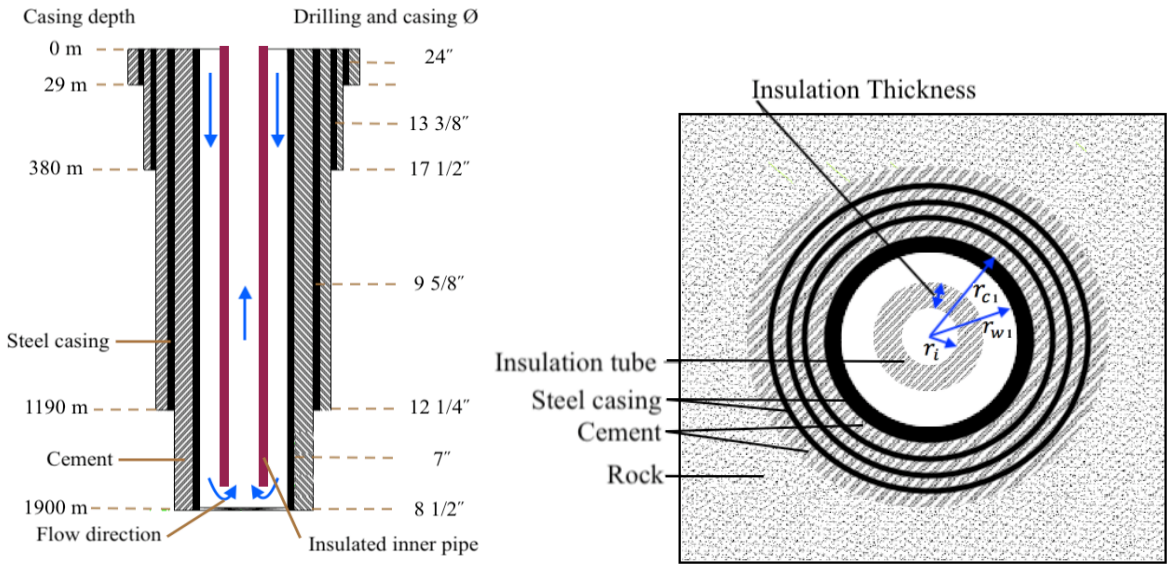

Figure 3-1 Left: Cross section of the well together with fluid flow direction, drilling and casing profile of the Grouw-01 well. Right: The top view.

3.2. The geology of the model

For the model the geological layering has been simplified. Particularly the thinner geological layers are left out of the model, what remains are three dominating geological layers which is the sandstone, siltstone and limestone. The model that has been created has a geological section of these three layers. with the rock types in these layers have different thermal conductivity values. In addition, layers saturated with water can have different thermal conductivities as well. For this simulation an average thermal conductivity value per dominating geological structure is used, and it is taken into consideration that there are large differences between the thermal conductive values of the rocks involved.

The three geological sections are selected based on their occurrence in the subsurface and thickness (Figure 3-3). The first section is built as a 300 meter sandstone layer (Table 9-4). The layer is described in the model as a fairly homogenous section with properties of an average sandstone (Table 3-1). The cement and surface casing are connected to the surrounding rocks, so there is direct heat exchange between these three different parts.

The second layer is siltstone, the depth of this section is between 300 and 1100 meters. The model has similar depth details as the stratigraphy in Figure 2-2, the intermediate casing is in contact with this section. Compared to sandstone in the upper section, the siltstone has lower thermal conductivity (Table 3-1). In the final segment there is an abundance of limestone, (Figure 3-3). This section starts after the siltstone section and continues to the bottom of the geothermal well. The third section is linked with the cement of the production casing and starts at a depth of 1100 meters. The end of the third layer is linked to the well depth. With a well depth of 2500 m, the layer would have a thickness of 1400 m. All the properties of the geology and well bore are constant (Table 3-1). The variables used here are the properties of the inner-tube, fluid properties, and the different fluid flowrates with changes in well thickness and injection temperatures.

Using cement between the steel casing and geological layering can increase the overall thermal conductivity (Iman Asadia, 2018). The cement used in well Grouw-01 has an overall density of $1900 - 2000\ \frac{kg}{m^3}$, and an average thermal conductivity that is almost half that of the geological sections as seen in Table 3-1. It is expected, however, that this will have a minor effect on the overall result since the cement layer is relatively thin compared to the geological sections.

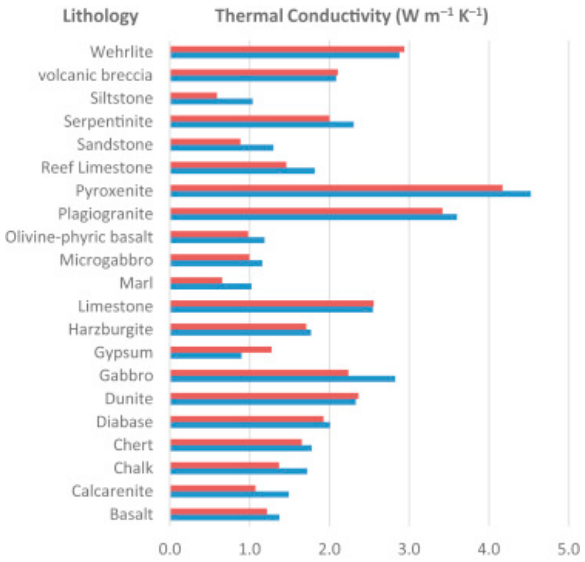

Figure 3-2 The thermal conductivity properties of several saturated (blue) and unsaturated (red) lithologies (Iosifina Iosif Stylianou, 2016).

Table 3-1 Thermal and hydraulic properties of the different layers around Grouw-01.

Parameters	Symbol	Dimension	Value
Sandstone			
Density	ρ_S	kg/m^3	2450
Thermal conductivity	λ_S	$W/(m * K)$	2.4
Heat capacity	c_S	$J/(kg * K)$	950
Siltstone			
Density	ρ_c	kg/m^3	2200
Thermal conductivity	λ_c	$W/(m * K)$	1.8
Heat capacity	c_c	$J/(kg * K)$	950
Limestone			
Density	ρ_l	kg/m^3	2550
Thermal conductivity	λ_l	$W/(m * K)$	2.8
Heat capacity	c_l	$J/(kg * K)$	1000
Cement			
Density	ρ_{ce}	kg/m^3	2000
Thermal conductivity	λ_{ce}	$W/(m * K)$	1.2
Heat capacity	c_{ce}	$J/(kg * K)$	1000
Wellbore radius	r_w	m	0.09
Inner-tubing radius	r_i	m	0.03
Inner-tubing thickness	t_i	m	0.02

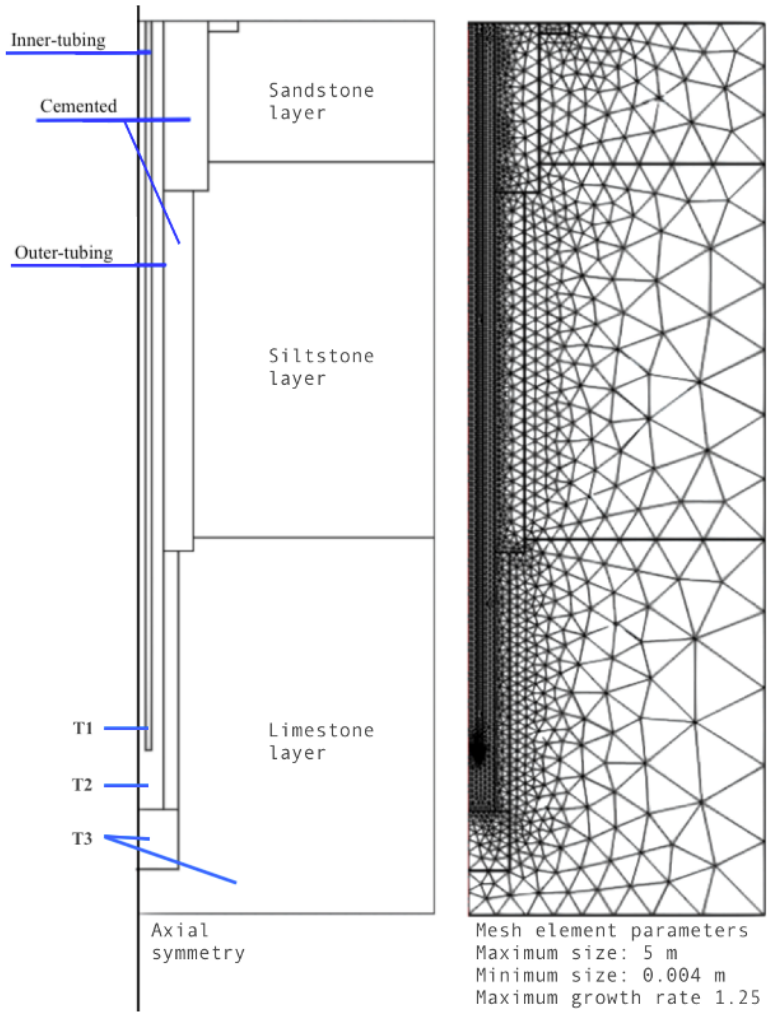

Figure 3-3 The wellbore model in terms of mesh grid parameters.

The model

COMSOL Multiphysics has been used for modelling of a DCBHE in this thesis. COMSOL is a finite element method (FEM) software, in which the laws of physics are expressed in mathematical models (COMSOL, 1986). The models are discretised by the FEM. The model created in this thesis is 2D axisymmetric (Figure 3-3) and the view of the model is in 3D. The main reason why the model is not built-in full 3D is the amount of mesh elements and hence the huge computational time. However, an axisymmetric model does not require the full 3D calculation and thus requires less mesh and less calculation time.

The element size (intensity) of the mesh grid close to the axial symmetry is more in the range of the minimum element size of 0.004 m. At the far ends of the axial symmetry the mesh grid size is close to maximum element size (Figure 3-3) (about 5 m). The reason for this difference is that the volume of space surrounding the well increases with an increase in radius from the axial symmetry point i.e., center point. Fine mesh grid results in higher accuracy of the desired output parameters, in our case the production temperatures.

3.3. Heat interaction in the different sections

In Figure 3-3 the well design is displayed. In this design the heat transfer is occurring between the different well sections. While fluid flows only in the inner-tubing and outer well (inside and outside of the tubing). The heat transfer interfaces define a partial differential equation for the temperature, T of the form stated in Equation 3-1 for the fluid. Heat is 'moved' or 'transported' by conduction and advection in a solid and fluid. The equations are solved with 2D triangular elements, where each of these elements contains 3 nodes. The solid and fluid temperatures are defined as follows; the inner-tubing with T1, working fluid T2 and all other metals, cement and geology as T3 (Figure 3-3). The numbering is based on which phase these materials are in, for example the insulation is in solid state.

Heat equation for the fluids

The created model can be explained in different steps, starting with the heat equation for the fluids. The equations used in this paragraph are heat transfer equations, with difference in the boundary conditions and initial temperatures. The discretization of the model for the fluid section has been solved by the linear method, meaning this method is connecting the triangulated nodes linearly.

Equation 3-1

$$\overbrace{\underbrace{\rho c_p \frac{\partial T_2}{\partial t}}_{Internal\ energy}}^{Storage\ term} + \overbrace{\rho c_p \mathbf{u} \cdot \nabla T_2}^{Convection\ term} + \overbrace{\underbrace{\nabla \cdot \mathbf{q}}_{\mathbf{q}=-\lambda \nabla T_2}}^{Conduction\ term} = \overbrace{\mathbf{Q}}^{source}$$

The heat equation (COMSOL, 1986) for the fluids and solids is described in Equation 3-1, where the storage term for the fluid has the density ρ $\left[\frac{kg}{m^3}\right]$, specific heat capacity at constant pressure c_p $\left[\frac{J}{kg \cdot K}\right]$ with the difference in injection and production temperature T_2 [°C]. The convection is dependent on the density, heat capacity, velocity vector $\mathbf{u}$ $[\frac{\mathrm{m}}{\mathrm{s}}]$ and is using the gradient of the fluid temperature. The conductive term uses the gradient of the conductive heat flux $\mathbf{q}$ $[\frac{\mathrm{W}}{\mathrm{m}^2}]$, thermal conductivity λ $[\frac{\mathrm{W}}{\mathrm{m}*\mathrm{K}}]$, the general heat source/sink $\mathbf{Q}$ $[\frac{\mathrm{W}}{\mathrm{m}^3}]$ and the fluid temperature. The description of the heat flux is also named Fourier's law.

Equation 3-2 initial values

$$T(x, y, o) = T_o$$
$$T_2 = T_o$$

T_o is the initial temperature at a certain location in the model at time 0, with T_2 indicating the working fluid (Figure 3-3). FEM needs boundary conditions and initial values in order to process the data. For our system the temperature log (Table 2-1) provides the geothermal gradient (Equation 2-1) and initial temperature (Equation 3-2). Dirichlet boundary conditions (Fabio Galbusera, 2018) are used here.

Equation 3-3

$$T_2 = T_3$$

The boundary in which heat is exchanged between the fluid (T_2) and production well (T_3) is described for its temperature exchange (Equation 3-3), with T_3 indicating the solid cemented well (Figure 3-3).

Equation 3-4

$$T_2 = T_1$$

In the well the working fluid has contact with the outer and inner side of the inner-tubing, also here the temperature is exchanged between the fluid (T_2) and inner-tubing (T_1) (Equation 3-4).

Equation 3-5

$$p_{inflow} = 5\ bar$$
$$T_{injection} = 12\ ℃$$

Equation 3-5 shows the fluid inflow initial conditions at the inlet (Figure 4-1) for the pressure and temperature. The p_{inflow} is based on the average pressure normal households have in their heating system (which can be different in most businesses and households and is around 5 bar).

Equation 3-6

$$-\mathbf{n} \cdot \mathbf{q} = 0$$

For the fluid outflow boundary condition (Equation 3-6), the flowrate will not be at a rate in which turbulence is reached; this is the reason why the fluid is expected to percolate by laminar flow (K.W.Oh, 2012).

Heat equation for the solids

In the model there are several different types of solids for example geological layering, cement, steel casing and the inner-tubing (Figure 3-3). Although these materials have different properties, the heat is transferred through the matter by conduction (Equation 3-7).

COMSOL has two options for discretization, the linear and quadratic Lagrange method. The discretization of the model for the solids section has been solved by the quadratic Lagrange method, this method is connecting the triangulated nodes in a much more accurate way compared to linear. If, for example, a curved object had to be discretized the quadratic method would select most of the curves, while the linear method would select the boundaries linearly (COMSOL, 1986).

Equation 3-7

$$\overbrace{\underbrace{\rho c_p \frac{\partial T_{1,3}}{\partial t}}_{Internal\ energy}}^{Storage\ term} + \overbrace{\underbrace{\nabla \cdot \mathbf{q}}_{\mathbf{q}=-\lambda \nabla T_{1,3}}}^{Conduction\ term} = \overbrace{\mathbf{Q}}^{source}$$

The inner-tubing

Equation 3-8

$$T = T_1$$

For the inner-tubing Equation 3-7 is used with the temperature function stated in Equation 3-8). The density, heat capacity and thermal conduction value is adjusted per insulation material.

Equation 3-9

$$T(x, y, o) = T_o$$
$$T_1 = T_o$$

The initial temperature values throughout the inner-tubing at t=0 (Equation 3-9).

Equation 3-10

$$-\mathbf{n} \cdot \mathbf{q} = 0$$

At the top section of the inner-tubing there is contact with the surface. At this contact there is no heat exchanged which creates a thermal insulation section (Equation 3-10).

Equation 3-11

$$T_1 = T_2$$

The inner and outer side of the tubing are in contact with the fluid. The boundary condition for this contact area is dependent on the fluid temperature (T2) (Equation 3-11).

The cement and geological layering

Equation 3-12

$$T = T_3$$

For the cement and geological layering Equation 3-7 is used, the temperature is also applied, with the definition of temperature changed (Equation 3-12).

Equation 3-13

$$T(x, y, o) = T_o$$
$$T_3 = T_o$$

The initial temperature values throughout the cement and geological layering at t=0 (Equation 3-13).

Equation 3-14

$$-\mathbf{n} \cdot \mathbf{q} = 0$$

The boundary condition between the surface and the cement, geological layering is expressed as in Equation 3-14. At these boundaries there is thermal insulation.

Equation 3-15

$$T_3 = T_o$$

The boundary on the right side of the geological layering as seen from the axial symmetry in Figure 3-3, has the same temperature distribution as the geothermal gradient (Equation 3-15).

For the steel casing the heat transfer Equation 3-16 is used, adjusted for the thickness of the production well.

Equation 3-16

$$\mathbf{q} = \mathrm{d}_s \mathrm{Q}_s - \mathrm{d}_s \rho c_p \frac{\partial T_3}{\partial t} - d_s \mathbf{q_s}$$
$$\mathbf{q_s} = -\lambda \nabla_t T_3$$

The conductive heat flux is shown by $\mathbf{q}$ $\left[\frac{\mathrm{W}}{\mathrm{m}^2}\right]$, the thickness of steel as d_s $[m]$, thin layer of heat source indicated with Q_s $\left[\frac{W}{m^3}\right]$, the density as ρ $\left[\frac{kg}{m^3}\right]$, specific heat capacity at constant pressure as c_p $\left[\frac{J}{kg*K}\right]$ and the thermal conductivity indicated with λ $[\frac{W}{m*K}]$.

3.4. Thermal power, energy and efficiencies

The power that the DCBHE system generates is based on the amount of heat that is stored in the working fluid. The power the system loses comes from the low pump efficiencies and the energy the different pumps in this system use. Subtracting the used from the generated energy for a designed system, results in the net remaining energy. The designed system has a heat pump and a DCBHE pump. The heat pump is a pump in a home that regulates the temperature and flowrate of the working fluid. The heat pump is set to provide heating for a floor heating system at $35°C$ (al, 2019), in this thesis. The DCBHE pump is a pump that circulates the working fluid in the well. The energy used by the DCBHE pump is estimated by first calculating the working fluid's Reynold's number (Equation 3-17), which describes the behavior of a fluid through the well. This behavior can be laminar or turbulent (Menon, 2015). The pressure required to compensate the losses of pressure during the pumping is stated in Equation 3-19 and Equation 3-17, which is occurring due to the friction with the well (Equation 3-18) (al, 2019). Using the pressure and properties of the fluid, the power used by the working fluid pump can be calculated with Equation 3-20, where the efficiency of the pump is assumed to be 70 % (Holmberg H, 2016).

Equation 3-17

$$Re_{inflow,outflow} = \frac{D v_z \rho}{\mu}$$

The Reynolds number is dimensionless and calculated for the inflow and outflow. In this equation, diameter of the well is D [m], the vertical velocity is v_z [m/s], density indicated by ρ $\left[\frac{kg}{m^3}\right]$ and the fluid viscosity by μ $[Pa * s]$.

Equation 3-18

$$f_{inflow,outflow} = \frac{1}{\left(0.79 \ln\left(Re_{inflow,outflow}\right) - 1.64\right)^2}$$

Equation 3-19

$$\Delta P = \frac{\rho_f f_{inflow} L v_{inflow}^2}{4(r_{w1} - (r_i + t_{insulation}))} + \frac{\rho_f f_{outflow} L v_{outflow}^2}{4 r_i}$$

where ΔP is the pressure $[Pa]$, density indicated by ρ_f during the inflow and outflow $\left[\frac{kg}{m^3}\right]$, the friction factor of the inflow and outflow as $f_{inflow}, f_{outflow}$ which has a dimensionless value, the length of the well is indicated by L [m], the inflow and outflow velocity is $v_{inflow}, v_{outflow}$ and the inner pipe radius is r_i [m] with the annular space of the co-axial BHE the difference between the radius of the inner-tubing, thickness inner-tubing as $t_{insulation}$ [m] and the radius of the well as r_{w1} [m].

Equation 3-20

$$W_p = \frac{m\Delta P}{\rho_f \eta}$$

The power of the pump is described with W_p [W], mass of the flowrate as m $\left[\frac{kg}{s}\right]$, the density as ρ_f of the working fluid $\left[\frac{kg}{m^3}\right]$, ΔP is the pressure $[Pa]$ and the efficiency of the pump as η which is a dimensionless number (Equation 3-20). This is used to pump the working fluid through the DCBHE.

Equation 3-21

$$\mathbf{P} = \rho_f c_f Q (T_{production} - T_{injection})$$

The power is indicated with **P** $[W]$, the heat capacity of the fluid as c_f $\left[\frac{J}{kg*K}\right]$, fluid density as ρ_f $\left[\frac{kg}{m^3}\right]$, the flowrate indicated as Q $[\frac{m^3}{s}]$, the production temperature as $T_{production}$ [℃] and injection temperature as $T_{injection}$ [℃]. This indicates the amount of power generated for the different working fluids.

Equation 3-22

$$COP_{heat\ pump} = -0.000158 * T_{production}^2 + 0.08 * T_{production} + 3.007$$

The coefficient of performance of the heat pump indicated as $COP_{heat\ pump}$ is dimensionless and the production temperature, $T_{production}$ [℃] (al, 2019). The COP of the heat pump is an indicator of how efficient a heat pump can perform.

Equation 3-23

$$Q = m\Delta H = mc_f\left(T_{production} - T_{injection}\right)$$

The heat generated is indicated as Q $[\frac{W}{m^3}]$, mass indicated with m $\left[\frac{kg}{s}\right]$, enthalpy as H $\left[\frac{J}{kg}\right]$, the heat capacity of the fluid is c_f $\left[\frac{J}{kg*K}\right]$ and the injection and production temperature as T [℃]. The Q is used to calculate the coefficient of the system performance CSP of the system.

Equation 3-24

$$Q_{heat\ pump} = Q\left(\frac{COP_{heat\ pump}}{COP_{heat\ pump} - 1}\right)$$

The heat of the pump indicated with $Q_{heat\ pump}$ and previously calculated coefficient of performance of the heat pump as $COP_{heat\ pump}$ (Equation 3-22).

Equation 3-25

$$W_{heat\ pump} = Q\left(\frac{1}{COP_{heat\ pump} - 1}\right)$$

The power of the heat pump indicated with $W_{heat\ pump}$ [W] and previously calculated coefficient of performance of the heat pump as $COP_{heat\ pump}$ (Equation 3-22). The heat and power of the heat pump are used in Equation 3-26 as a fraction to generate the COP.

Equation 3-26

$$COP = \frac{Q_{heat\ pump}}{W_{heat\ pump}}$$

The total coefficient of performance of the heat pump as COP which is dimensionless, power used by the heat pump indicated with $W_{heat\ pump}$ [W] and the heat of the pump as $Q_{heat\ pump}$ $[\frac{W}{m^3}]$.

Equation 3-27

$$CSP = \frac{Q_{heat\ pump}}{W_{heat\ pump} + W_{pump}}$$

The coefficient of the system performance CSP is dimensionless. CSP is a performance indicator for the system in which the heat used by the heat pump is in mathematical fraction to the total power used by the heat and working fluid pump.

Equation 3-28

$$Net\ power = P - W_{heat\ pump} - W_{pump}$$

The net power [W] of the system is created by subtracting the generated power from the power used by the heat and DCBHE pump.

4. Analysis and interpretation of the model

In order to understand the potential energy of a mono-well co-axial heat exchanger, it is important to understand the involved physics and design elements. For simulation, Grouw-01 is taken as the case study. The exact geometry of Grouw_01 well has been re-created in COMSOL based on the materials, geology and well design. The geology in the model is based on the actual geology surrounding Grouw_01, so this can vary if the model is applied for a different location. The model geology is a simplification of the real geology, as only the largest 3 layers have been selected, as explained in chap. 3.2. Each layer is assumed to have homogeneous properties in this model. The properties for cement, steel and inner-tubing are partly temperature dependent and partly constant (Table 4-1).

In order to use a model for simulation, first all the data to design the model need to be collected and interpreted. The properties of the geological units, steel casing and cemented sections with the well size are taken from Table 3-1. For all the different sensitivity analyses these properties remain the same. The initial temperatures of the geological units, steel casing and cemented sections are consistent with the geothermal gradient, which is related to the depth (Table 2-1). Temperature can be gained but also lost to the surroundings, for example, if the surrounding rocks have a lower temperature than the injected fluid (N.M. Wight, 2015).

After the data for the model is complete with the previously discussed initial conditions and geological setting a sensitivity analysis is conducted on the model. The sensitivity analysis is conducted to find the optimal design and performance conditions for the DCBHE. In the sensitivity analysis all parameters that can have an effect on the heat exchange are simulated, including flowrate, working fluid, inner-tubing material and thickness, outer-tubing thickness, well depth, injection temperature and reverse injection flow. This chapter also provides information of what can be expected in terms of depth-temperature relationship, production temperature, generated power, COP, CSP and net power.

4.1. Base case geology and well design

For the simulation a base case is created. The base case is a case to which one can compare the different simulations; it thus serves as a reference. For the base case we use a mass flowrate of 1 $\left[\frac{kg}{s}\right]$, which is approximately 86.4 $\left[\frac{m^3}{day}\right]$. Water is chosen as the working fluid, because of the many easy to work with benefits. Some of the benefits are the immediate availability in large quantities and having no environmental impact in case there is a leakage in the system.
However, water can cause corrosion if in contact with steel (M.M.Stack, 2012). Even though corrosion is a problem when working with steel casings, it is not within the scope of this thesis and will not be further investigated here. The water is injected at a temperature of $12°C$, this injection temperature is based on the average surface temperature around the Grouw-01 well ($15°C$) and the average surface temperature in the Netherlands ($10°C$) throughout a year (A. Lokhorst, 2007).

For the inner-tubing in the base case vacuum insulated tubing (VIT) is selected. VIT has a very low thermal conductivity value, which makes it an excellent insulating material. The VIT consists of two layered materials, between these layers there is empty space (which is vacuum). The properties of the VIT can vary per company and for this thesis an average estimation of the different industry values has been selected (Table 4-1).

Table 4-1 Properties of working fluid (water) and insulation material used in the base case.

Parameters	Symbol	Dimension	Equation used	At $T = 293$ K
Water (Wang P. , 2014)			(COMSOL, 1986)	
Density between $273K - 283K$	ρ_w	kg/m^3	$972.8 + 0.21 * T^1 - 4.0E - 4 * T\text{^}2$	
Density between $283K - 373K$			$345.28 + 5.75 * T^1 - 0.0157 * T^2 + 1.26E - 5 * T\text{^}3$	998
Thermal conductivity	λ_w	$W/(m * K)$	$-0.9 + 0.0084 * T\text{^}1 - 1.12E - 5 * T\text{^}2$	0.597
Heat capacity	c_w	$J/(kg * K)$	$4035.841 + 0.492312 * T\text{^}1$	4180
Dynamic viscosity $273K - 293K$	μ_w	$Pa * s$	$5.95 - 0.08 * T^1 + 4.29E - 4 * T^2 - 9.9E - 7 * T^3 + 8.65E - 10 * T\text{^}4$	0.000996
Dynamic viscosity $293K - 353K$			$0.41 - 0.005 * T^1 + 2.08E - 5 * T^2 - 4.06E - 8 * T^3 + 2.98E - 11 * T\text{^}4$	
Vacuum insulated tubing (COMSOL, 1986) (Tomasz Śliwaa, 2018)				
Density	ρ_{VIT}	kg/m^3	Constant	5500
Thermal conductivity	λ_{VIT}	$W/(m * K)$	Constant	0.08
Heat capacity	c_{VIT}	$J/(kg * K)$	Constant	500
Thickness	t_{VIT}	m	Constant	0.02
VIT radius	r_i	m	Constant	0.03
Mass flow rate	m_i	kg/s	Constant	1

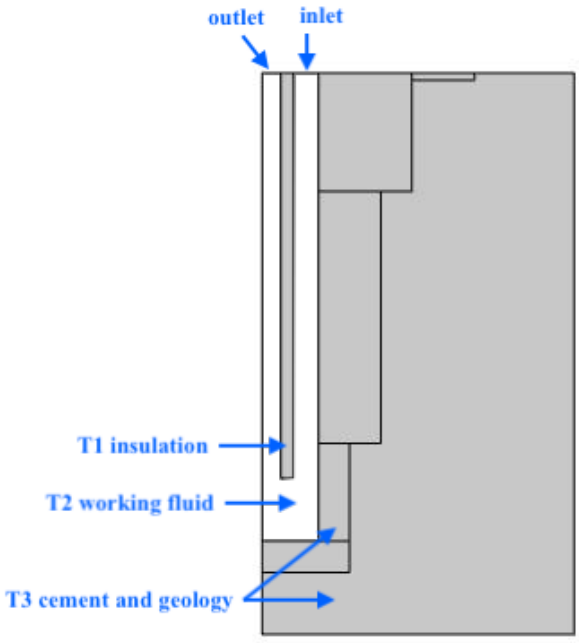

Figure 4-1 The inlet and outlet indications of the Grouw_01 model.

The base case heat exchange analysis

In the model, at t=0 water with $12°C$ is injected from the outlet (Figure 4-1). The fluid moves down towards the bottom of the well from where it moves up through the inner-tube towards the surface. As shown in Figure 4-2, as the water moves down, it gains heat from the surrounding rock layers. It will get the maximum temperature when it reaches the bottom of well. During the upward move, however, it loses heat to the inner-tubing material. This is where a good insulation becomes important. The simulations show that after one year, the BHT will cool down from $78°C$ to $45°C$, during this period most of the cooling occurs. After the first year to the 20^{th} year the BHT will cool from $45°C$ to $42°C$, the temperature drop has slowed down significantly. Between the 20^{th} and the 50^{th} year after injection the cooling is less than a degree, the BHT is stabilizing at $42°C$. The downward flow has an almost linear temperature gain during the first $1100 - 1200\,m$ depth, after this depth the slope becomes steeper (Figure 4-2). This change in slope coincides with the change in geological layering (Figure 3-3). At that depth there is a transition zone from the siltstone to the limestone. Compared to siltstone the thermal conductivity of limestone is significantly higher (Table 3-1), which can explain this difference in slope (Figure 4-2). A minor slope change could also be expected at around $300\,m$ deep, due to the change from sandstone to siltstone. During the upward flow of water there is only heat exchange with the insulation layer of the inner tube, which causes the slightly curved slope in Figure 4-2. In the first 24 hours there is cooling occurring within the working fluid during the transport from a BHT of $63°C$ to the production temperature at the outlet of $53°C$. After 1 year this cooling difference is also $10°C$ from BHT of $48°C$ to the production temperature of $38°C$. After 5 to 10 years the upward flow does not change much anymore and is similar in production temperature ($35.5°C$).

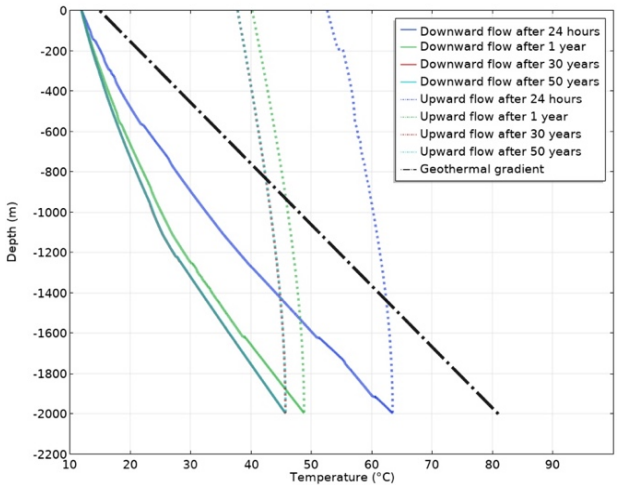

Figure 4-2 Depth and temperature relationship for the down and upward fluid flow at flowrate of 1 kg/s.

The production temperature and system performance

The production temperature increases in the first 4 hours after injection. The peak moment of this production temperature increase occurs between the 4th and 5th hour for the base case, after this peak the temperature gradually declines till the 10th year. The reason for the peak is that in the first hours the heat at short radial distance from the well can be extracted. With time the radial distance from which heat can be extracted expands. After 10 years the temperature is stable and continues at $35.5°C$ till the 50th year (Figure 4-3). The generated power has a similar pattern, since the production temperature and power are directly related (Equation 3-21). The generated power of the base case is around 108 kW after 3-5 years (Figure 4-4). For industrial purposes a unit change is applied to $[MW\ h]_{year}$ in Figure 4-4. For the unit change, the power (Figure 4-8) is multiplied with the number of hours in a year, the unit is for a year of power generation. The COP and CSP are at an average of 4.8 and 5.8 (Figure 4-5). Having a low COP, CSP would imply that the system is not efficient. After considering the energy used by the two pumps, a net power of 85 kW remains (Figure 4-6).

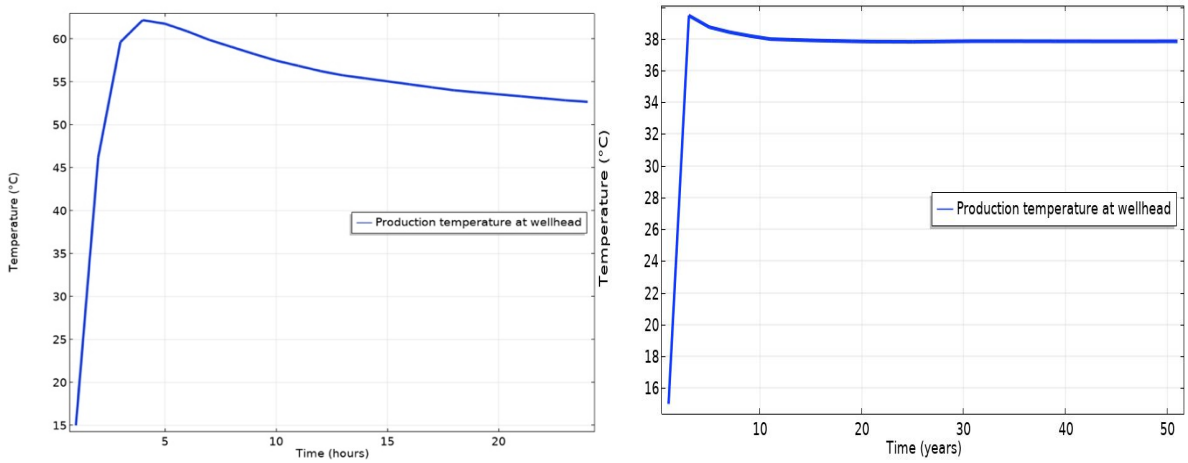

Figure 4-3 Production temperature at the well head during the first 24 hours (left) and for the first 50 years (right) after injection at a flowrate of 1 kg/s.

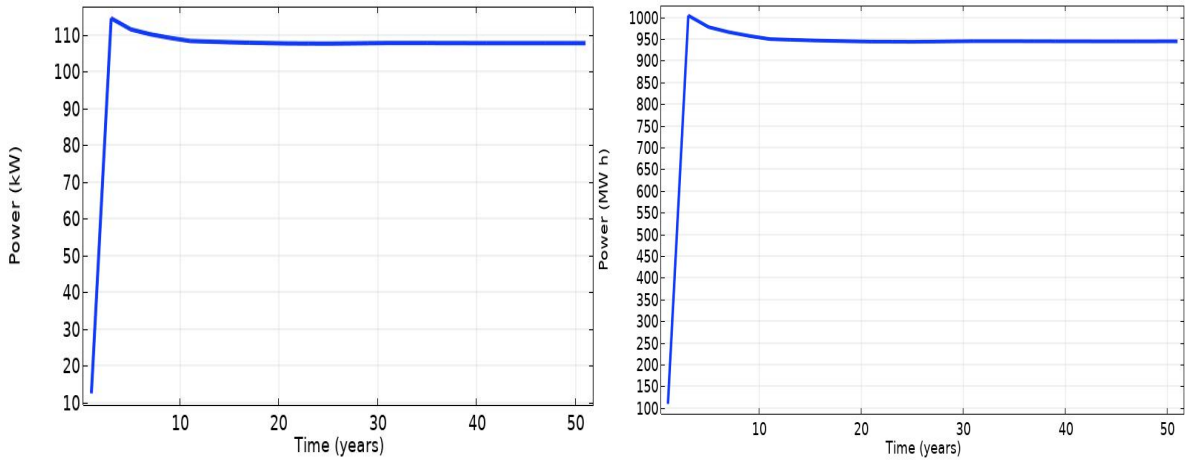

Figure 4-4 The produced power in [kW](left) and $[MW\ h]_{year}$*(right) at a flowrate of 1 kg/s.*

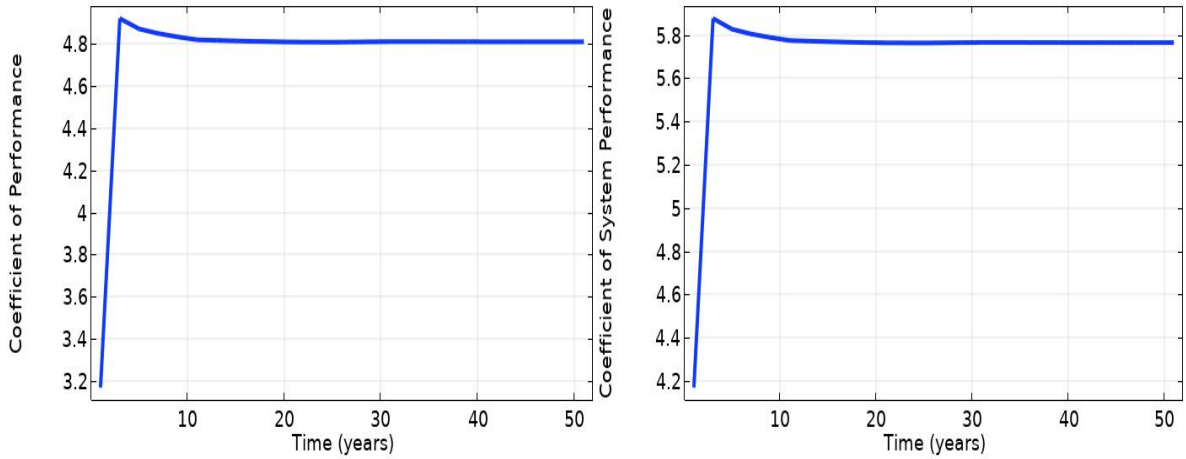

Figure 4-5 The COP (left) and the CSP of the system (right).

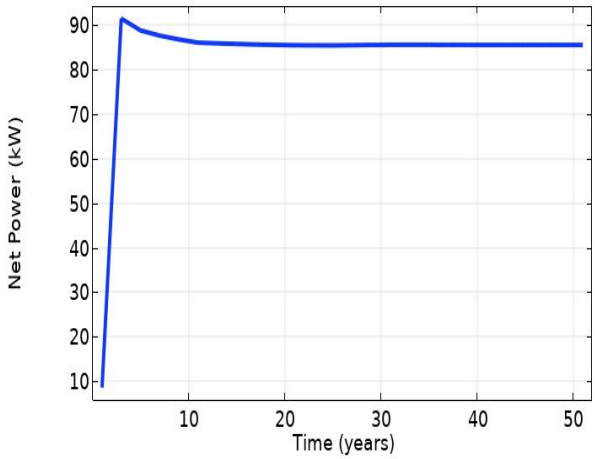

Figure 4-6 The net power of the system.

4.2. Parameter sensitivity analysis

In this paragraph the different parameter changes and their effect on temperature, power and efficiency are discussed. The changes are aimed at increasing the power and efficiency of the DCBHE. For the discussion sensitivity analyses are also conducted to find the optimal design conditions for the DCBHE. In the sensitivity analysis all the parameters that can have an effect on the production temperature, power generation and system efficiency are simulated, including flowrate, working fluid, inner-tubing material and thickness, outer-tubing thickness, well depths, injection temperature and the possibility of reversing the injection flow.

When changing the first parameter, which is the flowrate, an increase in flowrate leaves less time for the working fluid and surrounding rock to exchange heat. This should result in lower production temperature. However, since power generation not only depends on temperature but is also related to flowrate (Equation 3-21), and increase in power generation can be expected. The result of this parameter change is important to find the ideal flowrate for optimized power generation.

The thermal properties of the working fluid are also crucial for heat transfer within the geothermal system. Therefore, water, glycol and diathermal oil, gathered from literature are examined and compared in their simulation results. Water is further examined with assumed theoretical material property changes in thermal conductivity and heat capacity. An expectation for this change in heat capacity is that the working fluid should increase/decrease in temperature because of the internal energy change. For an increased thermal conductivity there should be more heat exchange occurring, resulting in a change in working fluid temperature. The results of this simulation should provide insight into an ideal working fluid.

The working fluid, is transported to the surface through the inner-tubing (insulation). During this transport cooling has to be kept at a minimum. Therefore, several inner-tubing materials - polypropylene, polyethylene and VIT - are analysed. VIT is further examined with material property changes in thermal conductivity and heat capacity in order to find the range in which the heat loss is kept to a minimum. Lowering the thermal conductivity of the material should provide a good insulation material, as with minimum thermal conductivity there is minimum heat exchange.

A property of the inner-tubing that can be changed is the thickness. The thickness of the VIT can cause the fluid to flow at a different flowrate by narrowing or widening the fluid flow area. Changing thickness, changes the volume of the insulation material to exchange heat with its surroundings. Both these factors play a major role, an expectation is that a better insulation material is created if the thickness is increased.

The heat extraction by the fluid can also improve in performance if surface contact area of the working fluid with the outer-tubing is increased. If surface contact area increases, this means more heat can be exchanged between rock and working fluid. The contact area increase, also affects the mass flowrate of 1 kg/s, more area for the fluid flow means that the flow velocity decreases. The heat exchange should increase with an increase in outer-tubing diameter, providing an improved overall performance.

A similar increase in surface contact area is seen between the working fluid and surrounding rock if the well depth increases. In this scenario different well depths are analysed, so a realistic expectation of the overall performance is created. Well depth change should provide a relationship in production temperature, power, COP and CSP with the depth in a linear form. This means one can expect an increase of performance with an increase of well depth and versa corresponding decrease in performance for decreasing well depth.

SO far, the discussed parameter and material changes are in the subsurface. At the surface there are also factors of influence which need to be taken into consideration, for example seasonal temperature fluctuations. These can affect the heat required or delivered to the closed loop system. To simulate these differences a case is created with different injection temperatures. In case the injection temperature is higher than the surrounding rock, then cooling will occur before stabilising and heating.

As in the summer the injection temperature can get hot, a case is created in which the well-is functioning as a cooling source. For this case the inlet and outlet are switched (Figure 4-1). In this way the working fluid is injected trough the inner-tubing and produced through the outer-tubing. The working fluid which has a high injection temperature during the summer months gets to cool down during transport to the surface.

4.2.1. Flowrate

For the sensitivity analysis with different flowrates, the flowrates used are 0.25 kg/s, 0.50 kg/s, 1.50 kg/s and 2 kg/s. The results for these flowrates are compared to the base case, which has a flowrate of 1 kg/s.

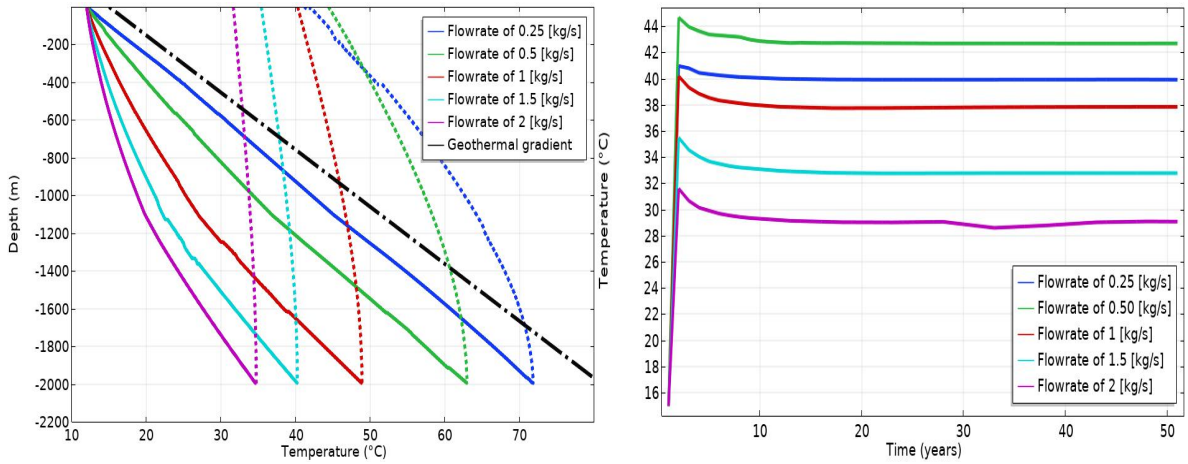

Figure 4-7 Depth and temperature relationship for the down and upward fluid flow (left) and the production temperature (right) at varying flowrates.

The heat exchange analysis

The working fluid requires time to exchange heat with the surrounding rock and gain temperature. Therefore, if the flowrate is high this results in lower BHT. If the flowrate is low a higher BHT is achieved (Figure 4-7). During the upward flow there is less heat exchanged with the VIT if the flowrate is high, such that the fluid temperature does not decline as much. The higher flowrate is causing the upward flow slope to be almost linear. For slower flowrates such as 0.25 kg/s and 0.50 kg/s working fluids tend to lose more heat during the upward flow.

The production temperature

In the first 5 to 10 years the production temperature declines until a stable production temperature is reached for all the flowrates. Generally, the production temperature decreases with increasing flowrate (Figure 4-7 right). However, the same trend does not exist for the flowrates less then 1 kg/s. The case with flowrate of 0.50 kg/s shows higher produced heat compared to 0.25 kg/s, where the production temperatures are $42.5°C$ and $40°C$, respectively. A possible explanation for this lower temperature lies in the heat exchange between the fluid and VIT during upward fluid flow. There is an optimum flowrate for which the heat exchange between the VIT and fluid is in balance with the downward flow, where at certain flowrate the maximum heat exchange can occur for a high BHT. At this optimum flowrate the production temperature is highest.

The power generation and system performance

Figure 4-8 left and right show the produced power in different units. As can be seen the generated power increases with increasing flowrate. The largest increase in the power generation is achieved for the increase in flowrate from 0.25 kg/s to 1 kg/s, where the power generated increases from 30 kW to 108 kW. During the first 10 years the flowrates of 1 kg/s, 1.50 kg/s and 2 kg/s tend to lose more energy compared to the flowrates of 0.25 kg/s and 0.25 kg/s. The highest loss of generated power (within 50 years of production) is with flowrate of 2 kg/s, where in the first year a power of 164 kW is generated and after 10 years this declines to 142 kW, at which point the generated power stabilizes. The higher flowrates transport a larger volume of working fluid per unit time, resulting in higher power generation.

The COP and CSP are at their highest for a flowrate of 0.50 kg/s and lowest for a flowrate of 2 kg/s (Figure 4-9). The system performs at its best when a high COP, CSP is achieved. After considering the energy used by the two pumps, the net power that remains is the highest for the flowrate of 2 kg/s (Figure 4-10). This was expected, since this flowrate generates the highest amount of power.

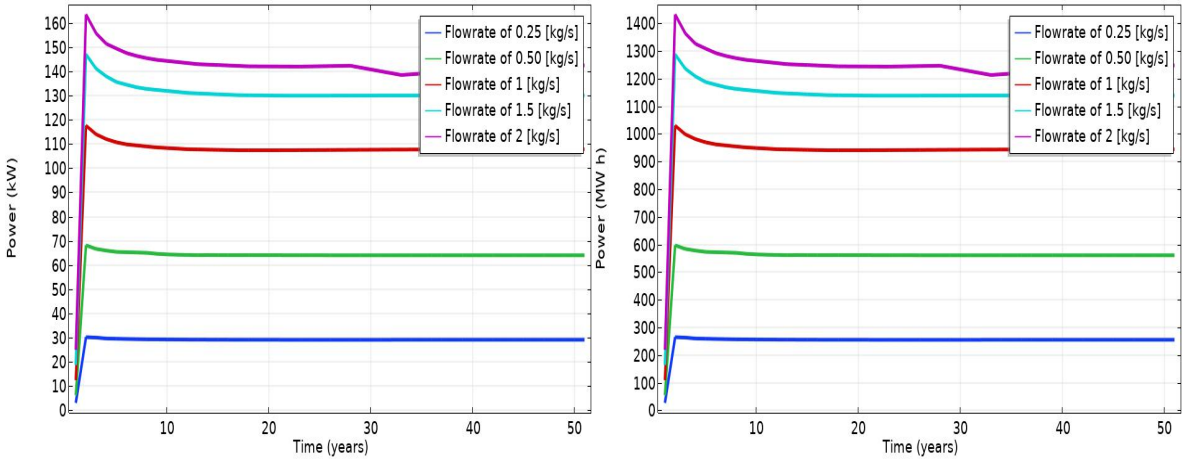

Figure 4-8 The produced power in [kW](left) and $[MW\ h]_{year}$ *(right) for different flowrates.*

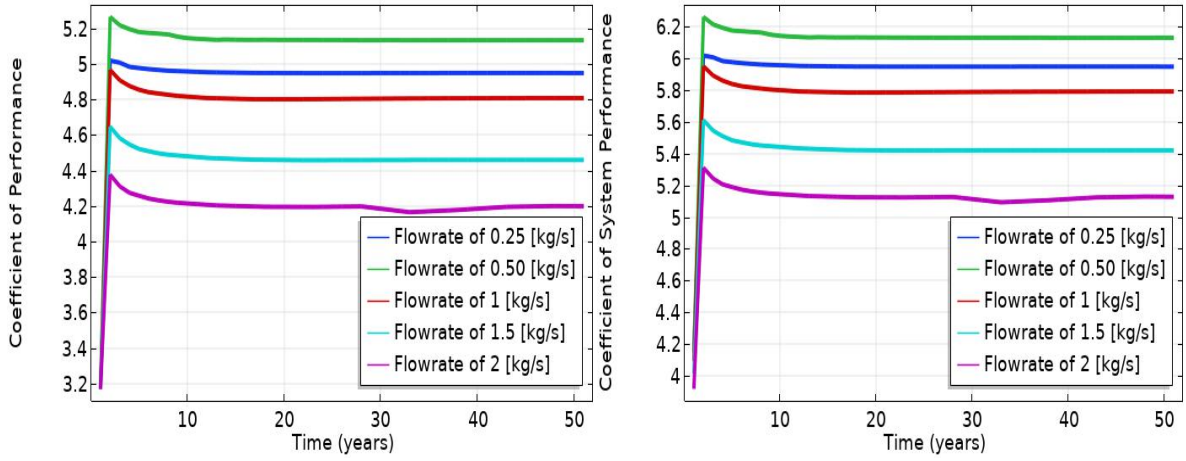

Figure 4-9 The COP (left) and the CSP of the system (right).

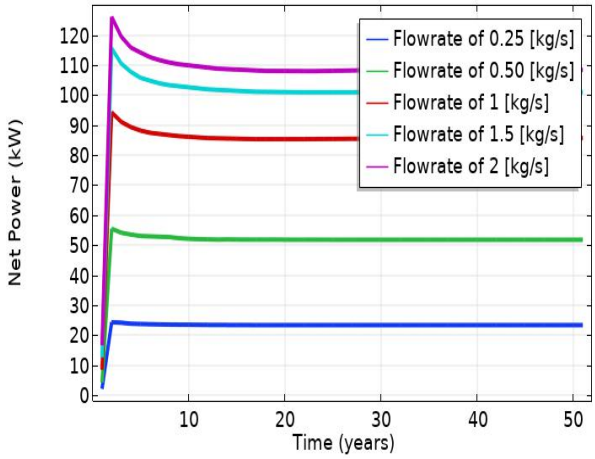

Figure 4-10 The net power of the system.

4.2.2. Working fluid

Several working fluids are analysed in this sensitivity analysis for their heat transporting properties. The examined working fluids are water, ethylene glycol and diathermic oil. An in-depth analysis is performed on water as working fluid, to find the degree in which properties of water influence production temperature. The properties changed are the heat capacity and the thermal conductivity, as these have influence on the heat exchange rate. Fluid A and B have higher and lower heat capacity, respectively, while all other properties are similar as of water. Fluid C has a higher thermal conductivity than water while all other properties are the same as of water. Table 4-2 lists the properties of the different working fluids except for water which is listed in Table 4-1 for the base case.

Table 4-2 Working fluid properties

Working fluid A	Symbol	Dimension	Equation	At $T = 293\ K$
Heat capacity	c_g	$J/(kg * K)$	constant	6000
Working fluid B				
Heat capacity	c_g	$J/(kg * K)$	constant	2000
Working fluid C				
Thermal conductivity	λ_g	$W/(m * K)$	constant	100
Diathermic oil (C. Alimonti, 2016)				
Density	ρ_g	kg/m^3	constant	762
Thermal conductivity	λ_g	$W/(m * K)$	constant	0.13
Heat capacity	c_g	$J/(kg * K)$	constant	2500
Dynamic viscosity	μ_g	$Pa * s$	constant	3.3
Ethylene glycol (Chan Soo Kim, 2003)				
Density	ρ_g	kg/m^3	$1322.68716 - 0.703271429 * T\hat{}1$	1117
Thermal conductivity	λ_g	$W/(m * K)$	$-0.0376511698 + 0.00162092411 * T\hat{}1 - 2.1875E-6 * T\hat{}2$	0.2495
Heat capacity	c_g	$J/(kg * K)$	$1071.4679 + 4.47428571 * T\hat{}1$	2382
Dynamic viscosity $273K - 313K$	μ_g	$Pa * s$	$58.7675977 - 0.715125609 * T\hat{}1 + 0.00326583487 * T\hat{}2 - 6.63118394E-6 * T\hat{}3 + 5.04966953E-9 * T\hat{}4$	0.0216
Dynamic viscosity $313K - 353K$			$1.59302422 - 0.0129863357 * T\hat{}1 + 3.54798736E-5 * T\hat{}2 - 3.24354812E-8 * T\hat{}3$	

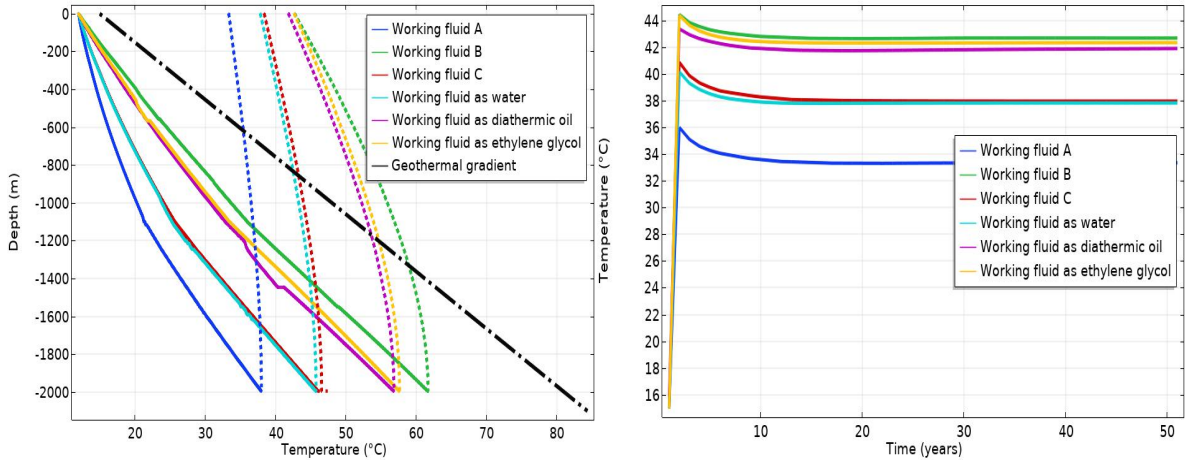

Figure 4-11 Depth and temperature relationship for the down and upward fluid flow (left) and the production temperature (right) for different working fluids.

The heat exchange analysis and production temperature

Figure 4-11 shows the heating, cooling and the production temperature of the different working fluids. Fluid B and glycol, which have the lowest heat capacity of all the working fluids, reach the highest BHT. If the heat capacity is high, the temperature of the working fluid increases at a slower rate. This is visible in the temperature behavior of working fluid A in Figure 4-11 (right). Ethylene glycol, which has slightly lower heat capacity and double the thermal conductivity than diathermic oil, results in higher BHT. During the upward fluid flow the working fluid B cools down fast, while working fluid A cools down extremely slowly (Figure 4-11 left). The change in heat capacity is creating this effect. The working fluids with relatively high heat capacity are better in sync with the temperature of the geological surroundings. This is seen in a slight increase of slope steepness at a depth of 1200 m for working fluids A, C and water (Figure 4-11-left).

Change in thermal conductivity however has less effect on the production temperature, increasing the thermal conductivity slightly increased the BHT. This is seen in the difference between the BHT of working fluid C and water.

The power generation and system performance

In Figure 4-12 (left) water and working fluid C are shown as almost one in the graph. These working fluids show similar power generation, this means that thermal conductivity does not have a significant effect on power generation. Contrary to this is the heat capacity, which is causing large differences in power generation. A working fluid with high heat capacity, for example working fluid A, generates the maximum amount of power. The working fluids ethylene glycol, working fluid B and diathermic oil have low heat capacity, these generate minimum power with a high production temperature. There is a big difference in power generated by glycol and diathermic oil while these have quit similar heat capacity and injection/production temperature. The difference can only be caused duo to the density differences between these fluids (Figure 4-12-left).

Looking at Figure 4-13 left and right, there are big differences in COP and CSP for diathermic oil. The DCBHE pump has difficulty transporting the diathermic oil into the well resulting in the lowest CSP value, this is caused by the higher viscosity of the working fluid (Table 4-2). Higher viscosity increases the friction factor and to overcome this, the pump needs more power which in return makes the system less efficient. The COP of working fluid A is the minimum, while working fluid B, C and diathermic oil are performing above average (Figure 4-13 left).

This means that working fluid A is the least efficient for a heating system because of the low production temperature. When comparing the net result to the power generation of Figure 4-12 (left), water and fluid C have lost 10 kW to overcome the power required for the heat- and DCBHE pump (Figure 4-14). A fluid like diathermic oil would not be recommended, since the working fluid uses more power in the pumps due to its density and viscosity properties than it generates from the DCBHE.

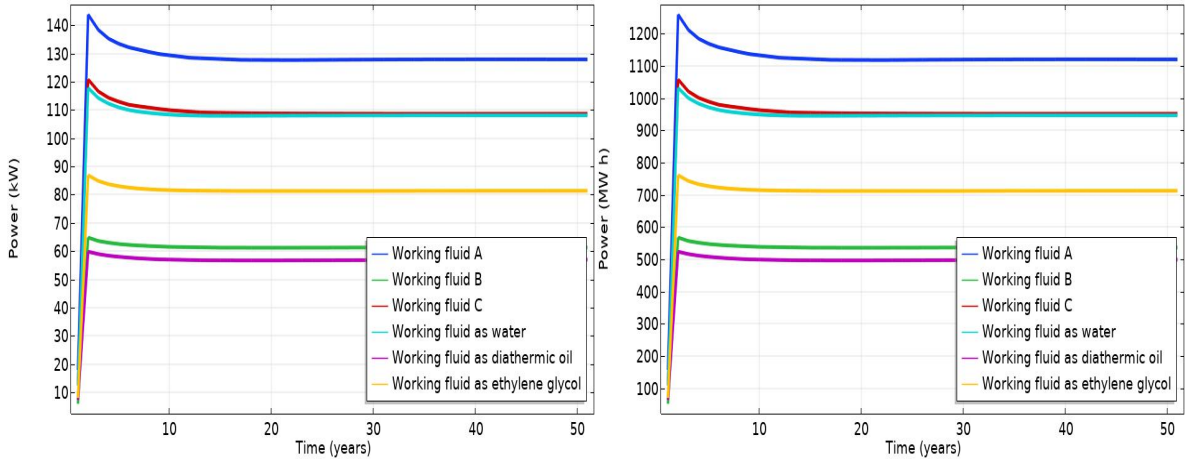

Figure 4-12 The produced power in [kW] and $[MW\ h]_{year}$ for the different working fluids.

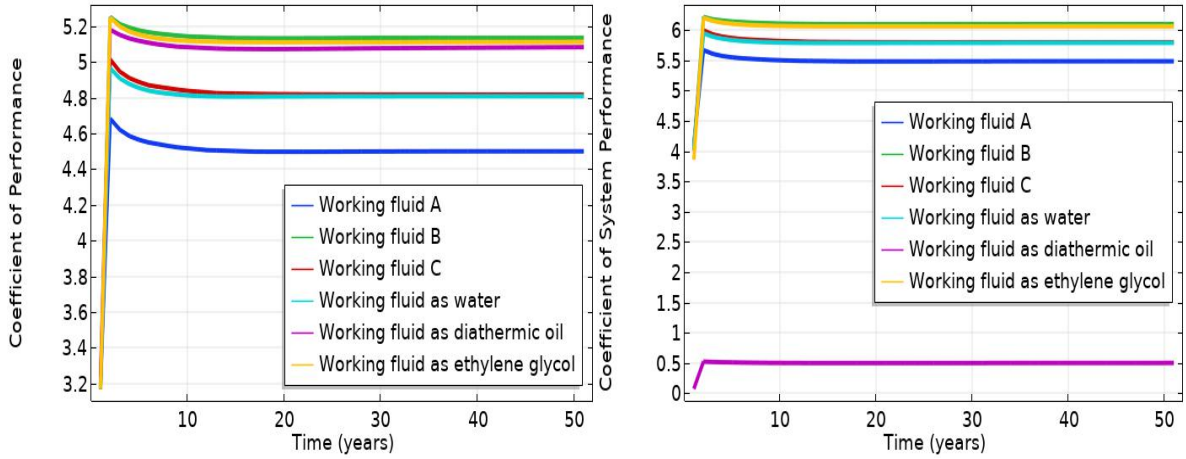

Figure 4-13 The COP (left) and the CSP of the system (right).

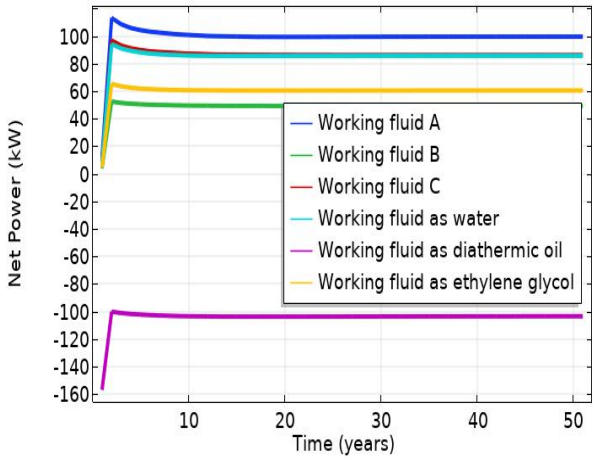

Figure 4-14 The net power of the system.

4.2.3. Inner-tubing material (insulation material)

The working fluid as previously discussed extracts heat from the subsurface, this heat should then be transported to the surface. During this transport to the surface, it is important that there is minimum cooling occurring. Materials that prevent cooling are insulation materials. In this chapter several insulation materials and the properties which are important for insulation are analysed. The studied insulation materials in this thesis are polypropylene, polyethylene, and VIT (base case). The properties of VIT are also adjusted, in order to find the degree to which property changes of VIT influence production temperature. The adjusted properties are the thermal conductivity and VIT with high and low heat capacity. Table 4-3 describes the properties of the different inner-tubing materials. The properties of normal VIT are presented in Table 4-1.

Table 4-3 Different inner-tubing materials

Polypropylene (COMSOL, 1986)	Symbol	Dimension	Value	At $T = 293\ K$
Density	ρ_{VIT}	kg/m^3	Constant	900
Thermal conductivity	λ_{VIT}	$W/(m * K)$	-1.844683+0.01728236*T^1-5.595958E-5*T^2+8.080328E-8*T^3-4.317061E-11*T^4	0.13
Heat capacity	c_{VIT}	$J/(kg * K)$	18307.07-217.3419*T^1+1.012687*T^2-0.002134645*T^3+2.075175E-6*T^4-7.361643E-10*T^5	1574
Polyethylene (Tomasz Śliwaa, 2018)				
Density	ρ	kg/m^3	1037.899-0.2652839*T^1	960
Thermal conductivity	λ_{VIT}	$W/(m * K)$	Constant	0.42
Heat capacity	c_{VIT}	$J/(kg * K)$	constant	2250
VIT high heat capacity				
Heat capacity	c_{VIT}	$J/(kg * K)$	constant	5000
VIT low heat capacity				
Heat capacity	c_{VIT}	$J/(kg * K)$	constant	50
VIT high thermal conductivity				
Thermal conductivity	λ_{VIT}	$W/(m * K)$	Constant	0.8

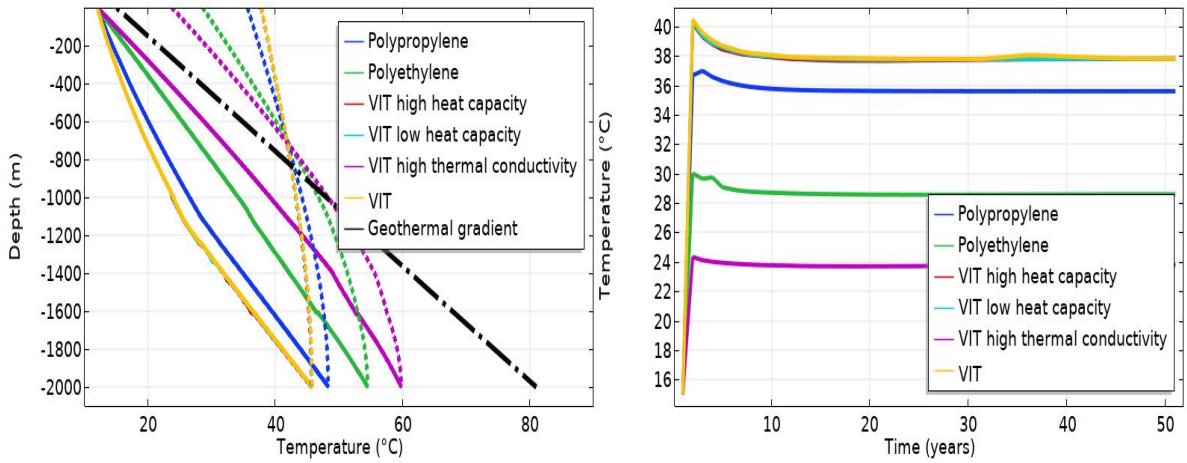

Figure 4-15 Depth and temperature relationship for the down and upward fluid flow (left) and the production temperature (right) with different insulation materials.

The heat exchange analysis

The polyethylene has a higher thermal conductivity and heat capacity value (Tomasz Sliwa, 2015) compared to the VIT (base case). This change in properties (Table 4-3) causes differences in the downward and upward flow. During the downward flow (of the polyethylene) the slope is almost linear, which is different from the base case. This effect on the downward flow is caused by the working fluid being heated from both the inner-tubing and outer-tubing. During the upward flow, the gained heat is lost to the unfavourable insulation material vice versa. The reason for this strong reaction is the thermal conductivity of the material, which is relatively high compared to the other insulation materials. Having a high thermal conductivity means that the material can conduct heat at a high rate. Vacuum insulated tubing on the other hand does not seem to respond if the heat capacity of the material is changed (Figure 4-15). Most of the change in temperature is caused by adjusting the thermal conductivity of VIT.

The production temperature and system performance

There are minor differences visible in the production temperature and power generated for VIT with low and high heat capacity (Figure 4-16). This means that the heat capacity is not an important material property for an insulation material. Under similar conditions a material with high thermal conductivity will perform less efficient as an insulation material. The least efficient insulation material is polyethylene and VIT with high thermal conductivity. This is explained by the high thermal conductivity (Figure 4-16). Similar graphs are shown for the COP, CSP and net power data (Figure 4-17) proving the importance of thermal conductivity for an insulation material.

A minor error is shown as a small peak in several images, for example in Figure 4-15 (right). This peak for polyethylene between the 5th and 7th year is caused by a simulation error. The software of COMSOL has a function in which the tolerance factor can be set. This number came by many trial and errors in which an increase in the tolerance factor would mean less accuracy of the model and a decrease would mean errors in the model. For this simulation a tolerance factor of 0.05 was selected. The error is the result of the extreme side in the tolerance of the simulation.

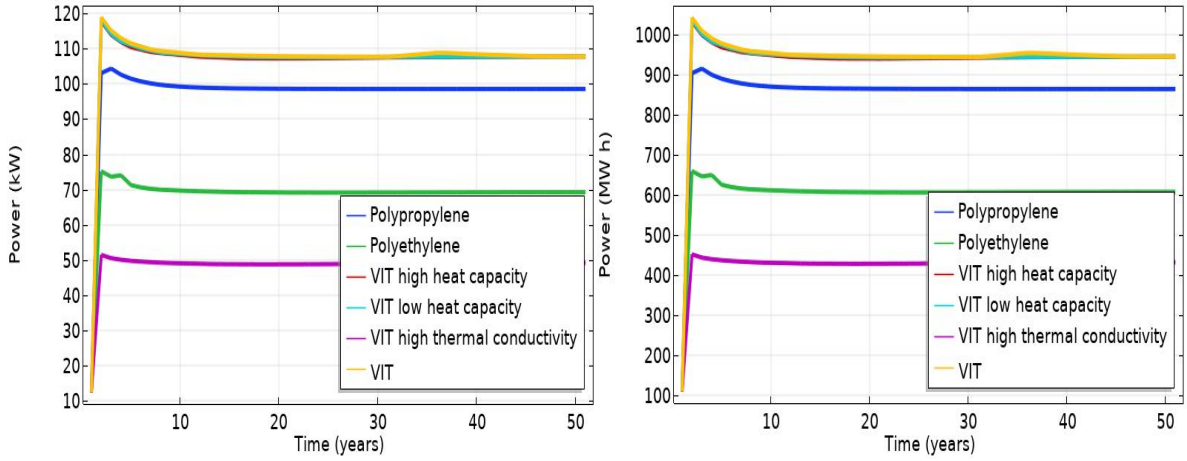

Figure 4-16 The produced power in [kW](left) and $[MW\ h]_{year}$ *(right) for the different injection temperatures.*

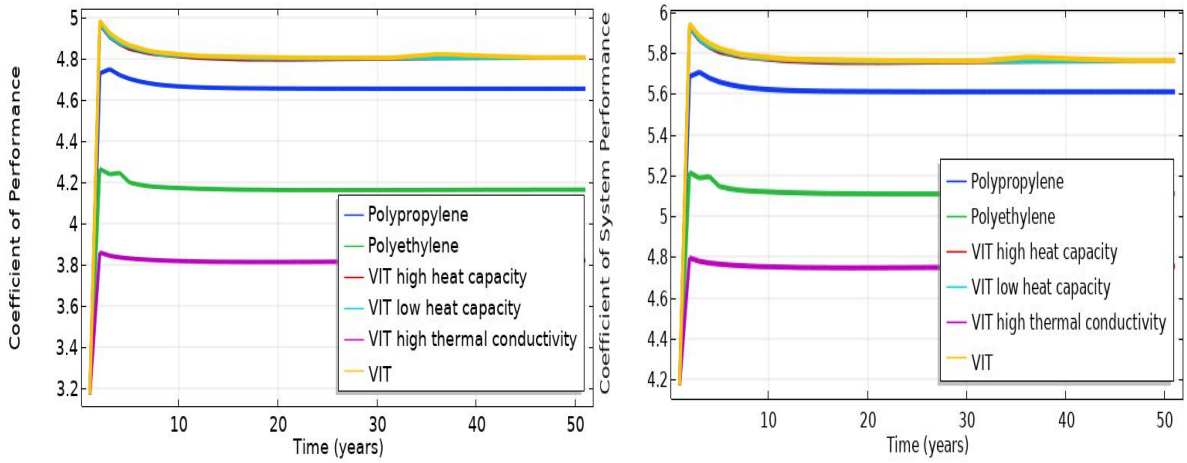

Figure 4-17 The COP (left) and the CSP of the system (right).

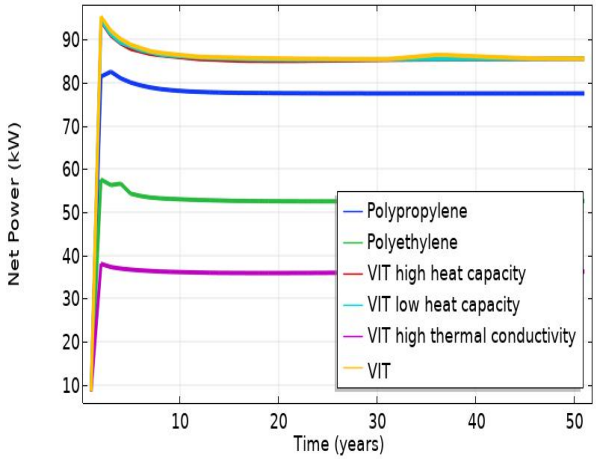

Figure 4-18 The net power of the system.

4.2.4. Inner-tubing thickness

Different production companies deliver VIT with similar properties but different thicknesses, with same material properties. In this simulation a sensitivity analysis is done for the different VIT thicknesses of 0.017 m, 0.022 m and 0.035 m. All other properties are the same for the different cases. Increasing or decreasing the VIT thickness also changes the inlet size (Figure 4-1). Changing the inlet size also affects the speed of the working fluid from the inlet to the outlet, which in turn affects thermal transport.

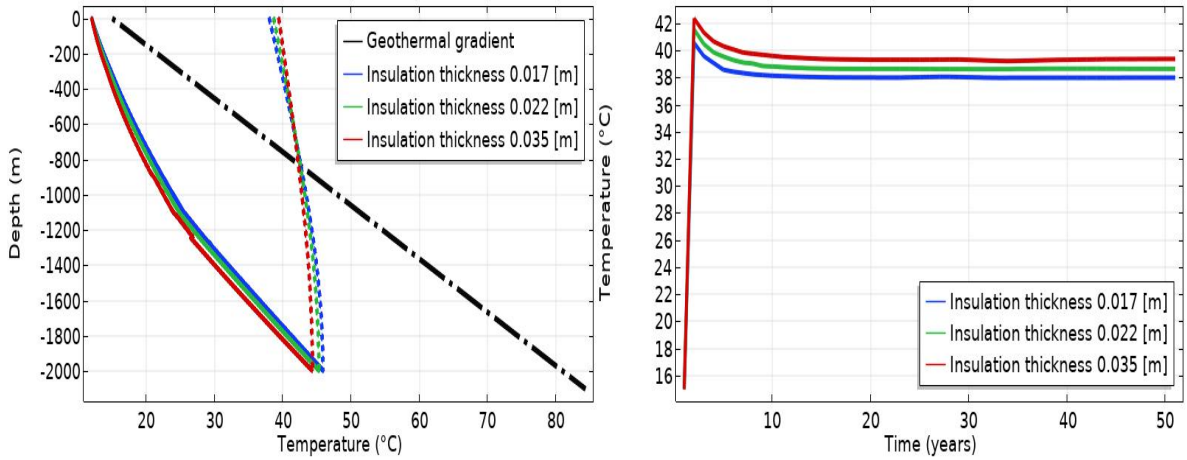

Figure 4-19 Depth and temperature relationship for the down and upward fluid flow (left) and the production temperature (right) for the different insulation thicknesses.

The heat exchange analysis

The temperature slope for the downward and upward flow is similar for different insulation thicknesses. When the VIT thickness of 0.035 m is applied, the working fluid reaches slightly lower BHT however slightly higher production temperatures compared to the base case (Figure 4-19 left). This increased VIT size is causing the fluid to move faster since there is less volume left in the inlet. With the faster fluid movement, there is slightly less time for heat exchange. During the upward flow of water there is only heat exchange occurring with the VIT and therefore the thickness of the VIT can improve or decrease the production temperature. Increasing the insulation thickness results in an increase of power generation. The difference between the minimum thickness of 0.017 m and the maximum of 0.035 m is 6 kW (Figure 4-20 left).

VIT of 0.035 m also has higher COP/CSP values (Figure 4-21) and a higher net power (Figure 4-22). For an ideal system the thickness of the VIT is as high as possible. The thicker the VIT thickness is, the better the system will perform as in Figure 4-21.

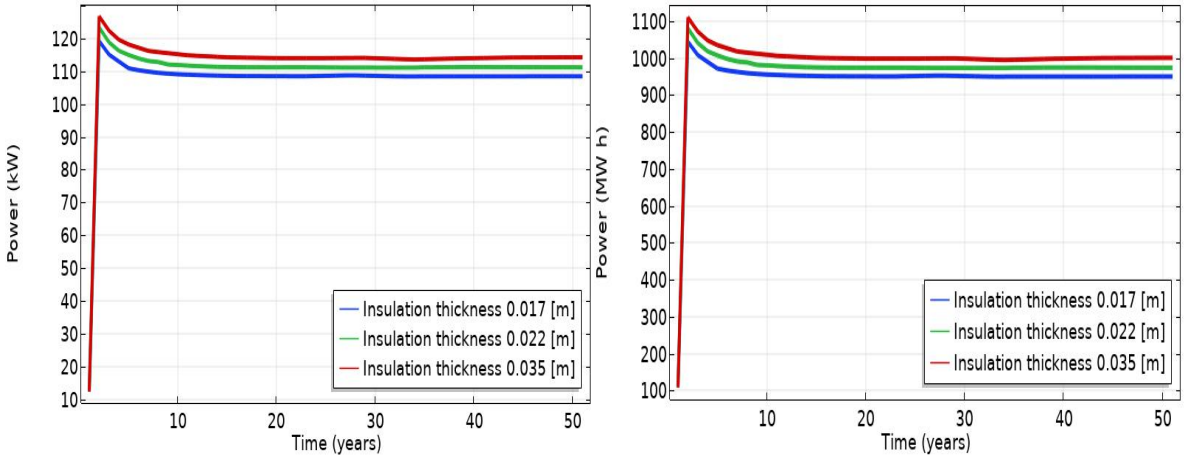

Figure 4-20 The produced power in [kW](left) and $[MW\ h]_{year}$*(right) for the different injection temperatures.*

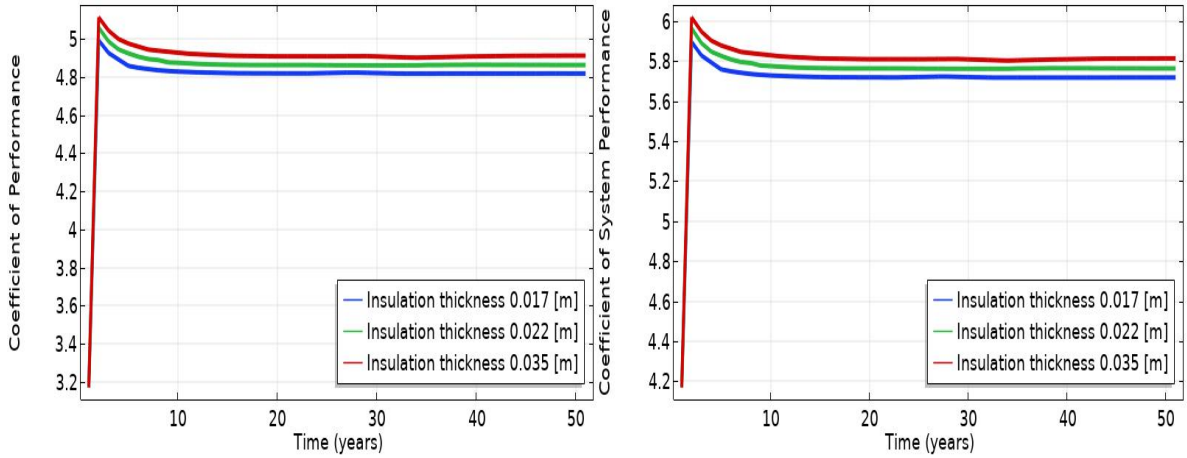

Figure 4-21 The COP (left) and the CSP of the system (right).

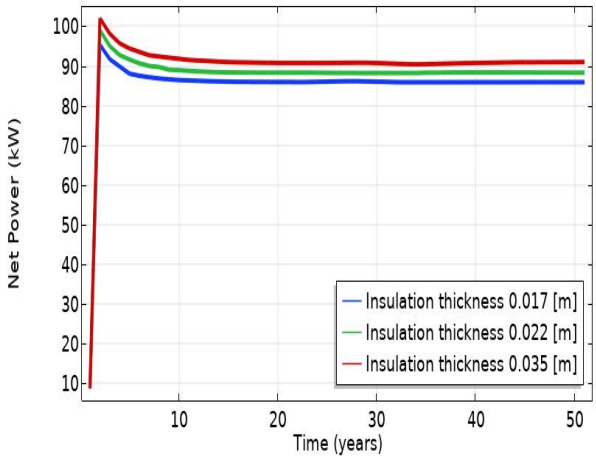

Figure 4-22 The net power of the system.

4.2.5. Outer-well thickness

The purpose of drilling a well can vary, this can be for hydrocarbons extraction or geothermal energy. Depending on what the purpose of a well is, a certain well size is selected. Increasing the outer tubing size also increases the subsurface contact area for the working fluid to interact with. Having a larger well also means that there is more volume for the working fluid to travel through, in this case the velocity decreases (if the injected mass of the working fluid stays the same). All these effects increase or decrease the heat transfer between the working fluid and the surrounding rocks. In this simulation the sensitivity analysis is created for an outer-well diameter of 0.16 m, 0.18 m, 0.22 m and 0.30 m. The well size of 0.18 m is the base case and all other properties of the materials are the same.

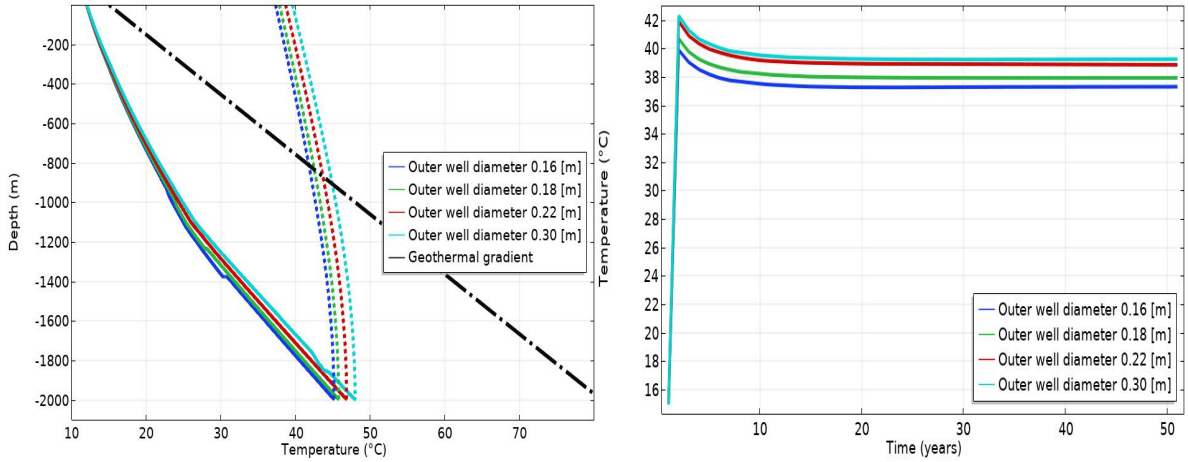

Figure 4-23 Depth and temperature relationship for the down and upward fluid flow (left) and the production temperature (right) for different outer well diameters.

The heat exchange analysis

A slightly higher BHT is reached when the diameter of the well is increased from 0.16 m to 0.30 m, as seen in Figure 4-23 (left). The four cases seem to be interacting in temperature increase in a similar way. Increasing the well size increases the BHT and production temperature (Figure 4-23). Increasing the outer well diameters also results in an increase of power generation. The power difference between the outer-well diameter of 0.16 m and 0.30 m is 10 kW (Figure 4-24-left), which is a low power addition for doubling the well diameter. The same positive results are seen for the COP and CSP, increasing the well size results in a slightly increased COP and CSP (Figure 4-25). The net power of the system is in line as with the results of COP and CSP, the larger outer-well diameters result in more net power (Figure 4-26).

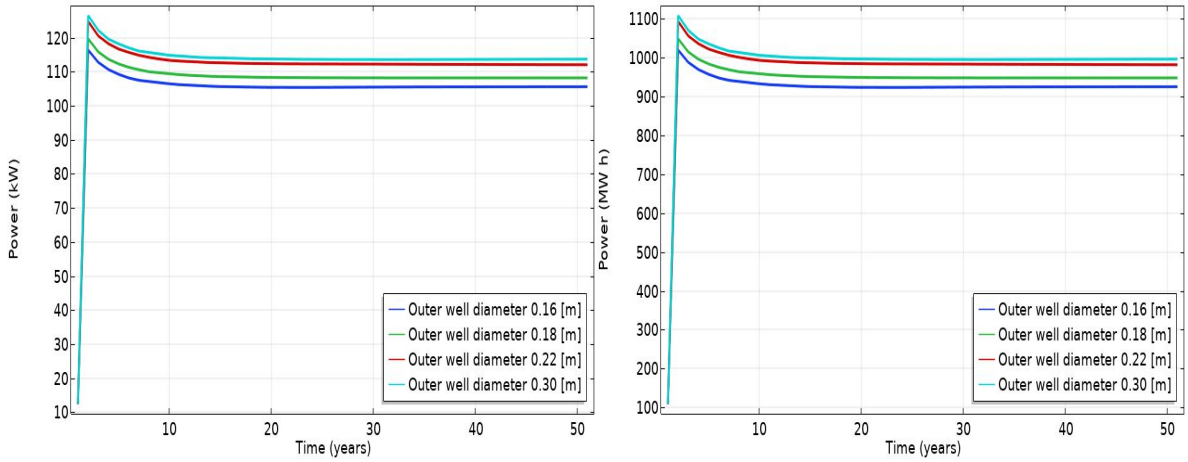

Figure 4-24 The produced power in [kW](left) and $[MW\ h]_{year}$ *(right) for different outer well diameters.*

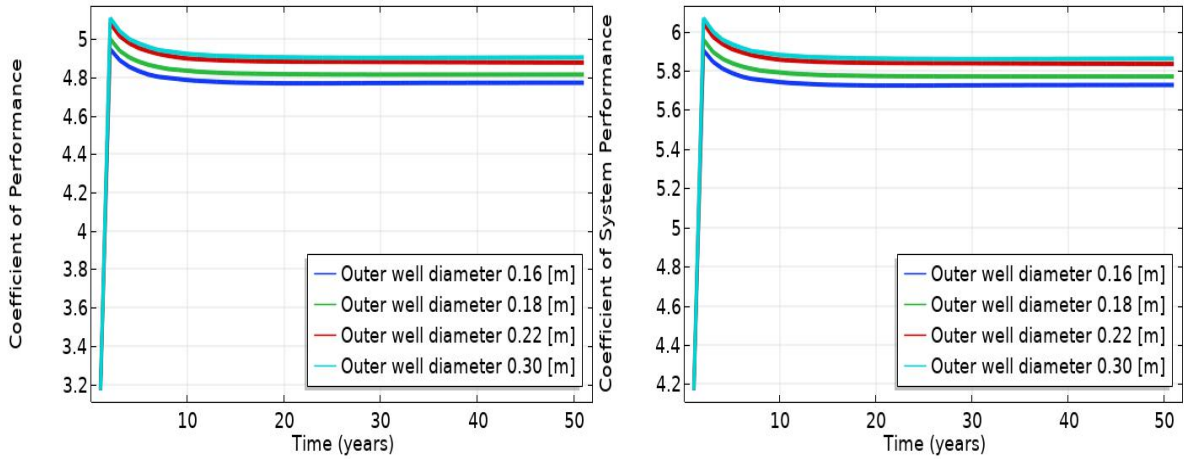

Figure 4-25 The COP (left) and the CSP of the system (right).

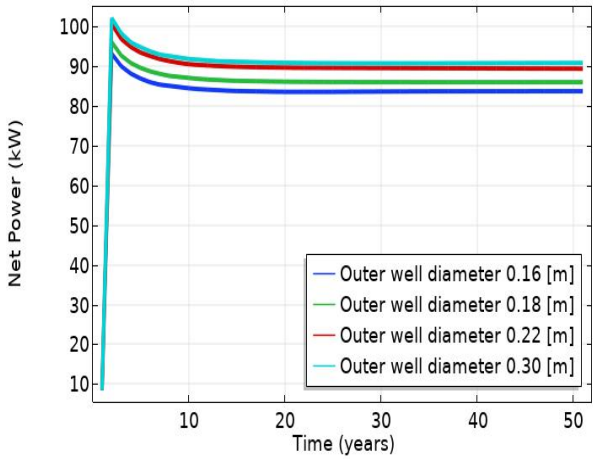

Figure 4-26 The net power of the system.

4.2.6. Well depth

In the Netherlands wells are spread throughout the country for different purposes and different depths as discussed in the introduction chapter. For the conversion to geothermal wells, it is important to know the heat exchange behaviour for these different well depths. For this part of the thesis water is further investigated for changes in production temperature with different well depths. The parameters changed are the simulated well depths of 1 km, 2 km, 3 km and 4 km and their geothermal temperature at these depths.

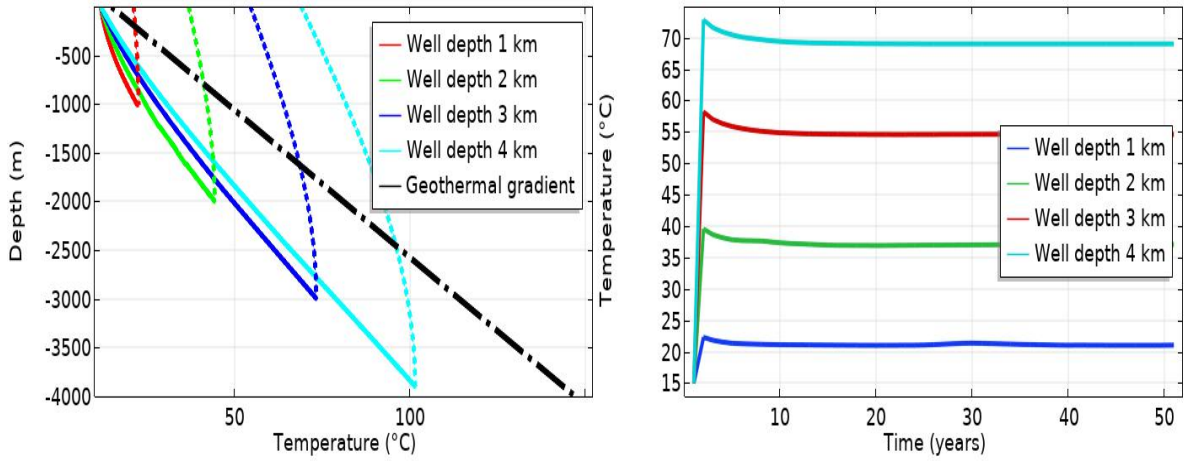

Figure 4-27 *Depth and temperature relationship for the down and upward fluid flow (left) and the production temperature (right) for different well depths.*

The heat exchange analysis

In Figure 4-27 (left) the different well depths have a linear relationship during the downward and upward fluid flow. However, there is more cooling occurring with the 4 km well during the upward fluid flow. Another observation is that with the increase in well depth there is relatively higher BHT reached for the same geothermal gradient. For example, the 1 km well has a BHT of around 25°C while the geothermal temperature is around 45°C, at 4 km these become 105°C and 145°C. Under the same flowrate and increased well depth, the working fluid has more time under similar circumstances to exchange heat with the surroundings. The deeper the well is, the higher the BHT will be, the corresponding working fluid temperature will also cool down faster during transport to the surface compared to shallower wells.

In Figure 4-27 (right) the production temperature and generated power of the different depths have an (almost) linear relation. When the depth is increased from 1 km to 4 km this provides a power generation of 40 kW to 240 kW (Figure 4-28 (left)).

The COP and CSP have similar linear relationship in Figure 4-29. The net power remaining in Figure 4-30 indicates that there is a 40 kW loss for the 4 km while this is 20 kW for the 1 km well, this is in line with efficiency of the system.

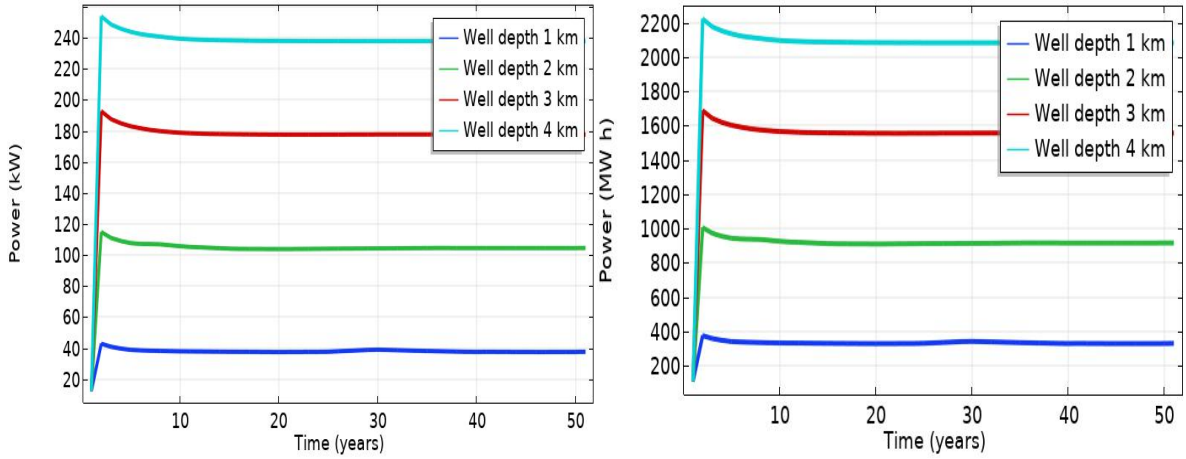

Figure 4-28 *The produced power in [kW](left) and* $[MW\ h]_{year}$*(right) for different well depths.*

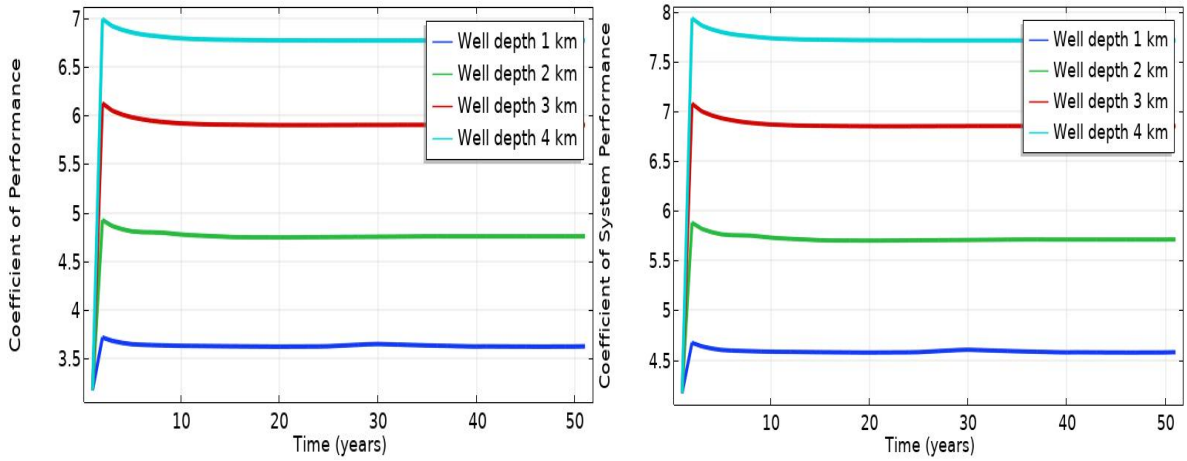

Figure 4-29 *The COP (left) and the CSP of the system (right).*

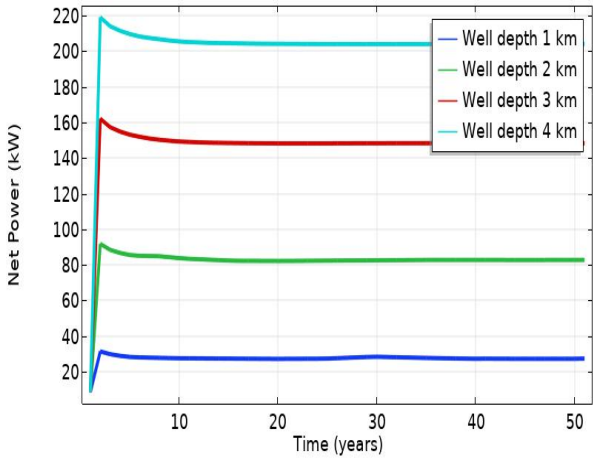

Figure 4-30 *The net power of the system.*

4.2.7. Injection temperature

During a year the weather has seasonal fluctuations, during the winter the surface temperatures can be around $3°C$ while during the summer this can increase to $18°C$ (instituut, 2020). If there is a summer season then the surface temperature will increase and the injection temperature of the working fluid will be higher. The injection temperature is expected to be higher because the working fluid needs to be transported through a possible circulation system in which the homes and businesses are the main source of heat demand or supply. To consider these changing conditions in the simulations, injection temperatures of $7°C$, $12°C$, $22°C$ and $32°C$ are investigated in this sensitivity analysis, with the base case having an injection temperature of $12°C$.

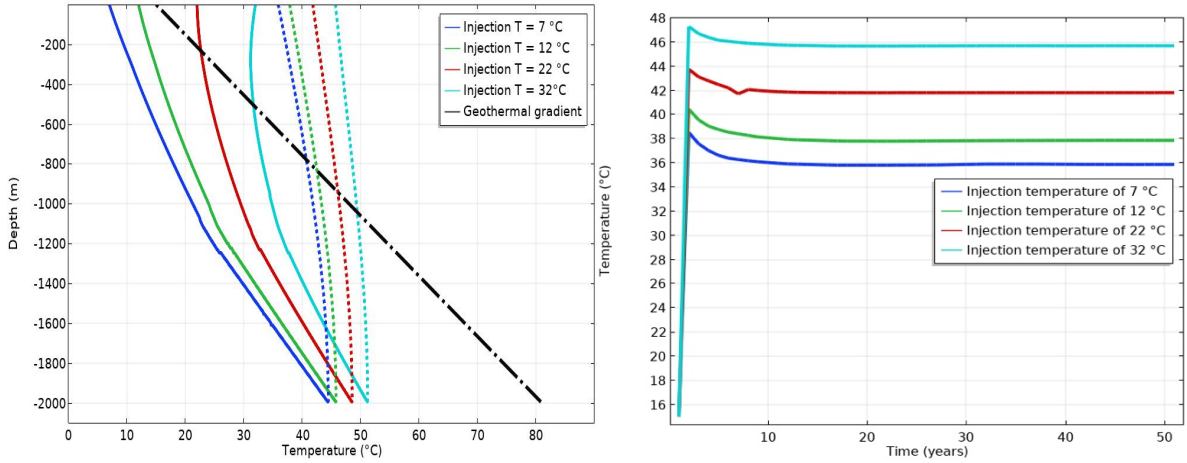

Figure 4-31 Depth and temperature relationship for the down and upward fluid flow (left) and the production temperature (right) with different injection temperatures.

The heat exchange analysis

In Figure 4-31 (left) the injection temperature of 32°C is slightly cooling down before gaining in temperature during the downward flow between a depth of 0 and 1000 m.
This is expected since the temperature of the subsurface (thermal gradient) is lower than the working fluid temperature at these depths. After the injection temperature reaches the same temperature as the subsurface, then heating of the working fluid starts. The higher injection temperatures also result in higher BHT, since less heating is required. During the upward flow there is a linear relationship between this BHT and the production temperature. This is expected since the temperature of the working fluid stabilizes at the bottom of the well and the working fluid is pumped to the surface with the same flowrate and well conditions (Figure 4-31-left).

The production temperature and system performance

The results of the production temperature in Figure 4-31 (right) indicate that there is minimum temperature gain for the working fluid with a high injection temperature. The highest injection temperature of 32°C only increases to a production temperature of 46°C. The difference is only 14°C, while for the lowest injection temperature of 7°C the difference is 29°C. Since the difference in temperature between the injection and production is higher for the lower injection temperatures, lower injection temperatures result in higher power generation (Figure 4-32).

The highest COP and CSP (Figure 4-33) is for the injection temperature of 32°C, indicating that this is the most efficient injection temperature. This high COP/CSP can be explained through the power required by the heat pump. Minimum power is used by the heat pump, since the working fluid temperature is high. The net power of this system, on the other hand, is the

lowest (Figure 4-34). For an ideal system an injection temperature around 12-22°C is recommended. At these temperatures the COP, CSP and the power generated are relatively high.

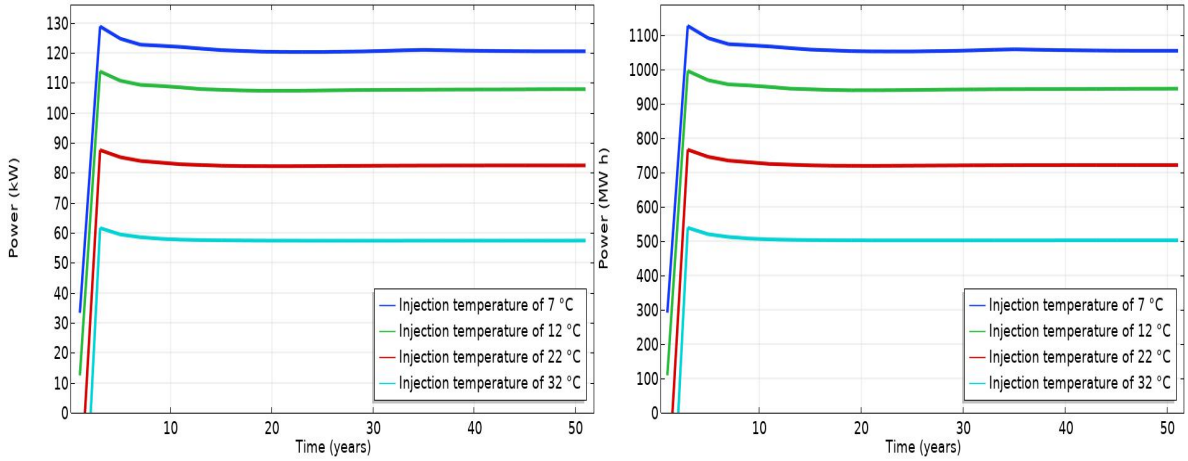

Figure 4-32 The produced power in [kW](left) and $[MW\ h]_{year}$ *(right) for the different injection temperatures.*

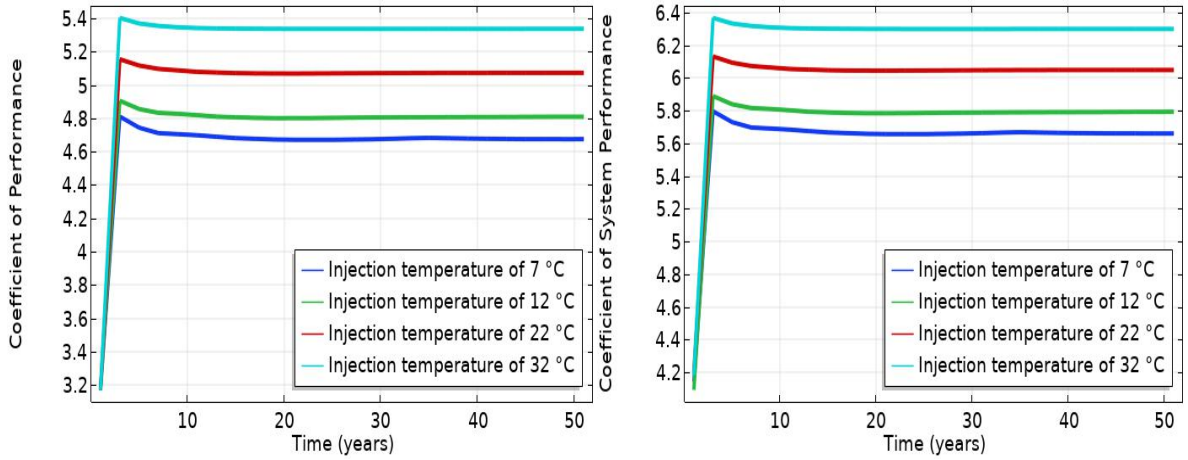

Figure 4-33 The COP (left) and the CSP of the system (right).

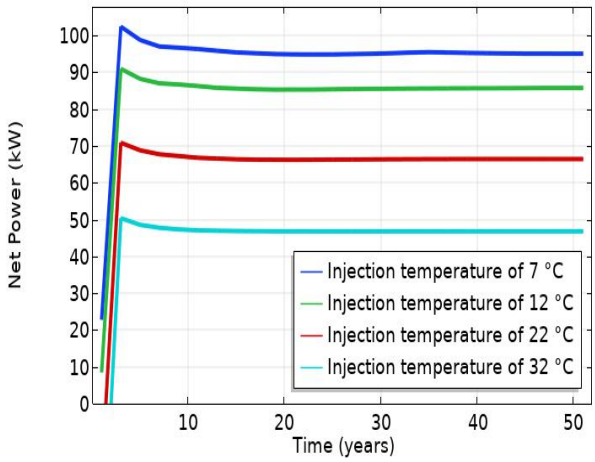

Figure 4-34 The net power of the system.

4.2.8. Reverse injection flow

During the summer season, the temperature of the homes and building can be quite high. As seen in Table 9-12 instead of requiring heat these homes and buildings prefer cooling. As the geothermal gradient stays quite stable throughout the year, a way to harvesting the cooling can be through reversing the injection and production. While flowing through the outer-well to the surface the temperature can cool down by exchanging heat. For this simulation the inlet and outlet of Figure 4-1 are changed. A sensitivity analysis with different flowrates was performed in order to have a better understanding of the heat exchange. The flowrates used are 0.25 kg/s, 0.50 kg/s and 1.5 kg/s and the injection temperature is increased to $30°C$. For the different flowrates all other parameters and materials remain the same as in the base case including the working fluid of water.

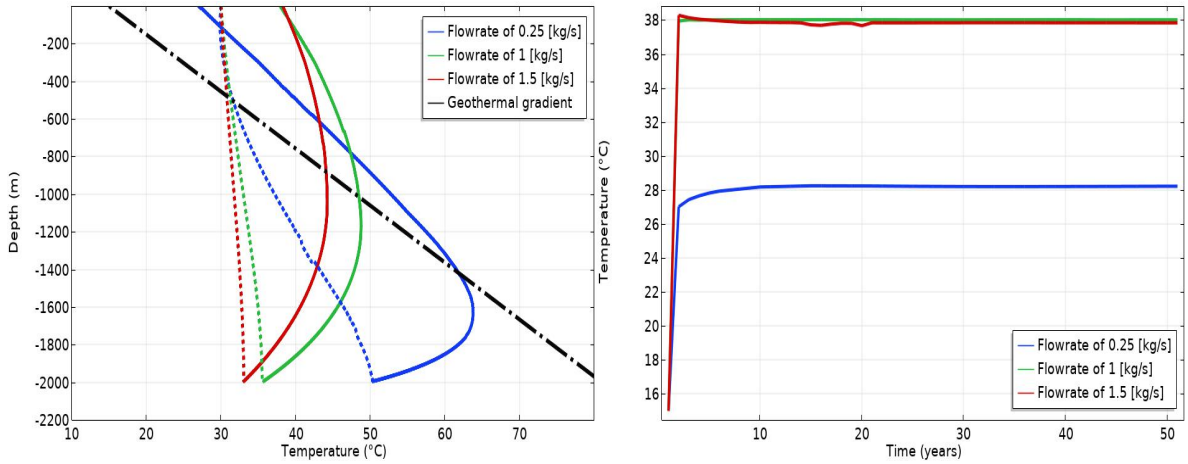

Figure 4-35 Depth and temperature relationship for the down and upward fluid flow (left) and the production temperature (right) for different flowrates.

The heat exchange analysis and system performance

During the down and upward flow the lowest flowrate adapts to the surrounding subsurface temperature. The base case and flowrate of 1.5 kg/s are flowing at a faster rate, resulting in almost no heat exchange during the downward flow. During the upward flow the temperature in these two cases is increased, such that the fluid reaches the surface with a higher production than injection temperature. For the flowrate of 0.25 kg/s, the production temperature is lower than the injection temperature (Figure 4-35). Since the flowrate of 0.25 kg/s has lost heat to the surrounding instead of gaining heat, this results in a net loss of power. The base case and flowrate of 1.5 kg/s gains in power, with the highest flowrate gaining the most power (Figure 4-36). Only the low flowrate of 0.25 kg/s, gives the working fluid time to cool down and be in sync with the temperature of the subsurface.

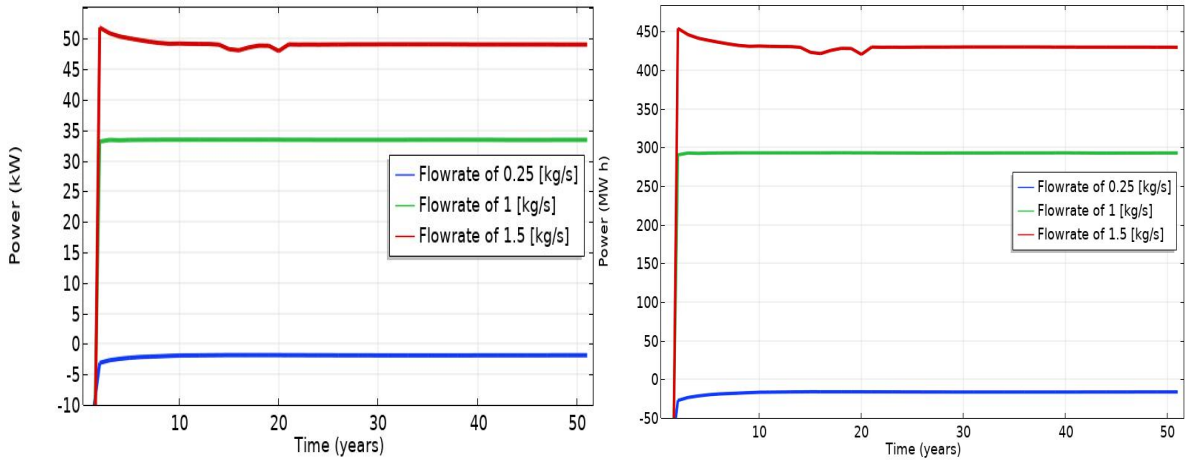

Figure 4-36 The produced power in [kW](left) and $[MW\ h]_{year}$(right) for different flowrates of the inversed flow.

4.2.9. Sensitivity analysis discussion

The data from the different sensitivity analyses are collected in this section, this gives an insight in the combined results of the parameter and material changes. Based on these combined data, optimal conditions for energy recovery from the well can be determined. The collected data are described in figures plotting temperature, COP, CSP and net power versus power.

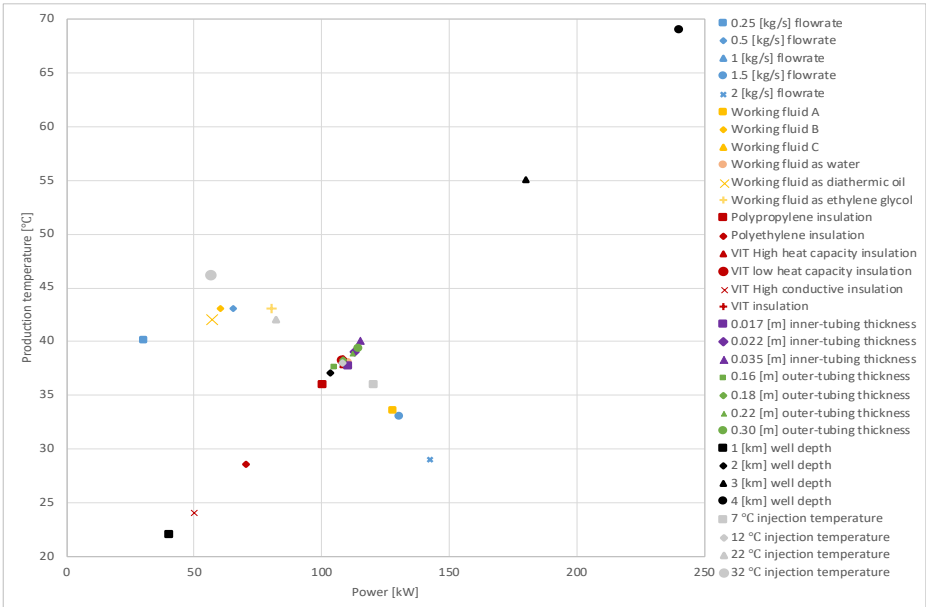

Figure 4-37 The power and temperature distribution of all the different property and material changes.

There is a linear relationship visible in Figure 4-37 between temperature and power. Several parameter or material changes produce a higher temperature, but lower power and vice versa. For example, when flowrate is decreased there is a trend visible to higher temperature and increase in flowrate generates higher power. Another trend is seen in increasing the well depths, this linearly increases temperature and power for increasing depths. Meaning that in an ideal well, the well is at maximum depth.

Generating the highest amount of power is the goal for the DCBHE system, the ideal case. In Figure 4-37, the collected data points show that a flowrate of 1.5 to 2 kg/s with working fluid A, injection temperature of 7°C, VIT as insulation, inner-tubing thickness of 0.035 m and outer-tubing thickness 0.30 m are ideal conditions.

In Figure 4-38 the ideal well conditions have similar parameters as Figure 4-37, except that the injection temperature is 22°C, flowrate 0.5 kg/s and glycol as working fluid are changed for a high COP, power relation. CSP and power distribution in Figure 4-39 has similar ideal parameters as with the temperature, power distribution. In Figure 4-40 the only negative net power is delivered by diathermic oil. This means that this working fluid should be left out as it is using more energy than it can provide.

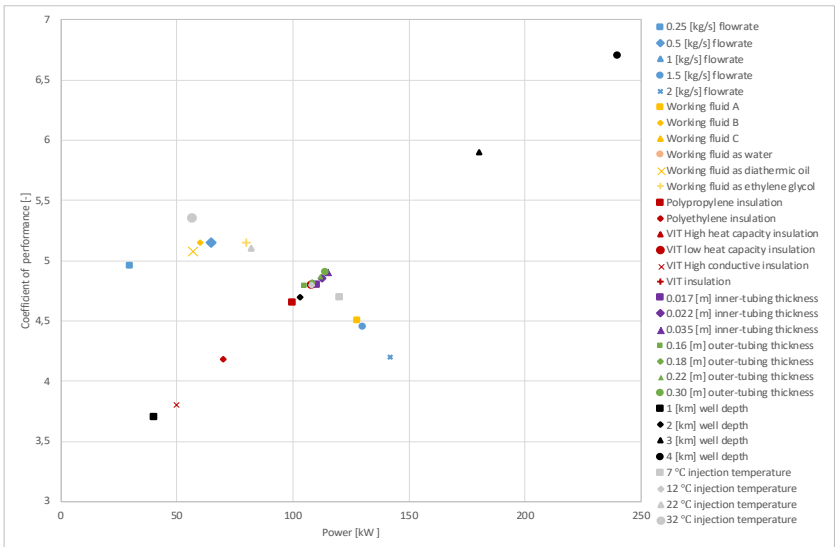

Figure 4-38 The power and COP distribution of all the different property and material changes.

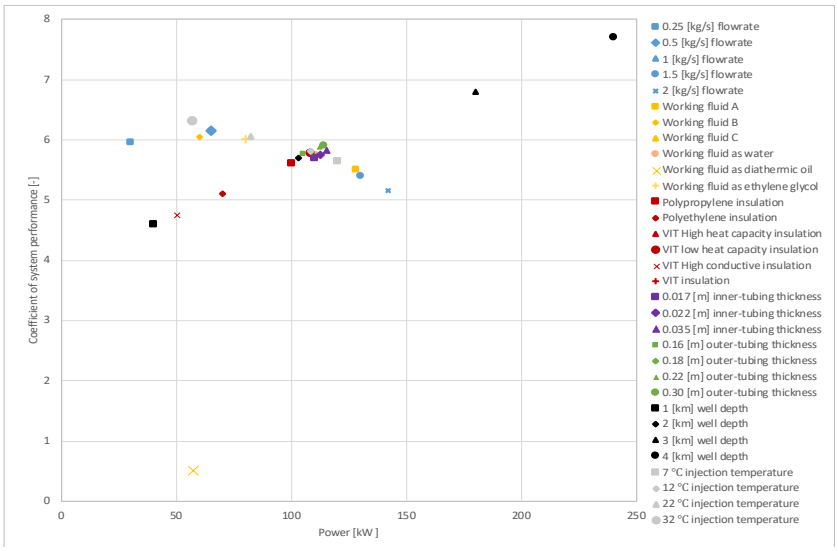

Figure 4-39 The power and CSP distribution of all the different property and material changes.

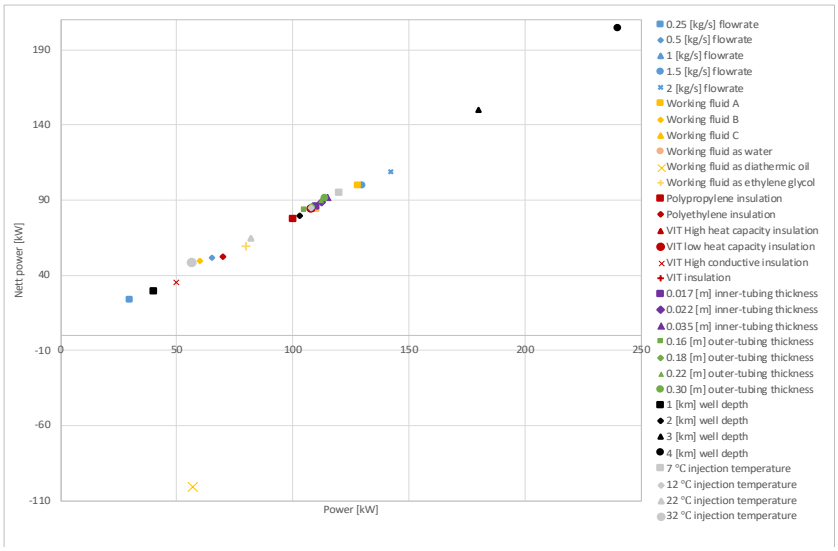

Figure 4-40 The power and net power distribution of all the different property and material changes.

5. Proposed DCBHE system and economic model

The coaxial heat exchangers in this research are limited to a depth of 1.8 kilometers. The well depth of 1.8 km is chosen since this is a realistic cement plugging depth for the Grouw-01 well. At this depth the BHT is lower than the boiling point of water (100°C). The heat losses during transport of the working fluid to the surface further cools down the BHT. By changing the flow rates for the given well design heat generation gained from DCBHE is calculated. On the basis of these data an economic model for the well and location is proposed.

5.1. The Grouw-01 data

Simulating the Grouw-01 well for the energy that the well can produce is a way in which the economic model can be built. For running the simulation all properties of the well are similar to the base case, except the well depth and the flowrate. The working fluid is water, as it showed to be the best of the fluids compared in the previous chapter.

The production temperatures calculated for the different flowrates from 1 kg/s to 2 kg/s are 34.5 °C, 30°C and 26.5°C (Figure 5-1). The power provided with these flowrates are 95 kW, 110 kW and 120 kW, respectively.

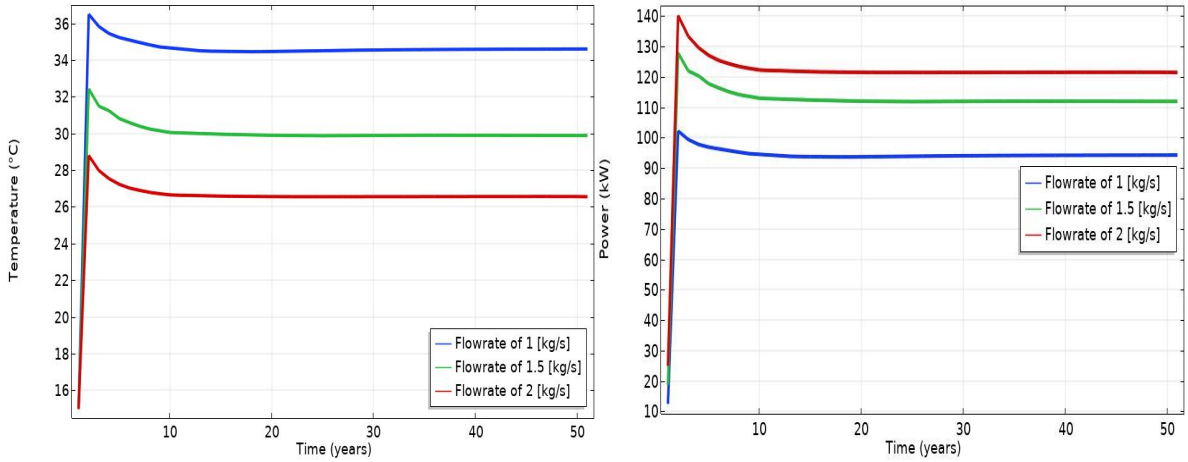

Figure 5-1 The production temperature (left) and the produced power in [kW] (right) for different flowrates at 1800 m well depth.

5.2. Deep coaxial bore-hole heat exchanging system for Grouw-01

DCBHE systems have several components in which the working fluid can circulate in a closed loop. The components for a shallow geothermal BHE (Figure 5-2) system consists of; fluid storage unit, heat pumps, pipelines and the DCBHE. The function of these different components are designed for a single housing system functioning in a closed working fluid loop. If a shallow BHE well were to be extended to depths over 500 m (as DCBHE) then there can be more components added to the system. some of these components are a DCBHE pump, which pumps the working fluid, and, as previously discussed, a VIT or an insulated tubing.

Similar as with a shallow BHE system, the DCBHE system through which the working fluid circulates is a closed circuit (Figure 5-2). The working fluid is circulated into the BHE to reach a desired production temperature. The working fluid coming from the BHE is stored in the thermal storage tank. The thermal storage tank contains a thermostat which is set at a certain temperature and consists of 2 units. The first unit is for storing the working fluid coming from the DCBHE and the second unit for the cooled water which goes in the DCBHE. The temperature of the first unit in the thermal storage tank should remain constant, this also requires energy. The working fluid is pumped from the thermal storage tank to the heat pump. The heat pump uses the heat from the working fluid and pumps colder working fluid to the storage tank (unit 2). From this unit in the storage tank, the DCBHE pump injects the working fluid into the DCBHE. The energy required by the DCBHE pump is dependent on the pressure loss between inner and outer-well, which is calculated by Equation 3-19.

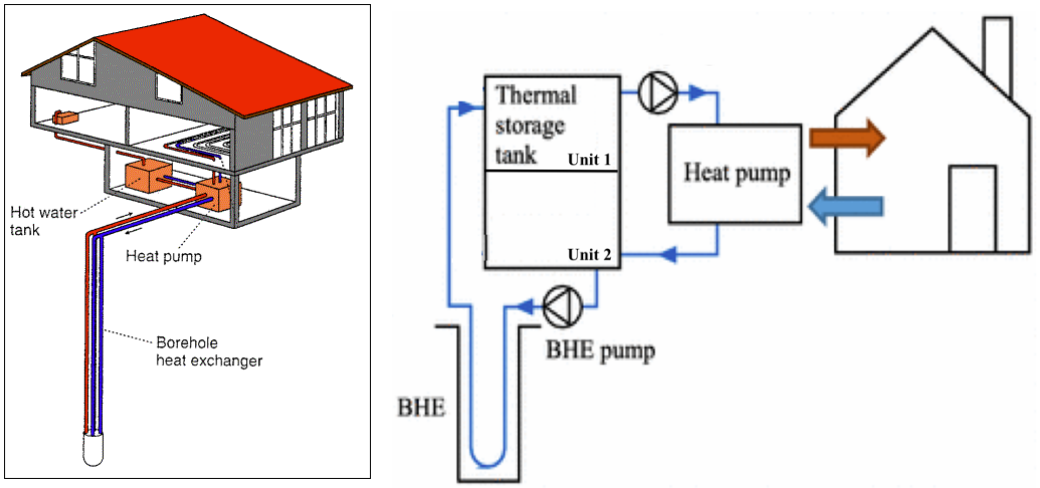

Figure 5-2. Shallow geothermal BHE system application (Zurich, 1986)(left) and schematic diagram of the proposed fluid circulating heating system(right) (H. Bilarian, 2019).

5.3. Proposed DCBHE system

Average households in the Netherlands use approximately 1240 m^3 of gas for heating the house throughout the year (CLO, 2019). This is around 1268 J/s of energy if we use $1 * 10^9\ J = 31.6\ m^3$ of natural gas (Rijkswaterstaat, 2020). For simulating water at a well depth of 1800 m from Figure 5-1 (right), the power generated of 97000 J/s can heat approximately 75 homes for a flowrate of 1 kg/s.

Applying the same concept of the shallow BHE system (Figure 5-2) here, and creating a new closed structure (Figure 5-4) requires more pumps and pipelines. The produced power from the Grouw-01 well with a flowrate of 2 kg/s is in theory enough power to replace the heating used by of 96 homes. The theoretical capacity has several flaws which lower the actual capacity and there are several aspects that need to be taken into consideration. for example; seasonal corrections, heat losses during transport at the surface, pumping system energy efficiency requirements losses (Figure 5-3).

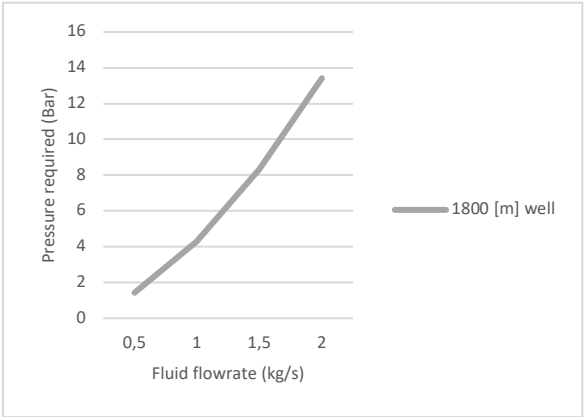

Figure 5-3 The pressure required to overcome friction for the DCBHE pump.

Based on the amount of energy that the Grouw-01 well can provide to the energy requirements for households, a system of heat supply and demand is created for the economic analysis. For the proposed system 10 buildings are connected to the closed loop, these buildings can contain normal households and businesses (Figure 5-4). The amount of 10 buildings is an estimation, since some businesses require more heating than an average home.

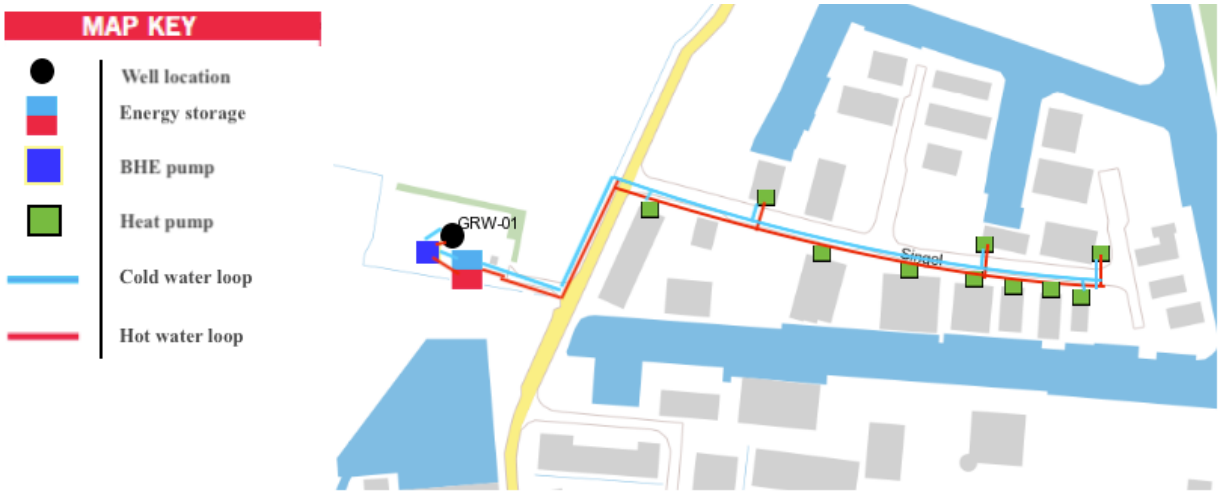

Figure 5-4. The closed loop system connected to a BHE system for the Grouw-01 well.

5.4. Economic model

The value of the different materials, project costs and revenues from a geothermal project are described in the economics. In this part of the thesis the economic potential of a DCBHE system is analyzed with three different cases. The cases are created by generating revenue and subtracting different costs. The costs involved are divided in capital costs, operational costs and a government take in the form of taxes.

If a project is financially viable, then a positive cashflow should be available after all the costs are subtracted from the revenue. The annual cashflow [F] in year [k] can be expressed as:

Equation 5-1

$$F_k = R_k - E_k = \underbrace{p_g N_k}_{Revenues} - \underbrace{O_k}_{Opex} - \underbrace{C_k}_{Capex} - \underbrace{T_R I_{bt,k}}_{Government\ take}$$

Where the expenses indicated with [E] are deducted from the revenue [R] throughout a year [k]. The revenue consists of the gas price [p_g] multiplied by the annual power production [N]. Operation [O] and capital [C] costs are the technical costs. The government costs are the tax rate [T] and income before tax [I] related (Seba, 1998).

The devaluation of money and if this money would have been invested in a different project, where a higher return could have been achieved, is taken into consideration with a discount rate. The discounted cumulative cash surplus is then the net present value (Equation 5-2).

Equation 5-2

$$NPV = \sum F_{disc} = \sum \left[\frac{F_k}{\left(1 + \frac{R_{disc}}{100}\right)^k} \right]$$

[R_{disc}] is the discount rate in percentage value throughout a year [k]. The annual cashflow is indicated with [F] and the discounted annual cashflow as [F_{disc}]. NPV is the net present value.

In the first years the NPV is negative for most geothermal projects since the total expenses due to OPEX, CAPEX and government take outweigh the revenue (Zaal, 2020). After the break-even point is reached in which the revenue and expenses are the same, a positive NPV will be reached.

Revenue

The income throughout the year is calculated by multiplying a certain gas price with the produced power in $[MW\ h]_{year}$. The number of hours that the installation should be operating throughout the year is dependent on the average consumer usage. In this research the assumption is made that throughout the winter the heat demand is higher and in the summer the demand is lower compared to yearly average (Table 9-12). For this reason, 6600 operational hours, which corresponds to approximately 9 months throughout a year, is used.

For the first 15 years of the project there is a government subsidy incentive scheme, SDE+, for renewable energy in the Netherlands providing a guaranteed payment. The subsidy scheme is created to make the renewable energy sector more profitable and to increase its contribution to

the national energy supply (policy, 2020). The subsidy price used for calculating the revenue is the difference between the cost price for the production of renewables (base amount) and the market value of the energy supplied (correction amount) in Table 5-1. During a year the subsidy can be used for 6000 operational hours, for the remaining 600 hours the market price of gas (which is estimated by PBL (leefomgeving, 2020)) is implemented into NPV calculations (Figure 5-5). The maximum period of the subsidy is 15 years, after these 15 years only the market price is used throughout every year. The future market gas price is certainly unknown, although based on the past the gas market price of the future is estimated.

Equation 5-3 (policy, 2020)

$$Maximum\ SDE + contribution = base\ amount - correction\ amount$$

Table 5-1 The subsidy scheme SDE+ (policy, 2020)

	Phase 1 From 9 am 17 March to 5 pm 23 March	**Phase 2** From 5 pm 23 March to 5 pm 30 March	**Phase 3** From 5 pm 30 March to 5 pm 2 April	Base energy price	Provisional correction amount 2020	Maximum full load hours per annum	Maximum subsidy period (years)	Operation must start at the latest within (years)
Geothermal	Maximum base amount / phase amount (€/kWh)			(€/kWh)				
Geothermal heat								
• ≥ 500 m deep	0.043	0.043	0.043	0.016	0.020	6,000	15	4
• Conversion of existing oil and/or gas wells, ≥ 500 m deep	0.043	0.043	0.043	0.016	0.020	6,000	15	4
• Expansion of production installation with at least one extra well, ≥ 500 m deep	0.031	0.031	0.031	0.016	0.020	6,000	15	4
• ≥ 4,000 m deep	0.065	0.065	0.065	0.016	0.020	7,000	15	4

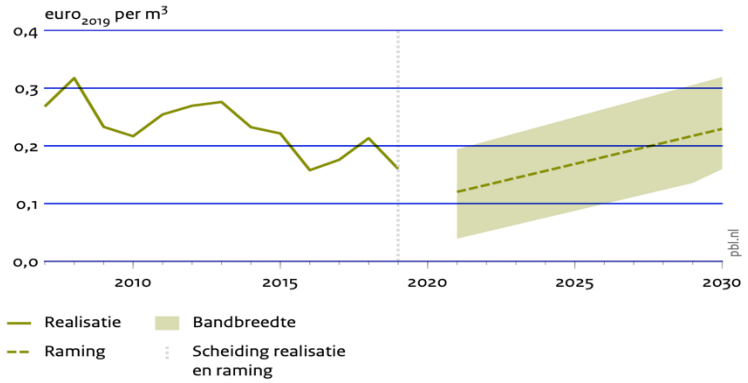

Figure 5-5. The expected market price for gas in the future (leefomgeving, 2020)

The capital expenditures (CAPEX)

The capital expenditures are all the costs the project is expected to have for setting up the proposed system. The capital expenditures are, for example, for installing VIT, well head, cementing the perforations and installing pipes and pumps. The set-up of this geothermal project can be done within a year in an existing well. The approximated CAPEX for the closed loop system is a one-time investment (Table 5-2). The CAPEX is depreciated over a number of years to obtain tax relief. Depreciation is the write-off of the asset's value over the period of its useful life. The government regulation defines how CAPEX is depreciated (Zitha, 2009). For most investments in the Netherlands the depreciation of the investment is set at 20 % per year (Belastingdienst, n.d.).

Table 5-2 CAPEX

Material	Value (€)	Source
BHE pump	1500	(Engeldot pomp- en leidingsystemen, n.d.)
Heat pump home (10 pc.)	20.000	(OfferteAdviseur, n.d.)
Pipelines	10.000	(OfferteAdviseur, n.d.)
Thermal storage tank (2 pc.)	4000	(Buffervaten, n.d.)
VIT (2000 m)	15.000	(20ht)
Isolating current perforations (case 2&3)	60.000	(Gibbons, 2020)
Tubing type used		
Installing VIT (case 1)	350.000	(Gibbons, 2020)
Pre-insulated water pipes (1800 m) (case 1&2)	20000	(Pre-insulated water pipe, n.d.) (Calpex Pre-Insulated PEX Pipe, n.d.) (Waterleidingen, n.d.) (20ht1)

The operational expenditures (OPEX)

The operational expenditures can be fixed per year as for example maintenance costs, or they can be variable, for example for pumping costs, thermal storage tank electricity costs. The operational costs are on a yearly basis (Table 5-3). The pumping costs are calculated by the amount of power these pumps use with Equation 3-20 multiplied with the price of electricity for the pumping (Table 5-4).

Government taxes

In the Netherlands a tax rate for company profits of under the € 200.000 is set at 16,5% (Tarieven voor de vennootschapsbelasting, n.d.). Since our profits do not exceed € 200.000, the tax rate of 16,5% is applied for all positive cashflow. For this research insurances and permits are left out.

The abandonment of Grouw-01

The well of Grouw-01 is in an observatory state, in which the perforations are not isolated and pressure is checked regularly for leaks. After depletion the well is in zonal or final abandonment. During the zonal abandonment the well perforations are isolated, the costs of this is described in Table 5-2. The final abandonment costs in which the well is completely sealed, cut off and cemented exceed € 500.000. This relatively high value (compared to the whole geothermal project) is not considered in the cashflow calculation, the abandonment could also be implemented if the geothermal project is beyond its lifetime.

Table 5-3 OPEX

	Value (€ annual rate)	
Thermal storage tank costs	500	est. based on normal systems
Pumping costs	7865	Equation 3-20 and Table 5-4
Maintenance	4000	Rough conservative value

Table 5-4 Market price and OPEX

Market price (first 15 years)	0,15	€ per kWh
SDE+ (first 15 years)	0,23	€ per kWh
Pumping	0,095	€ per kWh (Tabellen tarieven milieubelastingen, n.d.)
Market price (after 15 years)	0,25	€ per kWh

NPV

The economics gives an insight into the duration and profitability of the project. The profitability is dependent on the previously discussed revenue and costs. In this section the results of the previous discussed data have been processed and presented as a net present value based on three cases. The three cases are created with a difference in CAPEX. The first case is created with a reasonably low CAPEX (Table 5-5). In the first case the costs of isolating the current perforations are left out and a pre-insulated water pipe is used as insulation material (Table 5-2). The break-even point in this case is reached approximately after the 11th year of the project. At this point in the cash balance (Figure 5-6), the project has earned its investment costs and can provide the operational costs. After the 11th year the NPV is increasing and positive.

Table 5-5 The different cases

	Price index (€)
CAPEX case 1	55.500
CAPEX case 2	115.500
CAPEX case 3	460.500
OPEX (total)	12.365

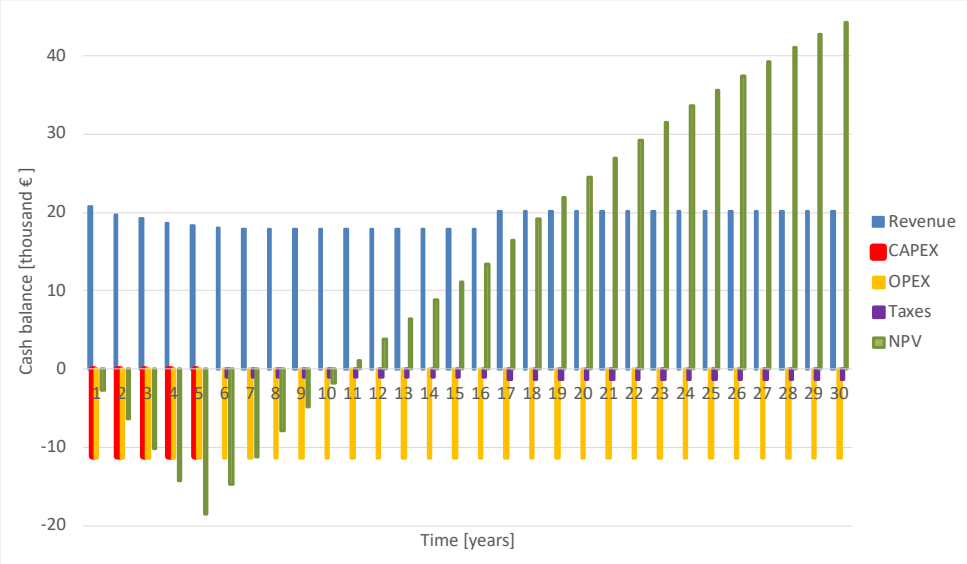

Figure 5-6. The cash balance of the first case with a depreciation period of 5 years.

In Figure 5-7 the first case is analyzed with and without depreciation of the CAPEX. If there was no depreciation of the CAPEX then the CAPEX is applied only in the first year. Having the project CAPEX linearly depreciated through several years delivers a higher NPV and cashflow since less taxes have to be paid over the profit. The second case does not reach a positive NPV within 30 years (Figure 5-7), if the project were to last longer than 30 years, a positive NPV would be reached. The third case also has a negative NPV, in this case a positive NPV cannot be reached (Figure 5-8).

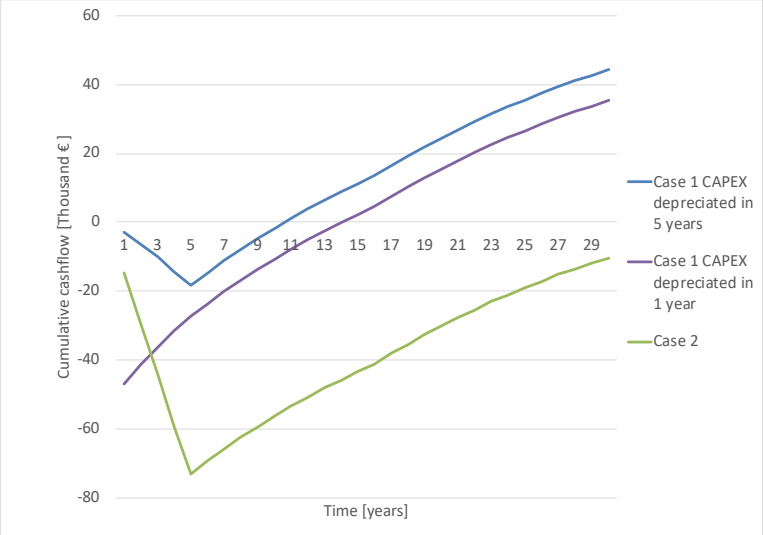

Figure 5-7. The first case with depreciation of 1 and 5 years, and the second case.

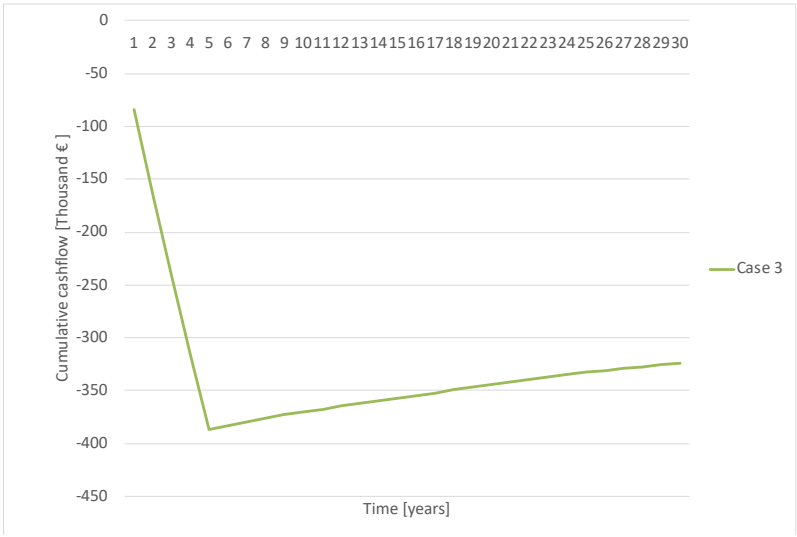

Figure 5-8. The third case with 5 years of depreciated CAPEX.

Sensitivity analysis

The economic calculation has several uncertainty factors influencing the results. For the economic calculation the uncertainty factors are influenced by technical issues or market and financial behavior. The technical factors can be, for example, the production temperatures, pressure distributions. The market and financial behavior are price related such as CAPEX, gas market price, OPEX and taxes. If the government in a country changes, this could affect taxes, which indirectly affects all the costs. All these different unknowns can have a positive or negative effect on the final projects net present value. In order to have a realistic and clear view of the financial effect of these estimations a sensitivity analysis is performed (Figure 5-9). For the sensitivity analysis, several parameters are changed to see the effect of this change on the net present value of the project. The changed parameters are the market price, material price, CAPEX, OPEX, load hours, taxes and the discount rate.

The data used for the base case in the sensitivity analysis are derived from the first case with 5-year depreciation. If all the parameters remain the same as with the base case (Table 5-6), the most sensitive parameters are the project load hours and OPEX as seen in the results of Figure 5-9. All the other parameters cannot cause the NPV to be negative even if their values were halved or doubled.

Table 5-6 Sensitivity data

Parameter change	Min	Base case	Max	Unit
Market price (after 15 years)	0,125	0,25	0,375	€ per kWh
Insulated water tubes price	10000	20000	30000	€
Total CAPEX	27750	55500	83250	€
Total OPEX	6183	12365	18548	€
Load hours	3300	6600	9900	hours
Taxes	8,25	16,5	24,75	%
Discount rate	2,5	5	7,5	%

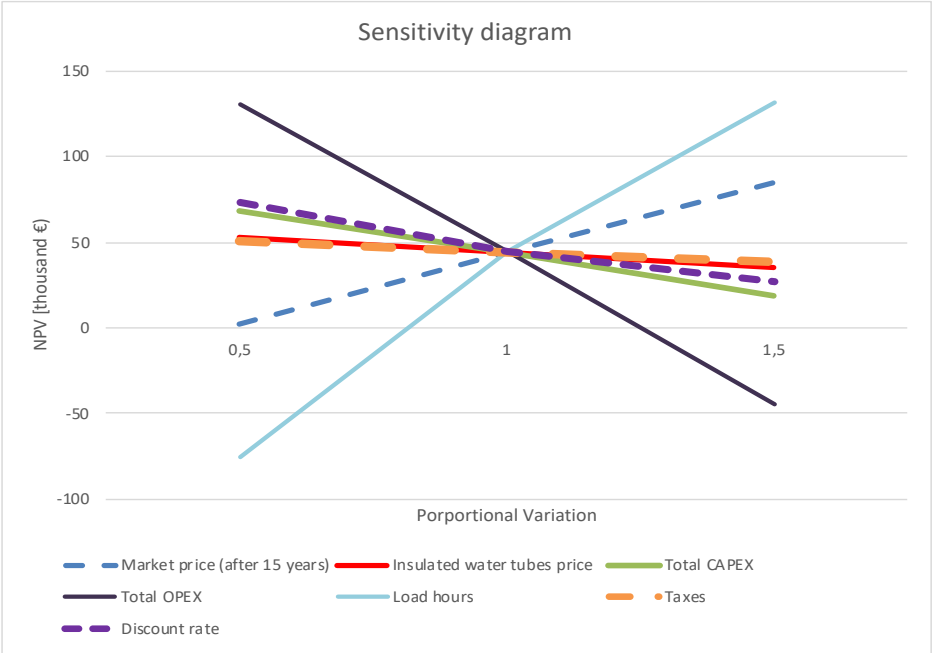

Figure 5-9. The sensitivity diagram of the NPV on different financial changes.

6. Discussion

In this section the factors which can cause a possible change in the end result of the many sensitivity analyses and economical calculations are discussed. These factors range from pore space in the geology, empty section between cement and geology, cement properties to the actual property changes of the different materials in the sensitivity analysis. The dimension of the model can also influence the outcome of the results. In COMSOL the difference between the dimensions is in the generated mesh grid. 1D requires for example 0.1 % (or less) of the mesh a 3D model requires. Less mesh means faster processing time of the simulation but also slightly less accurate in results. This is controversial, as one would say to select the highest possible accuracy. Both the processing time and accuracy had to be taken into consideration. For this reason, the co-axial 2D model is selected, if in the future faster computers are wide available the best option would be to run in 3D.

The second modelling related assumption is in the geology, which is a simplified solid and thermally conducting with an assigned constant value. In reality there is pore space in the geology, which can be filled with water or air. Both have different effect on overall thermal conduction, as air is a bad thermal conductor. These factors play a limited role, as there are no rocks known with porosity over 30% in these geological sections. Air in the subsurface could also be in the border between the cement layer and the geology. Assumption is made that this area is filled with water, because the Grouw-01 well is controlled yearly for pressure losses in the well. With pressure changes there is fluid between the rock and the cement. There is a possibility that this can change in the future and become a space filled with methane gas. In that case the void will function as an insulator, as the thermal conduction of methane gas is well below VIT value. Acting as an insulator will prevent heat exchange and therefore reduce temperature, power, COP and CSP of the system. In case this void is filled with cement, the thermal conduction will be higher. This is caused by the thermal conduction difference; cement has higher thermal conduction properties than water but lower than the geological surrounding. This will increase the over system performance. As water is in between the sections, it is safe to say that there is thermal conduction between the rock and well.

The geology can also regenerate heat, but in a slow pace compared to the extraction of heat. Heat regeneration is the process in which a volume of rock from which heat was extracted regains the original temperature. In the model heat regeneration is caused by the surrounding horizontal sides and bottom part of the model due to the assigned geothermal gradient. This means that if the heat extraction process is stopped, eventually (maybe over 100 years) the area will have the same temperature as the geothermal gradient. The rate in which this occurs is relatively slow, this is not further investigated in this thesis as the project duration is maximum 30 years. Dimensions of the geology in the model are determined by simulating different horizontal widths. In a study by Sliwa et al. (2015) (Tomasz Sliwa, 2015), the rock formation radius from the center of the well is approximately 30 m as seen in Figure 1-8. After having increased and decreased this dimension, the conclusion was that simulating past this radius would have a minor effect on the heat distribution. If less than this radius is simulated, then not all the heat can be extracted. In general, the further one is from the center of the well the less effect this has on the heat extraction.

The fluid through the well is in laminar flow, due to the low Reynolds number realised by the low flowrates. If the flowrates were high enough for turbulent flow, this could have a positive effect on the fluid heat distribution. Turbulent flow distributes heat in a chaotic matter, therefor increasing thermal mixing. As the flowrates are low, this is not further examined in this thesis.

The different sensitivity analyses showed a more detailed description of the temperature, power, COP, CSP result for the changes in flowrate, working fluid, insulation material and thickness, outer-tubing thickness, well depths, injection temperature and reversed injection flow. All these changes are important to know for designing a DCBHE. With the changed flowrates simulated, two important aspects were found. First that there is an optimum flowrate, through which a maximum amount of heat is exchanged with minimal loss during the upward transport. For the base case scenario this flowrate is between 0.5 kg/s and 0.75 kg/s. With the optimum flowrate the production temperature can reach the highest possible value. A second important aspect is the power generation. The power generation increases with fluid flow. However, it should be noted that increase of flowrate comes with increase of costs, especially for pumps. With the change in working fluids, it is found that ethylene glycol as circulation fluid is promising. The fluid has higher production temperatures compared to water, but due to its lower heat capacity the use of glycol would lead to less generated power. The most important material property for a working fluid is the heat capacity. Working fluids with high heat capacity tend to generate more power duo to the internal energy. As this thesis is limited to three working fluids, a future study could investigate more working fluids with high heat capacity. For this research the ideal working fluid is economically and technically viable.

The change of insulation material showed that, materials with low thermal conductivity like VIT perform overall better as an insulator. As VIT has high instalment costs, an alternative insulation is required for the project to be financially viable. Research in the economic chapter showed that there are insulating materials with similar properties and lower costs. Changing the thickness of the insulation improved the overall performance of the system in terms of temperature, power, COP, CSP. A thicker insulation material leaves less volume for the fluid to pass through, this would mean that the mass flowrate could be limited. Similar performance improvement is seen in the change in outer-well diameter. Increased surface contact area is the cause for the improved performance. Double the diameter of the outer well only delivers an almost 10 kW increase to the generated power of 105 kW. The overall performance of the system slightly improved in terms of temperature, power, COP, CSP. This information is good to know, but not practical. In practice there are almost no wells with those large thicknesses as this is not economically or technically viable for drilling to reach hydrocarbon reservoirs.

Changing the well depths, showed that there is an energy relationship between the different depths. The relationship between the depth and heat extraction in terms of temperature, power, COP, CSP is almost linear. This means that for a different well depth, the energy can be estimated as they are linearly dependent. An assumption made in this method is that the geology is also linearly extrapolated to the bottom of the well. Which is not the actual geology, but a simplified version. There is less porosity in deeper geological layers, so this can only have a positive impact on the data. As previously discussed, the rock has higher thermal conduction if not filled with water or air in the pore space.

Taking into consideration seasonal temperature fluctuations with the change in injection temperature, demonstrated the efficiency of low injection temperatures. The injection temperature of the system should remain low if maximum efficiency of the system is to be exploited. This also delivers lower production temperature, and fast cooling of the surrounding rock.

Reversing the injection flow, for reaching a cooling effect on the production temperature showed that this is only possible for low flowrates. The cooling is only a couple of degrees, on an injection temperature of $30°C$. This is not considered to be efficient as there is almost no cooling occurring. Having a cooling and heat unit at the simulated depth does not seem to be possible. Alternative methods, for example decreasing well depth can function as a possible cooling factor. As at lower depths the well reaches lower temperatures. This could make the project technically and financially complicated as there will be more costs for changing depth.

For the financial analysis, three cases were created in order to understand the effect of several factors on the NPV. There were only two factors which could negatively affect the NPV of the suggested project. These were the load hours and the OPEX. This means that these factors are very sensitive for having a successful project with positive NPV.
A different aspect to take into consideration are the heat losses at the surface from the transported working fluid, this is known to occur but not examined. This could decrease the energy productivity. As the tubes are insulated for transport, this heat loss is kept at a minimum. The abandonment costs were also not taken into consideration, since costs of the abonnement returns after the end of the project's life time.

7. Conclusion and recommendation

At the beginning of the report there were several research questions. These questions were formulated to answer the main question of 'How can a mono-well for efficient heat production be developed?'. I will answer the research questions by using the results of the numerical modelling part.

1) *How can energy extraction be optimized from the subsurface with a geothermal mono-well and under what condition?*
    a. Heat capacity of the working fluid has an important effect on temperature and produced power. For example, glycol has almost half the heat capacity of water. This makes glycol a better working fluid in terms of providing higher temperatures at the surface but also lower power. Decreased heat capacity results also in fast cooling of the fluid from the bottom hole to the surface. The most influential material property of a working fluid is the heat capacity.
    b. In general, as the flow rate increases, produced temperature decreases, however the produced power increases. It is important to note that increase of the flowrate usually leads to the increase of operational costs, mainly due to the energy used by the pump and the higher frequency of pump maintenance and/or exchange. Hence for a real optimization of flow rate in such systems economic considerations are of utmost value.
    c. Insulation material is crucial for an DCBHE, as this minimises the cooling during the upward flow. With this same insulation material and an increase in thickness, the heat loss is also reduced. In the example presented here, increasing the inner-tubing would lead to about 10 kW more power provided. The most important material property of an insulation material is the thermal conductivity.
    d. An increase in well depth increases the energy in a linear fashion.
    e. Having an injection temperature which is low compared to the subsurface temperature is crucial, as the efficiency of the extraction increases with a low injection temperature.

2) *Is the DCBHE economically viable?*
    a. The theoretical limit of power the DCBHE considered in this study provides enough heat for over 70 average households in the NL, in practice this amount is lower since there are losses due to efficiency and transport. For this project 10 household/companies were selected, which is a rough estimation.
    b. The financial sensitivity analysis showed what could make the project financially not viable. The OPEX and load-hours of the project are critical parameters. If, for example, the operational costs are 1.5 times as high as expected, then the project would not have a positive NPV.
    c. Based on the revenue and costs this project has, this project is economically viable in almost all scenarios where there is an alternative for VIT used. The high costs of VIT instalment makes the project financially not viable.

My studies showed that VIT (or a substitution with similar properties), water (or glycol for high temperature), a low injection temperature is crucial for designing an efficient DCBHE. The flowrate selection is based on the desired output temperature, so this can vary. The increased thickness of the inner-tubing and outer-tubing only increases the energy slightly. If the benefits (energy) outweigh the costs, then these are recommended.
The economic study showed a financially viable project, although there are some factors which can cause the project to have a negative NPV. These factors can be adjusted or changed (as with a replacement for VIT) to have a positive NPV. The heat delivered by one single well is enough for a minimum of 10 homes to have a lifetime of heating. There are many wells in this condition, unused and left in a shut-in state. If more wells were converted, then the costs of the project would reduce as collective maintenance and instalment costs become less. Making the project even more alluring to invest in.

With all these subjects discussed, the mono-well is an interesting asset. The energy is continuous for a long period of time, production temperature can be adjusted and the materials are environmentally acceptable. The Netherlands is currently in an energy transition, this project offers opportunities and earning potential.

8. Bibliography

Mary H. Dickson, M. F. (1995). *Geothermal Energy.* Pisa, Italy: John Wiley & Sons.

Grant, M. A. (n.d.). *Geothermal reservoir engineering* (second ed.). Burlington, Usa: Elsevier.

Scandiffio, G. P. (1995). Geochemical evolution of fluids in the Larderello geothermal field. *Proceedings world geothermal conference*, (pp. 1839-1843). Florence.

Horne, R. N. (1980). Design considerations of a down-hole coaxial geothermal heat exchanger. *4*.

Koji Morita, M. T. (1995). *Development of the Downhole Coaxial Heat Exchanger System: Potential for Fully Utilizing Geothermal Resources.* National Institute for Resources and Environment. Onogawa: GRC Bulletin.

Tomasz Śliwaa, M. K.-Ś. (2018). Potential application of vacuum insulated tubing for deep borehole heat exchangers. *75*.

C. Alimonti, E. S. (2016). Study of geothermal power generation from a very deep oil well with a wellbore heat exchanger. *Renewable Energy, 86*, 292-301.

Robert A. Caulk, I. T. (2017). Reuse of abandoned oil and gas wells for geothermal energy production. *Renewable energy, 112*, 388-397.

N.M. Wight, N. B. (2015). Geothermal energy from abandoned oil and gas wells using water in combination with a closed wellbore. *Applied Thermal Engineering, 89*, 908-915.

Sciencedirect. (n.d.). Retrieved from https://www.sciencedirect.com: https://www.sciencedirect.com/topics/engineering/colebrook-equation

Goepfer, R. (1990). *Static pressure and gradients.* Reservoir. The Hague: Elf petroland.

Horst, K. V. (1990). *Modified isochronal with memory gauges.* Elf petroland. Leeuwarden: Schlumberger.

Schlumberger. (1985). *Bottom hole pressure and temperature survey annexes.* Leeuwarden: Schlumberger.

Legendre, E. (1989). *Direction exploration.* Societe nationale elf aquitaine (production). Petroland.

Sponton, L. G. (1981). *Rapport d'analyze de gaz.* Den helder: Petroland.

Vassilis Belessiotis, S. K. (2016). Chapter Two - Water, the Raw Material for Desalination. In S. K. Vassilis Belessiotis, *Thermal solar desalination* (pp. 21-102). Elsevier.

Iosifina Iosif Stylianou, S. T. (2016, April). Renewable Energy. *Science Direct, 88*, 418-429 .

Iman Asadia, P. S. (2018). Thermal conductivity of cement – A review. *Journal of Building Engineering*, 81-93.

Robertson, E. C. (1988). *THERMAL PROPERTIES OF ROCKS.* UNITED STATES DEPARTMENT OF THE INTERIOR GEOLOGICAL SURVEY. Reston: U.S. Geological Survey.

Cermak, V. a. (1982). Zahlenwerte und funktionen aus naturwissenschaften un technik. *Physikalische eigenschaften der gesteine, 1A*, 305-343.

Petroland. (1979). *Draft of drilling program Grouw 1.* The Hague: Elf petroland b.v.

M.A.W. Vrijlandt, E. S. (2019). *ThermoGIS.* (TNO) Retrieved from ThermoGIS geothermal mapping: https://www.thermogis.nl/en/geothermal-family

Tomasz Sliwa, M. A. (2015, September). Natural and artifical methods for regeneration of heat resources for BHE to enhance the sustainability of underground thermal storage. (7).

Nlog. (1979, Oktober). *Data boring Grouw-01*. (Elf Petroland) Retrieved April 2020, from nlog.nl: https://www.nlog.nl/kaart-boringen
Zhang, H. (2011). *Building Materials in Civil Engineering.* Woodhead Publishing.
Chan Soo Kim, K. O. (2003). *Performance evaluation of an improved particle size magnifier for single nanoparticle detection.* Hiroshima: Aerosol science and technology.
Wang, P. (2014, October). A numerical investigation of impingin jet cooling with nanofluids. *18*(4).
COMSOL, i. (1986). *https://www.comsol.com/multiphysics/fea-software*. (COMSOL) Retrieved April 2020, from https://www.comsol.com.
Theo Wong, G. H. (2007, Jan). Cretaceous, in Geology of the Netherlands.
A. Lokhorst, T. W. (2007). *Geothermal energy.* (D. B. Th.E. Wong, Ed.) Amsterdam: oyal Netherlands Academy of Arts and Sciences KNAW.
M.M.Stack, G. (2012, January 27). Mapping erosion–corrosion of carbon steel in oil–water solutions: Effects of velocity and applied potential. *Elsevier, 274–275*, 401-413 .
Wang, M. W. (2009). A SINGLE-WELL EGS CONFIGURATION USING A THERMOSIPHON. Stanford: Stanford University.
Zhe Wang, M. W. (2009). A SINGLE-WELL EGS CONFIGURATION USING A THERMOSIPHON. Stanford: Stanford University.
D. Bonté, J.-D. v. (2012). Subsurface temperature of the onshore Netherlands: new temperature dataset and modelling. *Geologie en Mijnbouw*, 499.
Hanrahan, G. (2012). Key Concepts in Environmental Chemistry. *Elsevier Inc*, 73-106 .
Fabio Galbusera, F. N. (2018). Biomechanics of the Spine. *sciencedirect*, 239-255.
Mazumder, S. (2016). *Numerical Methods for Partial Differential Equations.* Elsevier Inc. .
K.W.Oh. (2012). 6 - Lab-on-chip (LOC) devices and microfluidics for biomedical applications. *MEMS for Biomedical Applications* , 150-171 .
CLO. (2019, Augustus 8). *Energieverbruik door huishoudens 1990-2018*. Retrieved June 1, 2020, from Rijksoverheid: https://www.clo.nl/indicatoren/nl0035-energieverbruik-door-de-huishoudens
Rijkswaterstaat. (2020, June 1). *Hoe is de omrekening van verbruik stadsverwarming naar m3 aardgas?* Retrieved from https://www.infomil.nl/onderwerpen/duurzaamheid-energie/energiebesparing/vragen-antwoorden/overige-vragen/omrekening-verbruik/
Zurich, I. o. (1986). *Shallow geothermal resources*. (Geothermics Radiometrics) Retrieved from http://www.gtr.ethz.ch/Projekte/ShallowGeothermics/shallow.html
dongen, B. v. (2019). *The economic potential of deep, direct use geothermal systems in the Netherlands.* Delft: Technical univeristy of Delft.
policy, M. o. (2020). *SDE+ spring 2020.* Zwolle: Netherlands enterprice agency.
leefomgeving, P. v. (2020). *Klimaat- en energieverkenning 2020.* Den Haag: TNO, Planbureau voor de leefomgeving, Rijksinstituut voor volksgezondheid en milieu, CBS.
instituut, K. N. (2020). *Grafieken van het afgelopen jaar*. (Ministerie van infrastructuur en waterstaat) Retrieved from https://www.knmi.nl/nederland-nu/klimatologie/grafieken/jaar
H. Bilarian, M. S. (2019). Economic and environmental assesment of a solar-assisted ground source heat pump system in a heating dominated climate. *International Journal of environmental science and technology*(May 2018), 3092.
Seba, R. (1998). *Economics of worldwide petroleum production.* Tulsa: Oil and gas consultants international.
Engeldot pomp- en leidingsystemen. (n.d.). (Engeldot) Retrieved December 2020, from https://www.engeldot.nl/pompen/cv-pomp/circulatie-en-inline-pomp/dab-enkele-circulatiepompen-klm-klp-in-line-flensaansluiting/

OfferteAdviseur. (n.d.). *Kosten warmtepomp*. Retrieved December 2020, from https://www.warmtepomp-info.nl/kosten-warmtepomp/
Buffervaten. (n.d.). (De Groene Hoed) Retrieved December 2020, from https://www.groenehoedduurzaam.nl/2000-liter-buffervat-2-warmtewisselaars.html
Gibbons, I. R. (2020, December). Engineer.
Pre-insulated water pipe. (n.d.). (Corelco) Retrieved December 2020, from http://www.corelco.com/pre-insulated-water-pipe/
Calpex Pre-Insulated PEX Pipe. (n.d.). (Polytherm) Retrieved December 2020, from http://www.polytherm.ie/p/calpex-pre-insulated-pex-pipe/pcalpex
Waterleidingen. (n.d.). (Wildkamp) Retrieved December 2020, from https://www.wildkamp.nl/assortiment/drukleidingen-fittingen/waterleidingsystemen/voorgeisoleerde-buizen-voor-waterleidingsystemen/17000010
Zitha, P. P. (2009). *Field development project AES2009.* Delft: Technical university of Delft.
Belastingdienst. (n.d.). *Afschrijven*. (Ondernemersplein) Retrieved December 2020, from https://ondernemersplein.kvk.nl/afschrijven/
Zaal, C. (2020). *Geothermal field development strategies based on economic and fault stability analysis.* Delft: Delft university of Technology.
Tarieven voor de vennootschapsbelasting. (n.d.). (Belastingdienst) Retrieved December 2020, from https://www.belastingdienst.nl/wps/wcm/connect/bldcontentnl/belastingdienst/zakelijk/winst/vennootschapsbelasting/tarieven_vennootschapsbelasting
Tabellen tarieven milieubelastingen. (n.d.). (Belastingdienst) Retrieved December 2020, from https://www.belastingdienst.nl/wps/wcm/connect/bldcontentnl/belastingdienst/zakelijk/overige_belastingen/belastingen_op_milieugrondslag/tarieven_milieubelastingen/tabellen_tarieven_milieubelastingen?projectid=6750bae7%2D383b%2D4c97%2Dbc7a%2D802790bd1110
Menon, E. S. (2015). Transmission pipeline calculations and simulations manual.
al, C. e. (2019). Numerical investigation on the performance, sustainability, and efficiency of the deep borehole heat exchanger system for building heating. *Geothermal Energy, 18*(7).
Holmberg H, A. J. (2016). Thermal evaluation of coaxial deep borehole heat exchangers. *Renew Energy, 97*, 65–76.
Klip, D. (2017). *The transition of the residential heating system.* The Hague: Clingendael internation energy programme.
R. Koelemijer, P. K. (2017). *Nationale kosten energietransitie in 2030.* Planbureau voor de leefomgeving.
Nijpels, E. (2019). *Climate agreement.* The Hague.
(n.d.). (High-quality and professional manufacturere of polyurethance insulation pipes in China) Retrieved December 2020, from http://www.tsxingbang.com
(n.d.). (Weifang Palconn plastics technology) Retrieved December 2020, from http://www.palconn.com

9. Appendix

Table 9-1 Bottom hole temperature calculations from temperature survey (Schlumberger, 1985).

FLOPETROL JOHNSTON Schlumberger

Base : ALKMAAR

Client : PETROLAND

Field : LEEUWARDEN

Well : Grouw 1

Section : ANNEX 1.3

Page : 1-1.3

Report No. : 17/85

Bottom Hole Temperature Calculations

INSTRUMENT DATA :

Temperature element No. 43924 Manufacturer G R C Range 0-300 °F

Recording element No. 36541 Clock No. 1506 Range 48 hr

DATE - TIME Time Hrs/	DATE - TIME Cumul Min.	Choke size	Depth Meter	W.H. temp.	Y Inches	Y + Yo	T °F	Remarks °C Units
30th.	May 1985							
16.35		Stylus on gauge						
17.15		Pressure up lubricator						
17.55		Gauge at survey depth						
17.55			1925		.453		168.0	75.6
18.00			1925		.457		168.7	75.9
18.30			1925		.462		169.5	76.4
18.45			1925		.468		170.5	76.9
19.00			1925		.469		170.7	77.1
20.00			1925		.472		171.2	77.3
24.00			1925		.474		171.5	77.5
31st.	May 1985							
12.00			1925		.474		171.5	77.5
24.00			1925		.474		171.5	77.5
1st.	June 1985							
08.00			1925		.474		171.5	77.5
08.02		Gauge at 1900 mtr.						
08.02			1900		.468		170.5	76.9
08.32			1900		.460		169.2	76.2
08.35		Gauge at 1850 mtr.						
08.35			1850		.439		165.5	74.2
09.05			1850		.427		163.4	73.0
		No further readings on this chart.						

DOP 117

Table 9-2 Analysed gas samples from GRW-01 (Legendre, 1989).

15.

TABLEAU 1 : PAYS-BAS TERRESTRES

COMPOSITION ET ISOTOPIE DES GAZ EN RESERVOIR CRETACE

DONNEES ISOTOPIQUES SUR LES CONDENSATS ASSOCIES

PUITS	FRA 1	HAR 5	FRA 1(*)	GRW 1	NWD 1d	ZDW-A1
Prof.(m/TR)	1056		1741-1747 et 1745	1927-1937	2247-2254	1856-1948
Réservoir	Cret.sup	Cret.sup	Cret.inf	Cret.inf	Cret.inf	Cret.inf
GOR (m3/m3)					96000	
N2	3.61	4.53	19.6/19.5	17.40	5.61	2.83
CO2	0	0	.54/.52	.49	.13	1.07
H2S	-	0	- / -	0	0	0
CH4	95.79	94.93	76.8/76.9	78.95	88.62	88.97
C2H6	.54	.46	2.3/2.2	2.62	4.00	5.06
C3H8	.03	.03	.54/.53	.36	1.00	1.17
i-C4H10	.01	.01	.11/ -	.04	.19	.20
n-C4H10	.01	0	.10/ -	.06	.23	.27
i-C5H12	.01	0	.05/ -	.01	.09	.10
n-C5H12	.01	0	.03/ -	.01	.07	.09
C6+	-	.04	- / -	.03	.06	.23
100xC1/Cn	99	99	96 / 96	96	94	93
d13C C1	-31.1	-35.7	-28.3 /-29.6	-28.8	-30.4	-32.0
C2		-17.5	- /-24.4	-25.4	-23.6	-22.8
C3				-21.8	-21.3	-21.0
C4				-22.5		-18.6
dD C1			- /-145	-156		-165
d13C CO2			-18.6(x2)	-13.6	-11.9	- 8.5
d18O CO2				+33.0		+35.0
d13C HT					-24.4	-24.5
d13C RD					-26.0	-26.3
dD HT						-89
dD RD						-84

(*) Deux analyses sont disponibles sur le gaz en réservoir crétacé inf.

EXPLICATIONS

Composition en % molaires

Isotopie des gaz :
Rapport isotopique du Carbone d13C en pour mille PDB
de l'Hydrogène dD en pour mille SMOW
de l'Oxygène d18O en pour mille SMOW

Isotopie des condensats :
Rapport isotopique du Carbone(d13C) et de l'Hydrogène(dD)
sur produit total(HT) et sur résidu de distillation(RD)

Table 9-3 Outer-well size and geological data from GRW-01 (Sponton, 1981).

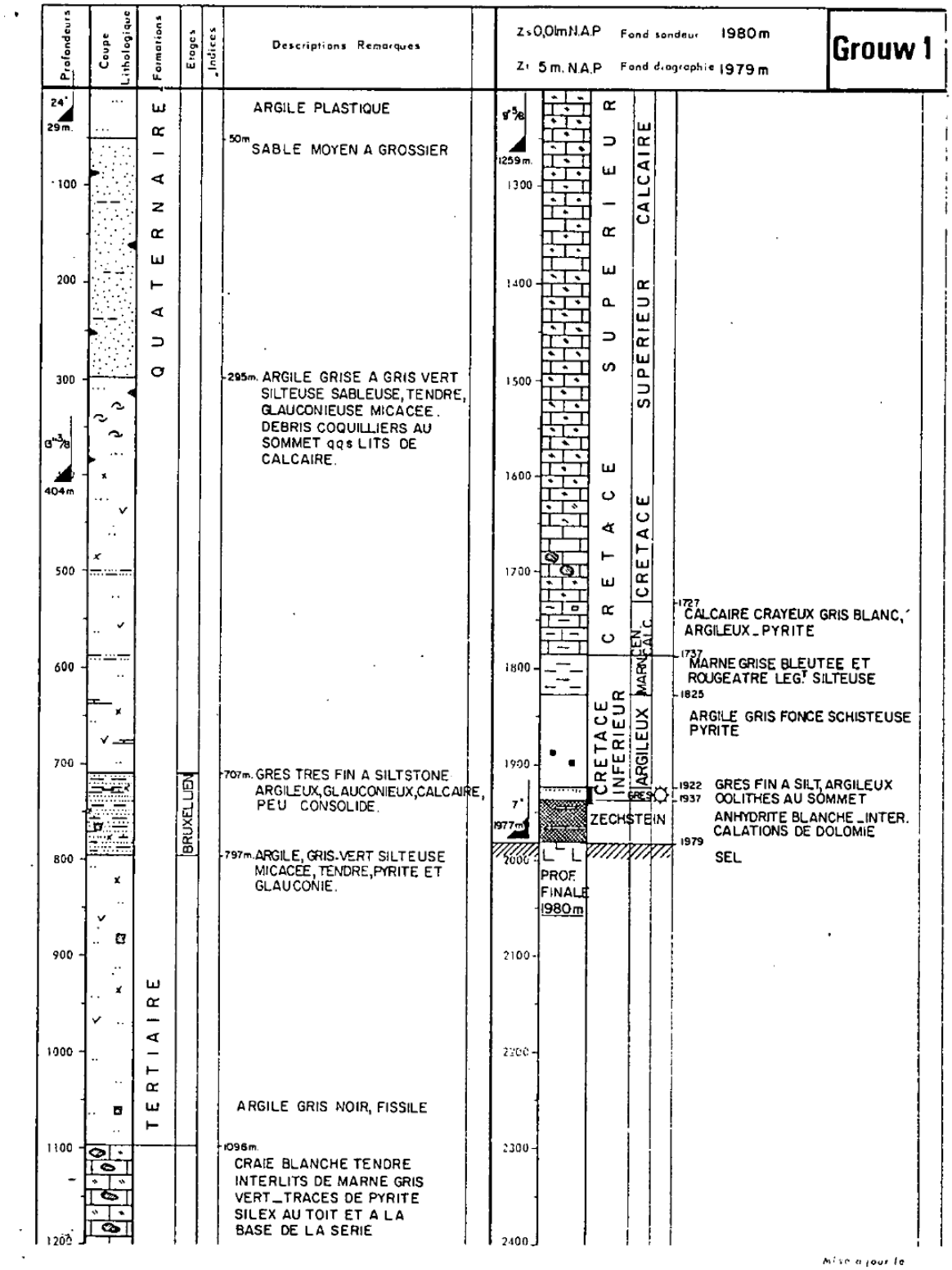

Table 9-4 The drilling program of Grouw-01 with casing program (Petroland, 1979).

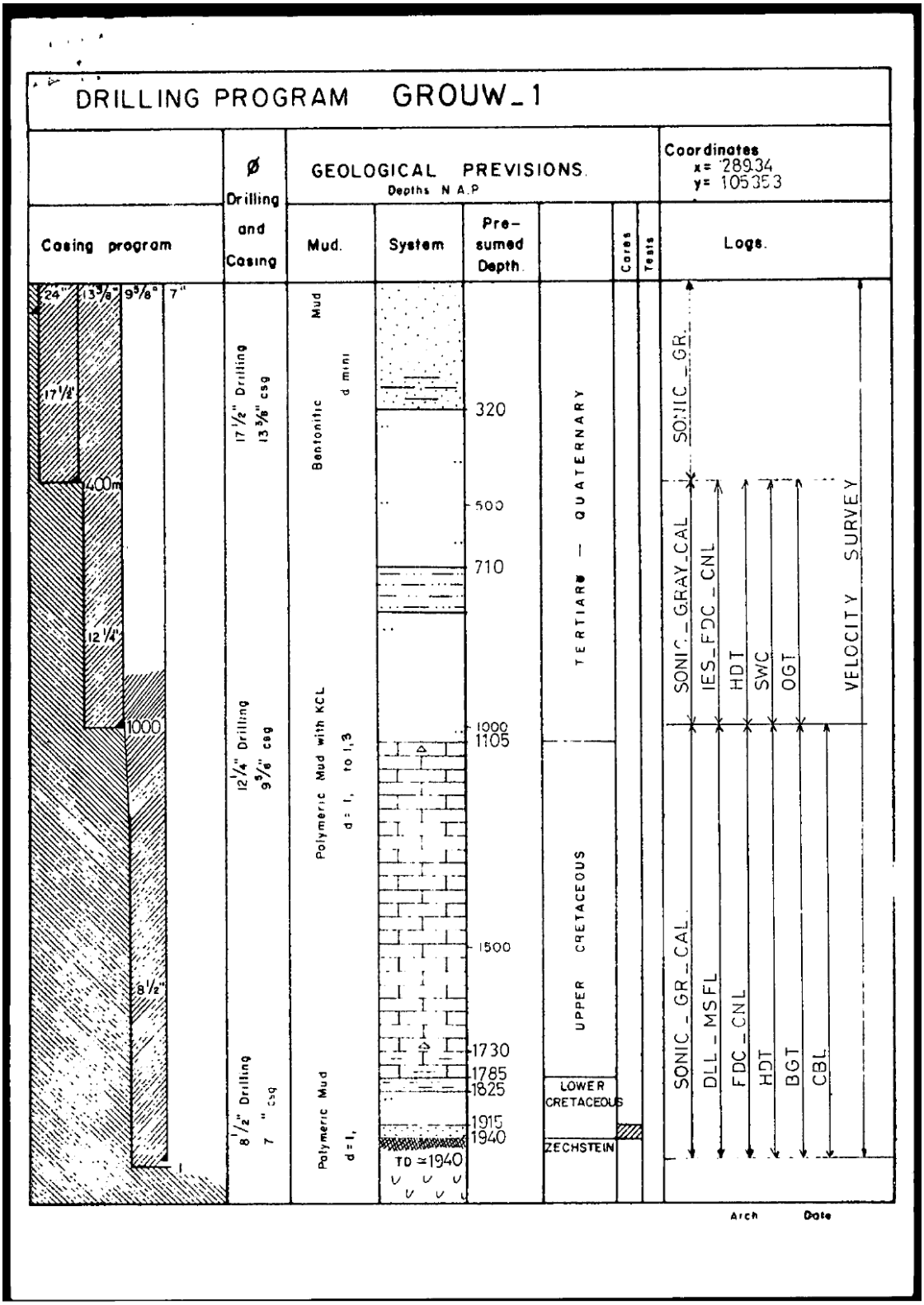

Table 9-5 Thermal conductivity of cement-based materials (Iman Asadia, 2018).

Type of concrete		Density (ρ) (kg/m^3)	Thermal conductivity (K) (W/m °K)
Concrete code	Description		
FC-1100	Foamed concrete with densities ranging from 1100 kg/m^3 to 1600 kg/m^3	1156	0.40
FC-1200		1192	0.41
FC-1300		1354	0.50
FC-1400		1409	0.54
FC-1500		1506	0.55
FC-1600		1594	0.57
OPSFGC13	Oil palm shell foamed geopolymer concrete with densities of 1300, 1500 and 1700 kg/m^3 and oil palm shell non-foamed geopolymer concrete	1291	0.47
OPSFGC15		1467	0.50
OPSFGC17		1721	0.54
OPSNFGC		1791	0.58
NP05-1700	Newspaper sandwiched aerated lightweight concrete panels with densities of 1100, 1400, and 1700 kg/m^3 aerial intensities of 0.05, 0.10, and 0.15 g/cm^2 of newspaper sandwiched	1700	0.50
NP05-1400		1400	0.39
NP05-1100		1100	0.31
NP10-1700		1700	0.49
NP10-1400		1400	0.33
NP10-1100		1100	0.30
NP15-1700		1700	0.40
NP 15-1400		1400	0.31
NP 15-1100		1100	0.30
PFC-150	Polystyrene foamed concrete with densities ranging from 150 kg/m^3 to 400 kg/m^3	150	0.08
PFC-200		200	0.08
PFC-250		250	0.09
PFC-400		400	0.15
SF10	Concrete containing silica fume and fly ash at ratios of 10–30% cement replacement	509	0.17
SF20		493	0.15
SF30		485	0.15
FA10		511	0.16
FA20		498	0.16
FA30		483	0.14
SF7.5	Concrete with silica fume in 7.5% and 15% cement replacement, fly ash and blast furnace in 15% and 30% cement replacement	2350	1.16
SF15		2335	1.05
FA15		2340	1.08
FA30		2290	0.95
BFS15		2355	1.09
BFS30		2340	1.04
SF + FA		2330	0.99
SF + BFS		2345	1.12
FA + BFS		2300	0.97
SF-10%	Mortar containing silica fume, fly ash and blast furnace as cement replacement in 10%, 20% and 30% weight	1920	0.97
SF-20%		1880	0.81
SF-30%		1790	0.71
FA-10%		2020	1.01
FA-20%		1950	0.87
FA-30%		1920	0.79
BFS-10%		2106	1.03
BFS-20%		2010	1.03
BFS-30%		1990	1.01

Type of concrete		Density (ρ) (kg/m^3)	Thermal conductivity (K) (W/m °K)
Concrete code	Description		
REF	Different types of normal concrete, magnetite concrete, graphite concrete, graphite and magnetite concrete, steel fiber concrete, steel fiber concrete with high fiber concentration, concrete with brass shavings, concrete with copper wires, concrete with PCM pellets, concrete with micro PCM, concrete with PCM dispersion, and cement paste	2240	2.24
MAG		3650	2.57
GRA		1890	3.52
GAM		2810	3.85
ST1		2330	2.57
ST2		2441	2.95
BRA		2520	2.71
COP		2438	3.63
PEL5		1790	1.23
MIC5		1570	0.83
MIC50		1570	0.77
DIS5		1900	1.47
DIS50		1900	1.63
PAS		1510	0.58
Silica fume (0%) + Silane (0%)	Concrete containing 0–2% silane and 15% silica fume (by weight of content) as admixtures	1990	0.52
Silica fume (15%) + Silane (0%)		1980	0.40
Silica fume (15%) + Silane (0.2%)		2070	0.61
Silica fume (15%) + Silane (0.5%)		2060	0.64
Silica fume (15%) + Silane (0.75%)		2050	0.66
Silica fume (15%) + Silane (1%)		2080	0.68
Silica fume (15%) + Silane (1.5%)		2070	0.69
Silica fume (15%) + Silane (2%)		2070	0.71
CCM	Cement matrix and wooden aggregate in 10–30% of mass fraction	1283	0.43
10WA		1065	0.34
20 WA		908	0.23
25 WA		862	0.22
30 WA		800	0.21

Table 9-6 Specific heat of common rocks at various temperature (Robertson, 1988).

Rock type	Specific heat (10^3 J/kg K)					
Temp. (°C)	0	50-65	200	400	800	1200
Granite..... 0.65		0.95	1.07	1.13		
0.80	0.77	0.95	1.09	1.39		
Granodiorite..... 0.70		0.97	1.09	1.18		
Diorite..... 0.71	0.81	0.99	1.09	1.18		
Basalt..... 0.85		1.04	1.15	1.32	1.49	
Diabase..... 0.70		0.87	0.98	1.19	1.36	
Gabbro..... 0.72		0.99	1.10	1.18		
Gneiss, granitic... 0.74	0.79	1.01				
Slate..... 0.71		1.00	1.10	1.20	1.27	
Quartzite..... 0.70	0.77	0.97	1.13	1.17	1.33	
Marble..... 0.79	0.85	1.00	1.13			
Sandstone.....	0.93					
Micaceous sandstone		0.73				
Clay, amorphous.... 0.75		0.94	1.13	1.51		
Clay, kaolin..... 0.80		0.94	1.08	1.78	1.78	
Shale.....	0.77					
Limestone.....	1.00					
	0.83					

Table 9-7 Bulk density of common rocks (Robertson, 1988, p. 74).

Rock type	Decimal porosity ϕ	Bulk density (g/cm^3)
	Igneous [1]	
Granite.....	----	2.67
Granodiorite.....	----	2.72
Syenite.....	----	2.76
Quartz diorite.....	----	2.81
Diorite.....	----	2.84
Gabbro.....	----	2.98
Diabase.....	----	2.97
Peridotite.....	----	3.23
Dunite.....	----	3.28
	Metamorphic [2]	
Granite gneiss.....	----	2.7
Quartz mica schist	----	2.8
Slate.....	----	2.8
Amphibolite.....	----	3.0
Eclogite.....	----	3.4
	Sedimentary [3]	
Sandstone.....	0.007	2.7
	0.10	2.5
	0.20	2.3
	0.30	2.2
Limestone.....	0.005	2.7
	0.05	2.6
Chalk.....	0.30	2.2
Dolomite.....	0.03	2.8
Shale.....	0.05	2.6
	0.20	2.4
Sand.....	0.50	1.9
Silt.....	0.75	1.5

[1] Averages from Daly, 1966; porosity not recorded.

[2] Averages from Clark, 1966; porosity not recorded.

[3] Averages from Manger, 1966. Bulk densities of sedimentary rocks are for samples saturated with water. Representative values of density and corresponding porosity are given; therefore, only two significant figures are shown.

Table 9-8 Thermal conductivity of limestone with water in the pores, showing variation with solidity, at 300 K and 5 MPa (Robertson, 1988, p. 21).

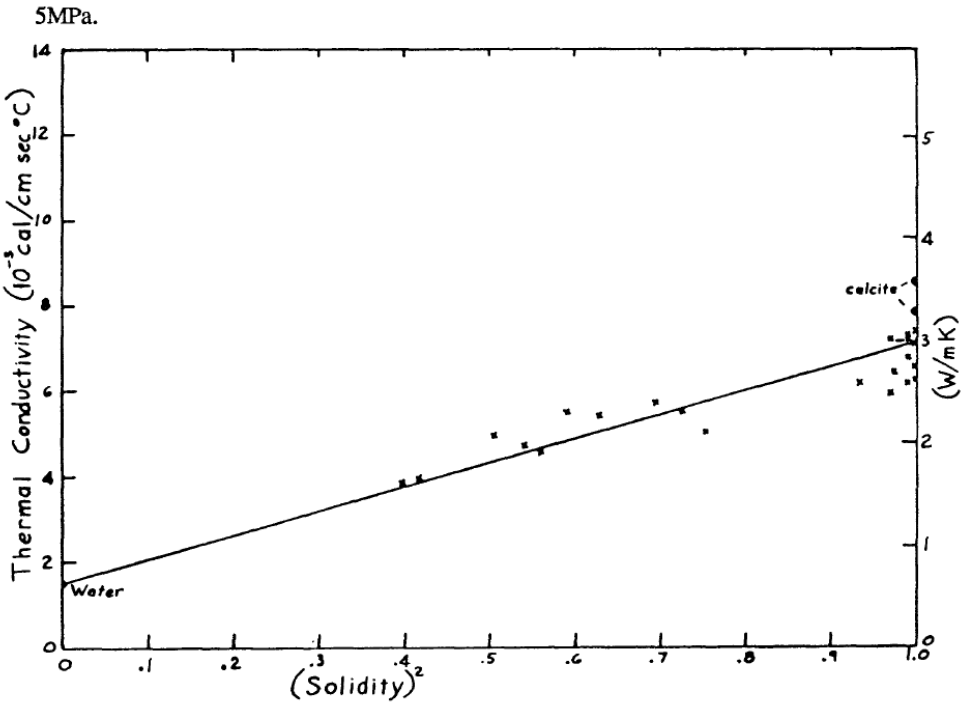

Table 9-9 Thermal conductivity of limestone with air in the pores, showing variation with solidity, at 300 K and 5 MPa (Robertson, 1988, p. 21).

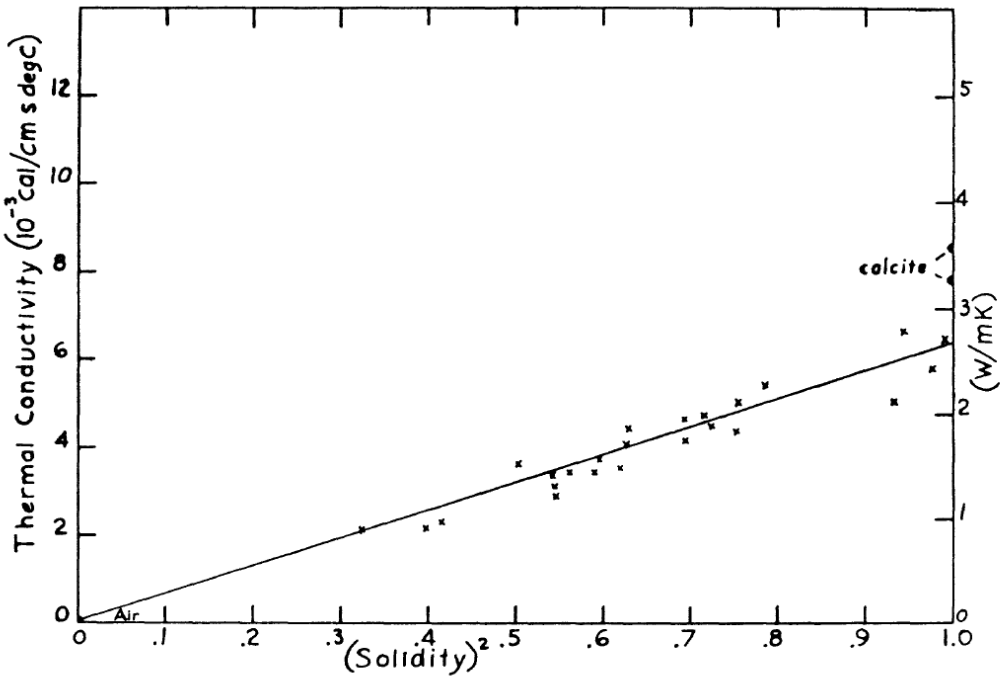

Table 9-10 Thermal conductivity, k, of some sediments as a function of density (Cermak, 1982).

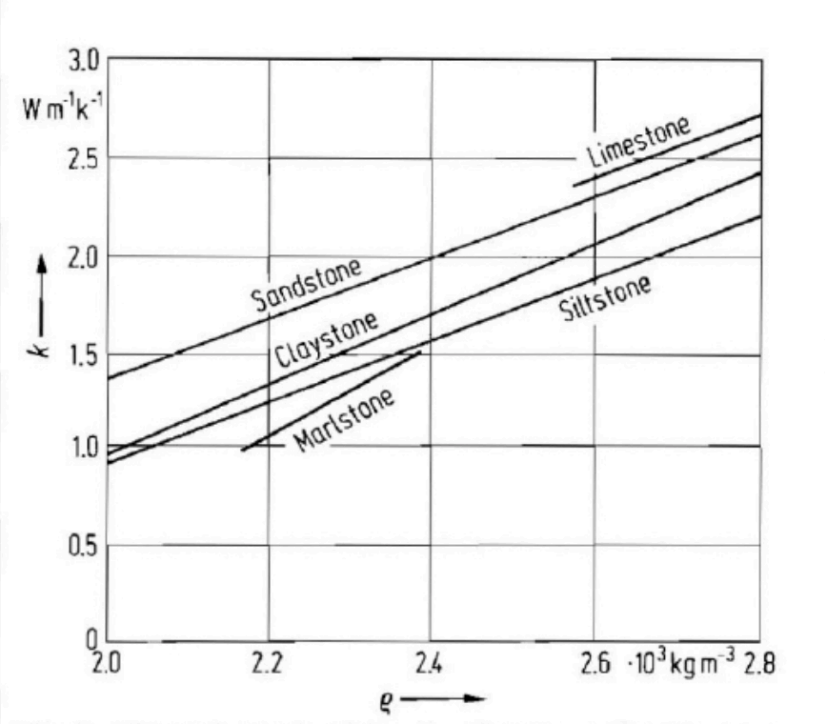

Table 9-11 Thermal conductivity ranges of common rocks (Cermak, 1982).

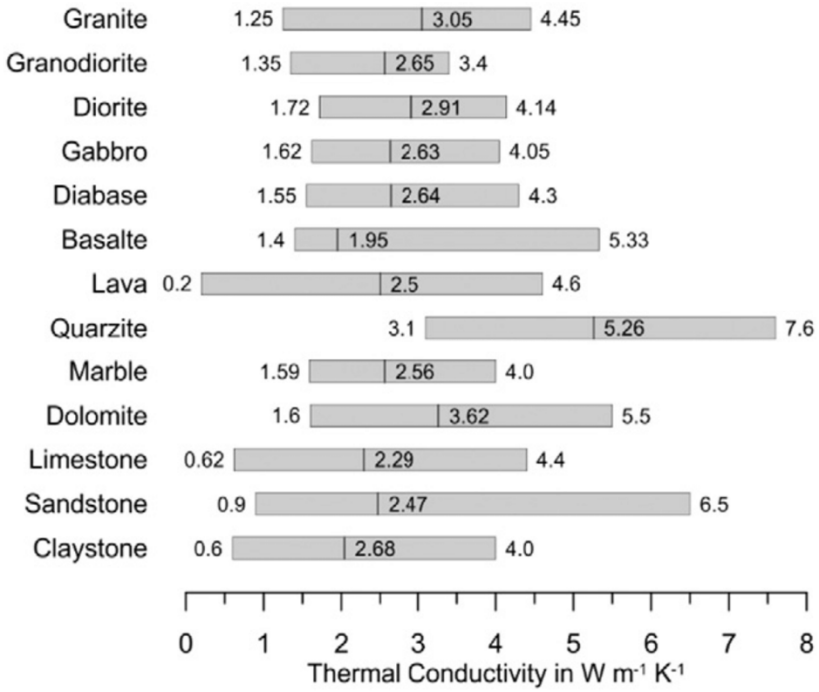

Table 9-12 The energy consumption of all the Dutch households throughout a year (Klip, 2017).